Testing Unified Models of Active Galaxies through Infrared Spectroscopy

Philip Rodriguez Blanco

Ph.D. Thesis

University of Edinburgh

1991

This thesis has been composed by me and consists entirely of my own work except where indicated in the text.

Philip R. Blanco

September 1991

Acknowledgements

After spending a nearly a quarter of my life in the field of research which eventually led to this thesis, there are many whom I must acknowledge for playing a role in its completion.

I would like to thank my original supervisors Peter Brand and Pat Roche, for tolerating my roundabout routes back from the AAT in the early stages. I am also especially grateful to my "adopted" supervisor Martin Ward for boldly entrusting me with the task of reducing the data, and for his clarity of expression and exemplary scientific method in our mutual endeavours, from which I hope I have learned a great deal. This work also benefited greatly from the encouraging comments, vociferous objections and occasional long silences of my other collaborators: Minoru Nishida, Andrew Wilson and Gillian Wright; I look forward to continuing these collaborations. It is also a pleasure to thank Mark Yates, who took the time five years ago to patiently explain the essentials of astronomy to a befuddled first-year research student, and who subsequently coached me (succsssfully) in the ancient art of applying for telescope time.

Many other astronomers have contributed their advice and encouragement free of charge, and I still hope to provide a return on their investment in the future: Marshall M^{c}Call, Keith Thompson and Hans Zinnecker did much to boost my morale at just the right time through their genuine interest and enthusiasm. At the telescope, Jeremy Bailey, Tim Hawarden and especially Tom Geballe ($1\,\mathrm{Gb}=10^{-20}\,\mathrm{W\,cm^{-2}\,\mu m^{-1}}$) helped to make real astronomy a much less daunting prospect—learning from their example was much more pleasant than learning from my own mistakes!

The conscientious labours of the technical and computing staff at the Royal Observatory, Edinburgh also also deserve a mention. Much of my time in Edinburgh was spent reducing and analysing data on the evolving STARLINK computer system at ROE, which is superbly managed by John Barrow. Steven Beard and latterly Horst Meyerdierks contributed excellent software and algorithms to the Great Cause. Rosemary Glendinning and her colleagues provided a steady supply of *CGS*s for astronomers to play with; CGS2, CGS3 and CGS4 have all contributed to the results presented in this volume.

It is still an enviable necessity for British astronomers to travel. To this end, the staff of American Express (Business Travel) in Edinburgh provided a high degree common sense every time I asked their advice, and never complained about my convoluted itineries. Of those folks in the US whose hospitality I was privileged to enjoy, Nancy M^{c}Daniel deserves special mention for her long letters from California and for sacrificing

her valuable time to cater for my flying visits. Thanks are also due to Donna Womble for making fun of my "British accent", and Pauline McMahon and Eric Gotthelf for providing a safe haven in New York City.

Of the handful of people who have made my stay in Edinburgh more bearable. Richard Dixon provided a much-needed dog-biscuit of insanity as a flat- and office-mate, and instinctively knew when I needed help with something. As a flat-mate Andrea McNicoll shared friendship, conversation much-appreciated veggie things to keep me alive and sane, and has obviously instructed her best friend Nina Sobecka to take over these responsibilities!

I would also like to acknowledge the Department of Astronomy, University of Edinburgh, and the Department of Housing, City of Edinburgh for encouraging me to move on to better things, and *Star Trek* for much sound advice on decision-making and personnel management over the past few years. My name would be held in contempt forever if I did not crack at least one in-joke connected with the student population, especially by Penelope Smith who kindly proof-read some most of the text of this thesis. Instead I shall wish those who shall follow me every success in their research.

This work is hardly worthy of dedication. Nevertheless it allows me to express my love and gratitude to my mother, Joan Mary, for the sometimes painful task of helping me grow up, and to my father, John Rodriguez Blanco, a peaceful man of science and rational thinking, who in countless ways has done much to improve this work, but sadly did not live to see me finish it.

Abstract

New near-infrared spectroscopic observations of several Active Galactic Nuclei (*AGN*) are presented. In combination with existing data and X-ray, visible and far-infrared frequencies, these data are used to investigate the effects of interstellar extinction on their observed spectral energy distributions. The derived intrinsic properties of these sources are compared in detail with those expected in terms of current "unified schemes" of AGN, which seek to relate the various observational classes through the parameters of luminosity, viewing angle and obscuration.

After first presenting the methods of data reduction and analysis appropriate to infrared spectra, I use observations of the Paschen β hydrogen recombination line in three so-called *Narrow Line X-ray Galaxies* to show that their *intrinsic* (extinction-corrected) broad-line and X-ray properties can be accounted for in terms of normal Seyfert 1 nuclei obscured by moderate interstellar extinction along our line of sight.

Near-infrared spectroscopy of the luminous radio galaxy Cygnus A at $\lambda \simeq 2\,\mu$m reveals strong narrow line emission from H_2 v=1–0 S(1), [SiVI] and H^+, which I argue is excited by a highly-obscured quasar nucleus obscured by $A_V = 37 \pm 7$ mag. Wavelength-independent electron scattering of this continuum plausibly accounts for the observed optical and near-infrared non-stellar continuum. I also demonstrate that the quasar nucleus is also able to power the observed far-infrared continuum through heating of interstellar dust by the (unobserved) ultraviolet continuum.

Similar observations of the infrared-luminous galaxy merger Markarian 463 are presented as part of a multiwavelength study to determine the origin of the high far-infrared luminosities of such systems. In Markarian 463 this luminosity is provided almost wholly by an optically-obscured Seyfert 1 nucleus, which I predict should be detectable as a hard X-ray source. Using ultraviolet, optical and near-infrared line observations I am able to quantify or set limits on the roles of various emission mechanisms and the roles of interstellar dust and gas in shaping the appearance of Markarian 463(E) from hard X-ray to sub-millimetre frequencies.

These results demonstrate the utility of near-infrared spectroscopy in testing schemes which seek to unify the observational classes of AGN, and in providing important links between emission mechanisms over a wide range of frequency. I propose further observational tests for the AGN under study here, and for larger, unbiased samples of AGN for which such observations should be possible in the near future.

Contents

Chapter 1

Introductory remarks

A few percent of the galaxies we see are host to scenes of intense activity in their nuclei. Historically such activity has been identified using the techniques available to optical astronomers, but the past two decades in particular have brought us a wealth of new information on these objects at wavelengths extending across the electromagnetic spectrum. Infrared spectroscopic observations of these nuclei, and their combination with the relatively recent results from studies at other wavelengths, are the subjects of this dissertation.

The earliest spectroscopic observations of spiral nebulae identified a small fraction of galaxies as 'active' from the appearance of nebular emission lines in their optical spectra (e.g. Fath 1908). The first systematic study of activity in the nuclei of galaxies was performed by Seyfert (1943), who included the 'classical' active galaxies NGC 4151 and NGC 1068 in his sample. The classification which bears his name has since been extended to cover all radio-quiet galactic nuclei with high ionization spectra. Although Seyfert saw similarities between his spectra and those of high excitation planetary nebulae in our own Galaxy, it was not until the advent of radio astronomy that attention turned towards explaining the origin of the line emission. Baade & Minkowski (1954) identified the radio source Cygnus A with a faint elliptical galaxy at a redshift z=0.05, whose rich emission line spectrum resembled those of Seyfert's galaxies. However, it was only after the subsequent discovery of the more luminous, but spectroscopically similar, quasars (e.g. Schmidt 1963) that observational and theoretical studies confirmed the intrinsically *non-stellar* origin of this activity (see Section 9.1 of Chapter 5 for a *post facto* application of these arguments to the near-infrared spectrum).

1 Multiwavelength observations of active galaxies

Since that time the nuclei of active galaxies have been detected at every waveband for which instruments have been constructed. Satellites observing at X-ray energies have

delineated the most energetic processes, while the continuing mission of the *International Ultraviolet Explorer* has extended our knowledge of their line and continuum properties shortward of the cut-off imposed by the earth's atmosphere at 300 nm. In the far-infrared domain (12–100 μm), the *IRAS* satellite's all-sky survey opened up a whole new window to the universe, and confirmed that many galaxies emit most of their energy in this part of the spectrum. Most recently the sub-millimetre region has become accessible to ground-based astronomers, and although most active galaxies lie below current sensitivity limits, studies of the nearest and brightest examples are already bridging the gap between our understanding of the far-infrared and radio emission seen in these objects. In the 1960's radio astronomy played the leading role in the discovery of quasars, the most luminous and most distant galaxy nuclei. Since then we have learned that only a small fraction of active galaxies are "radio loud". Present day radio techniques allow us to probe the structure of *all* classes of active nuclei in unprecedented detail through the techniques of high-resolution interferometry.

2 Infrared spectroscopy of active galaxies

This dissertation is concerned with ground based near-infrared (1–5 μm) spectroscopy of a small sample of AGN in which extinction and viewing angle are suspected of being *mainly* responsible for their distinction from broad line AGN. Although such observations are much more difficult to perform than in the neighbouring visible window (330 nm to 1 μm), we shall see that they provide important new insights into the workings of obscured active nuclei, principally because infrared radiation is better able to penetrate the interstellar dust along our line of sight to them (Figure 1). Since the first infrared spectrum was obtained of NGC1068 by Thompson, Lebofsky & Rieke (1978) this relatively new observational field has already proven invaluable for exploring the dusty central regions of AGN and the molecular material associated with it (through measurements of the vibration-rotation transitions of H_2), but it is only recently that the available technology facilitated the use of grating spectrometers and linear arrays of detectors in the infrared for extragalactic work. The results presented in these thesis were performed with "state-of-the-art" instrumentation available at the time, including (in the case of Chapter 5) data obtained with a second-generation, 2-D infrared array spectrometer.

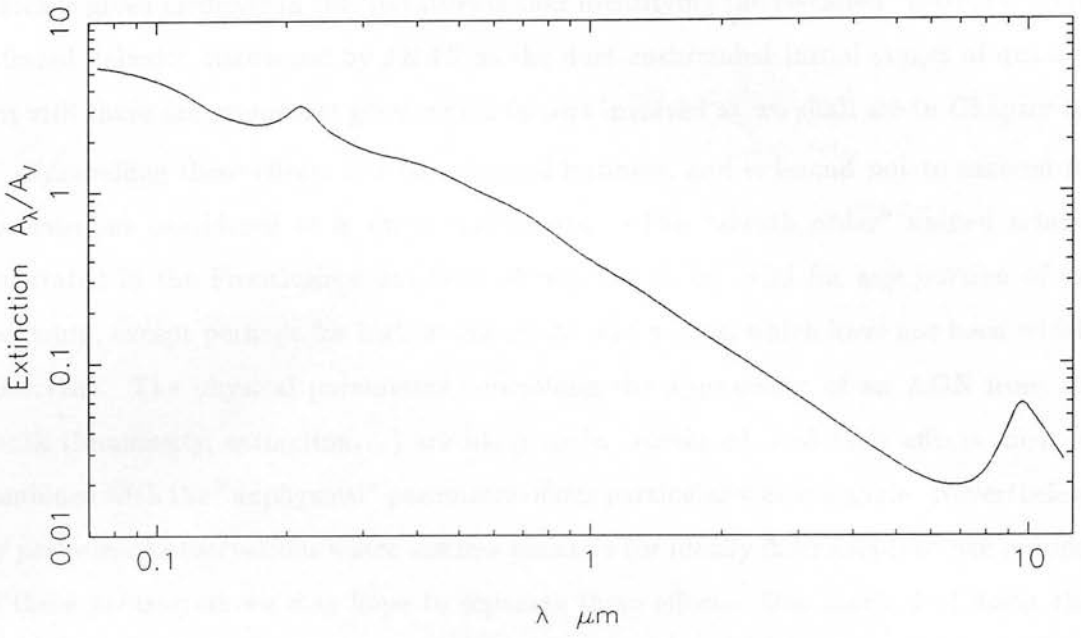

Figure 1*: The interstellar extinction curve, interpolated from the values tabulated by Mathis (1990) assuming a total-to-selective extinction ratio R=3.1. Note the logarithmic axes, and the greatly-reduced extinction at near-infrared wavelengths compared to the visible and ultraviolet. Two main features visible on this curve are the 217.5-nm absorption "bump" in the ultraviolet, and the 9.7-μm silicate absorption feature. Both of these features, and the value of R, are a function of grain composition and environment, but in the absence of further information we adopt the average extinction curve shown. Also apparent from the Figure is the approximate power-law behaviour of the extinction curve at near-infrared wavelengths, which appears to remain roughly constant in shape in a variety of environments.*

3 Classification and "unified models" of active galaxies

The large quantity of data at every wavelength has shown that nuclear activity has many manifestations, and numerous attempts have been made to unify the observational classes.

Given the time constraints of both author and reader, I shall spare ourselves the usual leisurely stroll along the foreshore of the subject. The taxonomy of AGN, and possible schemes for unifying them, are laid out in an excellent review by Lawrence (1987); I shall assume that the reader is familiar with the results reviewed in this paper. The most fashionable current schemes explain the difference between broad- and narrow-line AGN in terms of the joint effects of obscuration and viewing angle, with the addition of relativistic beaming in the case of radio-loud AGN. The remaining "evolutionary" model

which is given credence in the literature is that identifying the so-called "ultraluminous" infrared galaxies discovered by *IRAS* as the dust-enshrouded initial stages of quasars, but still there are important geometrical factors involved as we shall see in Chapter 5.

Unravelling these effects is a complicated business, and is bound not to succeed for observations considered at a single wavelength. (The "zeroth order" unified scheme illustrated in the Frontispiece has been shown *not* to be valid for any portion of the spectrum, except perhaps for highest-energy X- and γ-rays, which have not been widely observed). The physical parameters controlling the appearance of an AGN from the Earth (luminosity, extinction...) are likely to be correlated, and their effects must be combined with the "unphysical" parameter of our particular viewing angle. Nevertheless, by performing observations which are less sensitive (or ideally insensitive) to one or more of these parameters we may hope to separate these effects. One method of doing this is through carefully-selected statistical samples; the route pursued here, however, is to confront the predictions of unified schemes with detailed observations of individual objects.

4 Thesis rationale

In this thesis, infrared spectroscopic observations of a number of active galaxies are utilized in conjunction with data at optical, X-ray and other wavelengths (most of which have only become available over the past decade) in an attempt to both separate and quantify the effects of excitation and extinction in their nuclei. These results are compared with the the naïve expectations of current "unified schemes", which seek to explain the diverse observational classes of active galaxies in terms of a prototype AGN modified by the effects of extinction, viewing angle and (in the case of powerful radio galaxies) relativistic beaming. The chapters which follow represent some of the first steps taken in the near-infrared to test these unified models in a small selection of the nearby active galaxy population. This selection is unashamedly biased; the AGN were selected from optical samples of emission-line AGN principally because they were thought to be excellent candidates for obscured nuclear activity, they were overhead in a clear skies on the allocated nights at the telescope, and bright enough at near-infrared wavelengths for us to perform useful observations.

5 Thesis Guide

Each chapter has been written as a more-or-less self-contained unit, with all the relevant material included except where repetition would be tedious. The Prologue at the start attempts to convince the reader of the motivation for performing the research described, and a brief Summary highlights the major findings in a succinct manner. The Introduction to each chapter also contains material which would normally be found in a wide-ranging review at the start of the thesis, but it was thought best to introduce the concepts behind particular predictions of unified schemes where they were most relevant.

In the next chapter I present a step-by-step account of the data reduction and analysis methods which have been applied to much of the infrared spectra used in this volume. Chapter 3 presents the first results of a programme to search for broad infrared line emission from optically-obscured nuclei of galaxies with Seyfert 2 spectra; to ensure a degree of initial success we chose to observe those Seyfert 2s which have been detected in hard X-rays, to test whether their intrinsic broad line properties do indeed conform to those expected of Seyfert 1 AGN. Chapter 4 presents new near-infrared measurements of atomic and molecular lines in the luminous radio galaxy Cygnus A, while in Chapter 5 we present a similar multiwavelength study of the (Seyfert 2) nucleus of the infrared-luminous merger Markarian 463.

In keeping with the modular nature of this dissertation, predictions arising from our results for individual galaxies, and suggested observational tests arising therefrom, are presented at the end of each chapter, but a more global view is taken briefly in the closing remarks at the end of the thesis.

6 Conventions and Definitions

Astronomy is a science steeped in history and folklore, and as such has inherited a number of peculiarities in its system of units. Despite the preponderance of obsolete (cgs) units in the astronomical literature, the author has tried to adhere to the *Système Internationale* (*SI*) as far as possible in the physical units, and has converted pertinent data from other sources onto this system, apart from the few exceptions itemized below:

i. The unit of distance is the parsec (pc) ($1\,\mathrm{pc}=3.08\times10^{16}\,\mathrm{m}$)

ii. Number densities and column densities are given in their cgs form (cm^{-3} and cm^{-2} respectively). This is partly because the density of the diffuse interstellar medium in our Galaxy is believed to be $\sim 1\,cm^{-3}$.

iii. The unit of flux density (flux-per-unit-frequency) is the Jansky (Jy), where $1\,Jy = 10^{-26}\,W\,m^{-2}\,Hz^{-1}$. There is no such unit for flux-per-unit-wavelength, which we normally express in $W\,m^{-2}\,\mu m^{-1}$. (A small prize awaits the person who informs the author of the first published use of this unit).

iv. The concept of *magnitude* is defined in Chapter 2. Note that an extinction value given in magnitudes can be converted to the more conventional *optical depth* through the relation $\tau_\lambda = 0.4 \ln 10 A_\lambda$.

v. Spectral lines are identified by their wavelengths in this thesis, and here an inconsistent notation has been propagated for the sake of clarity. Whilst ultraviolet (λ<330 nm) and infrared (λ>1 μm) lines are referred to by their *in vacuo* wavelengths, spectral lines in the intervening visible domain are labelled by their wavelengths *in air*. The reader should be aware that whatever the notation, vacuum wavelengths have been used in calculations where accurate values are critical.

vi. A standard cosmology with H_0=50 km s^{-1} Mpc^{-1} and q_0=1/2 has been used to calculate distances from a galaxy's redshift cz, except where specifically indicated. These values are primarily chosen for consistency with other workers.

References

Baade, W. & Minkowski, R., 1954. *Astrophys. J.*, **119**, 206.

Fath, E. A., 1908. *Lick Observatory Bulletin*, **5**, 71.

Lawrence, A., 1987. *Publs astr. Soc. Pacific*, **99**, 309.

Mathis, J. S., 1990. *Ann. Rev. Astr. Astrophys.*, **28**, 37.

Seyfert, C. K., 1943. *Astrophys. J.*, **97**, 28.

Schmidt, M., 1963. *Nature*, **197**, 1040.

Thompson, R. I., Lebofsky, M. J. & Rieke, G. H., 1978. *Astrophys. J. Lett.*, **222**, L49.

Chapter 2

Reduction and Analysis of Infrared Spectral Data

Prologue: Ground-based spectroscopy of galaxies at near-infrared wavelengths requires a number of special observing and data reduction procedures. In this chapter an overview these methods is presented, with specific reference to data taken with CGS2 on UKIRT. This is followed by a brief description of the estimation of line fluxes and profiles from infrared spectra. As an illustration of these methods we follow these steps in the reduction of a K window spectrum of Markarian 463(E). It is hoped that this chapter may serve as an introduction to the subject for the non-specialist astronomer.

1 Introduction

Observing at infrared wavelengths from the ground has been likened to observing in the visible during the daytime with the dome lights on, since the background radiation incident on a detector from the sky and surroundings is typically far higher than the feeble astronomical signals one wishes to observe (Figure 1). In addition, the attenuation of incoming signals by water vapour, CO_2 and O_2 molecules in our atmosphere can be severe, and can change rapidly with wavelength, especially at the edges of the atmospheric "windows" (Figure 2; see also Figure 1 of Chapter 4). Even though space-based infrared observatories (e.g. *ISO* and *SIRTF*) are planned to start work by the end of the millenium, these satellites will have relatively small light-gathering apertures ($\lesssim$1.0 m), and hence will only surpass the performance of 4-metre class ground-based telescopes outside the atmospheric "windows" through which near-infrared light may reach the ground, and at the longer infrared wavelengths ($\lambda \gtrsim 20\,\mu$m) where ground-based astronomy is virtually impossible.

As we shall see in subsequent chapters, infrared emission lines in AGN typically have much lower equivalent widths than their optical counterparts. This is partly due to the physics of the transitions themselves (e.g. the Balmer, Paschen and Brackett series of hydrogen recombination lines), and partly due to the strong continua of AGN

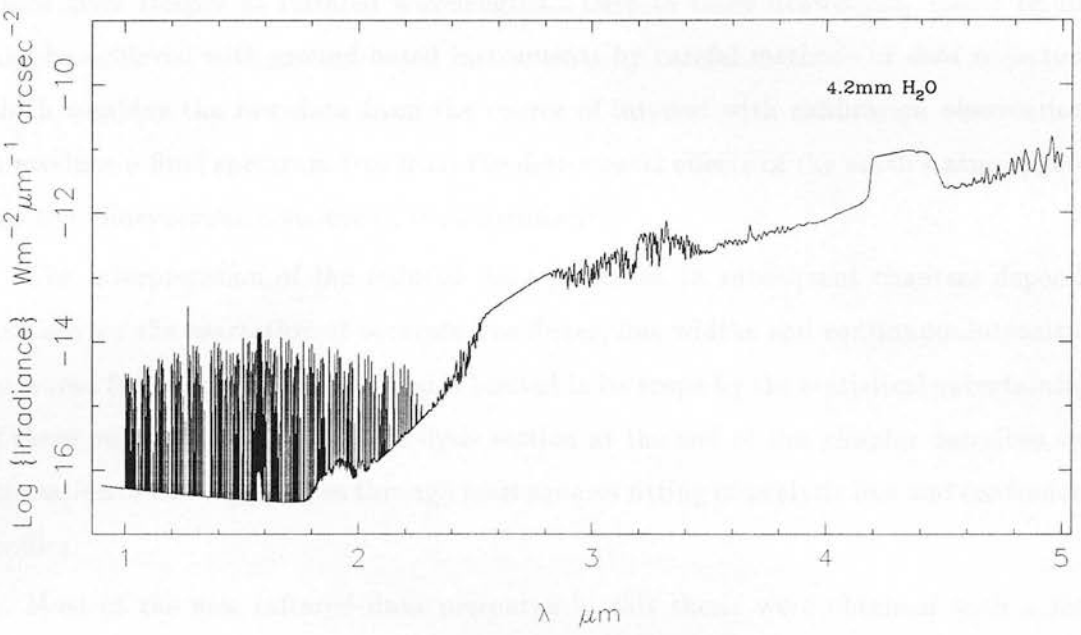

Figure 1: *The emission from sky and telescope at Mauna Kea, as seen by a focal plane instrument. The telescope is assumed to have an emissivity of 0.15 and a temperature of 275 K. To this emission has been added a model atmospheric emission spectrum for a zenith angle of 0 degrees and a water vapour column of 4.2mm, including emission from non-thermal OH airglow which produces the 'forest' of lines visible at the shorter wavelengths. These data have been kindly provided by Alistair Glasse.*

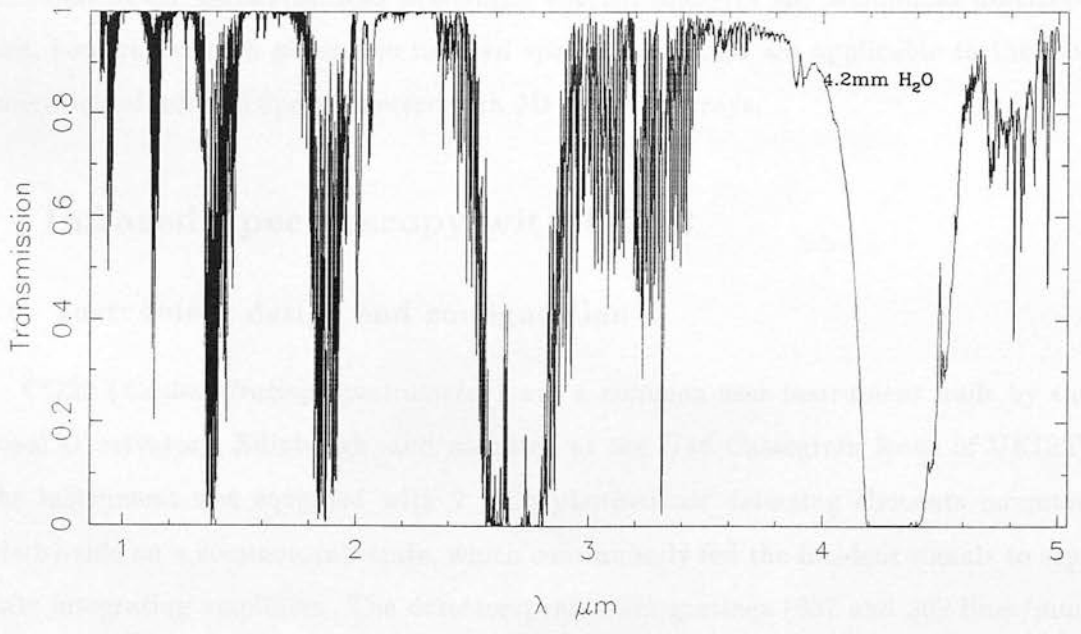

Figure 2: *Transmission of the atmosphere at Mauna Kea, modelled with the same parameters as the emission spectrum in Figure 1. It can be seen that emissivity and opacity of the atmosphere at the longer wavelengths (the "thermal infrared" are related through Kirchoff's law.*

which rises steeply at infrared wavelengths. Despite these drawbacks, useful results may be achieved with ground-based instruments by careful methods of *data reduction*, which combine the raw data from the source of interest with calibration observations to produce a final spectrum free from the detrimental effects of the earth's atmosphere, and the idiosyncratic response of the instrument.

The interpretation of the reduced data presented in subsequent chapters depends crucially on the extraction of accurate line fluxes, line widths and continuum intensities measured from infrared spectra, and is limited in its scope by the statistical uncertainties of these parameters. The data analysis section at the end of this chapter describes the estimation of these quantities through least squares fitting of analytic line and continuum profiles.

Most of the new infrared data presented in this thesis were obtained with a single instrument (CGS2) mounted on the 3.8-metre United Kingdom Infrared Telescope (*UKIRT*), which is situated at 4200 m above sea level on the summit of Mauna Kea, Hawaii. For this reason, and to aid the reader's understanding of the methods introduced later, a brief description of the instrument is given first. To serve as a concrete example of these techniques, we follow the stages in reduction and analysis of a K-window spectrum of the galaxy nucleus Markarian 463(E). Many of the techniques described here, however, remain general to infrared spectroscopy, and are applicable to the new generation of infrared spectrometers with 2D detector arrays.

2 Infrared Spectroscopy with CGS2

2.1 Instrument design and configuration

CGS2 (*Cooled Grating Spectrometer*) was a common-user instrument built by the Royal Observatory, Edinburgh, and mounted at the f/36 Cassegrain focus of UKIRT. The instrument was equipped with 7 InSb photovoltaic detecting elements mounted side-by-side on a common substrate, which continuously fed the incident signals to separate integrating amplifiers. The detectors, reflection gratings (637 and 302 lines/mm, mounted back-to back), broad-band filters and apertures were housed in a dewar cooled to 77K by solid and liquid nitrogen. The resolution of this Littrow-design spectrometer

was limited by the finite size of the detector elements (or rather the angle they subtended at the grating). The instrument and data acquisition system are described by Chapman *et al.* (1990), and references therein.

2.2 Exposure times and sky subtraction

Subtraction of the sky background was achieved by "chopping" the secondary mirror of the telescope to measure the sky emission at a small displacement (30–45 arcsec) from the source. At wavelengths less than 2.5 μm a chop cycle consisted typically of two 2-second exposure (one on source, one on sky) for observations of faint sources, or two 50-millisecond exposure for bright stars and planetary nebulae (which would otherwise saturate the detectors). At longer wavelengths the background thermal emission from sky and telescope was so intense (Figure 1) that the detector amplifiers would soon reach saturation, so a 2×50-millisecond exposure was used for all such observations. For reasons of efficiency, it was usual to perform 8–12 of these chop cycles at each grating position, and these were then averaged to yield the sky-subtracted signal for each detector at a wavelength determined by its position relative to the grating.

2.3 Stepping the grating

In order to fully sample the instrumental resolution of CGS 2 (i.e. the line profile generated by passing a monochromatic light through the instrument), and to cover a useful wavelength range it was necessary to step the grating through a number of positions to generate a "scan". For the data presented in this thesis the grating was stepped in increments of 7/3 detector spacings such that 3 measurements were made within the instrumental profile (i.e. a "sampling factor" of 3). The grating positions for the scan used to observe Markarian 463(E) are displayed in Figure 3. One important consequence later) of stepping the grating in this manner (as we shall see later) was that points at adjacent wavelengths in the scan were not produced by the same detector.

These spectral scans comprised the raw data to which the observer had access for subsequent reduction; sky subtraction and co-addition of source signal within individual chop cycles having been performed by the data acquisition software. To achieve a useful signal-to-noise ratio it was necessary to co-add a number of such scans.

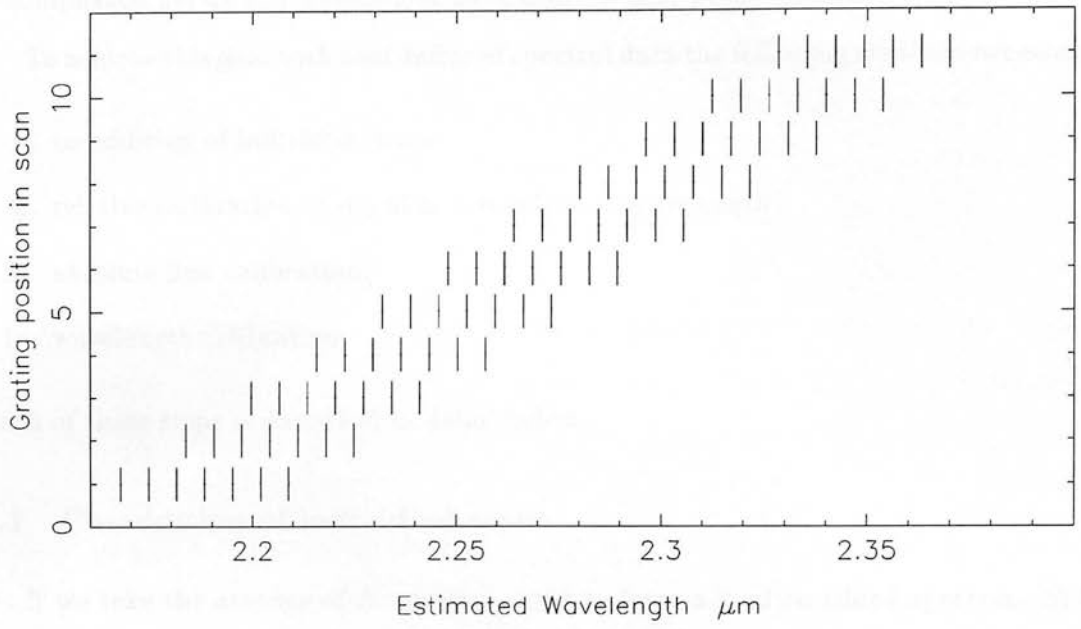

Figure 3: *Scan definition for the CGS2 spectrum of Markarian 463(E)discussed later in this chapter, showing the detector wavelengths as a function of grating position, which was stepped in increments of 7/3 detector spacings. It can be seen that a given detector contributes to every 7th point in the final spectrum, in the fully sampled region.*

2.4 A spectrum of Markarian 463(E)—an example

In subsequent sections we shall use as an example a K window spectrum of Markarian 463(E), taken on 1990 April 15 with CGS2. The 302 lines/mm grating was employed, giving a resolution of approximately 920 km s^{-1}. Unfortunately, two of the seven detectors were not working on this occasion and the output from them had to be discarded. The seeing was estimated to be $\lesssim$1.5 arcsec and the sky was clear throughout the observation. The eastern nucleus of Markarian 463 was centred in the 5 arcsec circular aperture by maximising the combined signal from all 5 working detectors. The secondary chop throw and exposure times were the "typical" values quoted above. A total of 29 scans were performed with these settings.

3 Data Reduction

One of the common aims of ground-based astronomers is to remove as far as possible the effects of atmosphere and observing apparatus from their data. This must be

accomplished before any meaningful data analysis may be attempted.

To achieve this goal with near-infrared spectral data the following steps are necessary:

i. co-addition of individual scans

ii. relative calibration of signal as a function of wavelength.

iii. absolute flux calibration.

iv. wavelength calibration

Each of these steps is described in detail below.

3.1 Co-addition of individual scans

If we take the average of N spectral scans to form a final co-added spectrum $S(\lambda)$ where:

$$S(\lambda) = \frac{\sum_{i=1}^{N} S_i(\lambda)}{N} \tag{2.1}$$

the error $\sigma(\lambda)$ on each point at wavelength λ will be given by

$$\sigma(\lambda) = \sqrt{\frac{\sum_{i=1}^{N} (S_i(\lambda) - S(\lambda))^2}{N(N-1)}} \tag{2.2}$$

As expected, the signal-to-noise on a typical spectral point is proportional to $\sqrt{N}$, or the square-root of the on-source exposure time.

A refinement to this simple co-addition is often necessary due to the different mean levels of scans as a result of guiding errors, seeing changes or "grey" (wavelength-independent) changes in atmospheric transmission between scans, as may be produced by cirrus clouds.[1]. To account for these variations each scan had to be normalized to the same mean level. Firstly, for each scan i the wavelength-averaged signal $\overline{S(i)}$ was calculated, from which the mean level $\overline{S}$ of *all* scans (i.e. the mean level of the final co-added spectrum) is determined. Individual scans were then normalized to this mean level (by multiplication of $\overline{S}/\overline{S_i}$) before co-addition. At this stage a few scans which were obviously affected by adverse conditions (usually resulting in a signal far below the mean) could be rejected, since the signal-to-noise of points in these scans was typically much worse than the others. The remaining scans, appropriately re-normalized,

[1]These clouds also scatter optical radiation in a wavelength-independent manner: they look white!

were averaged to produce the final spectrum $S(\lambda)$. By replacing $S_i(\lambda)$ in the equations above by $\overline{S}/\overline{S_i} \times S_i(\lambda)$ it can be seen from Equations 2.1 and 2.2 that the signal in the final spectrum remains unchanged, but the errors assigned to each point become more representative of the point-to-point deviations *within* this spectrum. The remaining uncertainty in the mean flux level $\overline{S}$ averaged over wavelength is calculated as part of the absolute flux calibration (see later).

Obviously, for very faint sources one should *not* attempt to re-scale the spectral scans in this manner, as some of the scans may have negative mean levels $\overline{S_i}$ as a result of the large random (additive) errors on individual points, which would in this case dominate any error in the (multiplicative) factor for the entire scan.

The co-added spectrum of Markarian 463(E) is shown in Figure 4, which is the average of 22 scans (7 scans were rejected as containing far too little signal due to guiding errors; the fraction of bad scans is not usually as high as this).

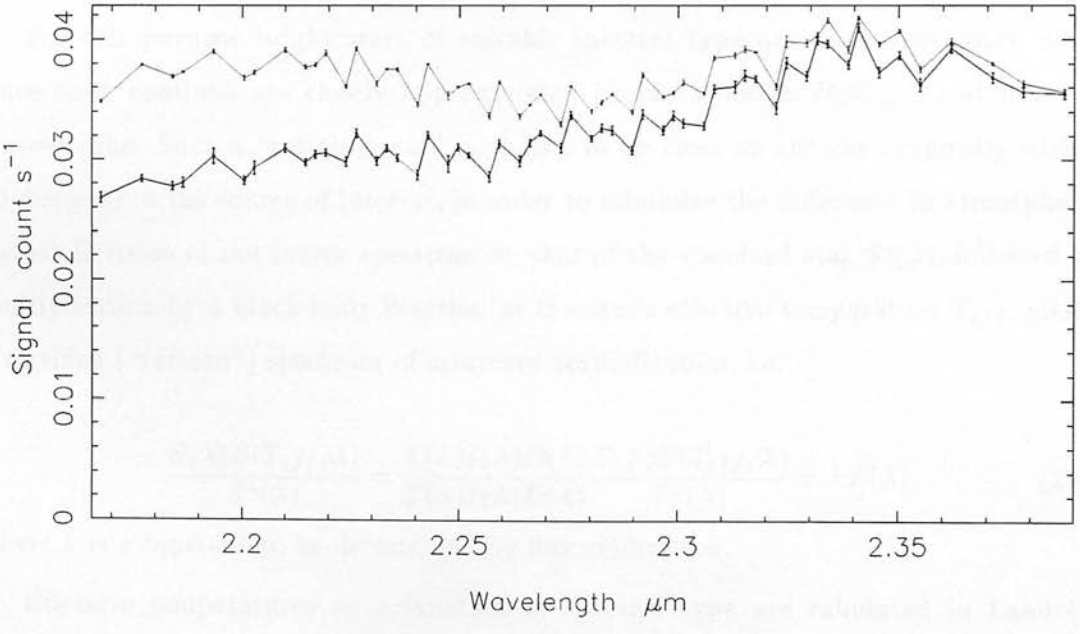

Figure 4: *Coadded raw spectrum of Markarian 463(E), shown together with a spectrum of the standard star BS5235 (thin line) taken with the same grating settings—this spectrum has been scaled to fit on the same plot. The spectral features are dominated by the individual responses of the detectors ($D(\lambda)$ in the notation introduced later), but the significantly redder continuum of the AGN relative to the star is readily apparent.*

3.2 Wavelength-dependent effects

The co-added spectrum produced by a ground-based infrared spectrometer is often radically different in form from the intrinsic spectrum of the source $F(\lambda)$ incident at the top of the earth's atmosphere. This is mainly due to the transmission of the atmosphere $T(\lambda)$, which is a strong function of wavelength (Figure 2), and to a lesser extent the (smoothly-varying) wavelength-dependent response of the instrument $I(\lambda)$. For reasons which will become apparent later, we also consider explicitly the variation of relative gains between detecting elements $D(\lambda)$, where each detector position in the final spectrum is labelled by its wavelength λ. These effects combine to distort the measured spectrum $S(\lambda)$ from its intrinsic spectral shape:

$$S(\lambda) = F(\lambda)T(\lambda)I(\lambda)D(\lambda) \tag{2.3}$$

Restoration of the intrinsic shape is achieved simply by observing an astronomical source of known spectrum along a similar path through the atmosphere.

For this purpose bright stars of suitable spectral type are most commonly used, since their continua are closely approximated by black-bodies $B(T_{eff}, \lambda)$ at infrared wavelengths. Such a "ratioing star" is chosen to be close on the sky (typically within 10 degrees) to the source of interest, in order to minimize the difference in atmospheric paths. Division of the source spectrum by that of the standard star $S^*(\lambda)$, followed by multiplication by a black-body function at the star's effective temperature T_{eff}, yields a rectified ("ratioed") spectrum of arbitrary normalization, i.e.

$$\frac{S(\lambda)B(T_{eff},\lambda)}{S^*(\lambda)} = \frac{T(\lambda)I(\lambda)D(\lambda)}{T(\lambda)I(\lambda)D(\lambda)}\frac{F(\lambda)B(T_{eff},\lambda)}{F^*(\lambda)} = kF(\lambda) \tag{2.4}$$

where k is a constant to be determined by flux calibration.

Effective temperatures as a function of spectral type are tabulated in Landölt-Bornstein (1982). Early type (A–F) stars selected from the Yale Bright Star catalogue (Hoffleit & Jaschek 1982) are often used as standard stars for extragalactic work, since (i) they are common and one can be found close in the sky to the source and (ii) their smooth black-body continua are punctuated only by Paschen and Brackett absorption lines of H^+. If these lines are in a relatively clear part of the atmospheric window (e.g. Brackett γ at 2.166 μm) one may interpolate across such absorption features in the

standard star spectrum before division.

The equivalent widths of the hydrogen absorption lines in cooler stars (spectral type later than type G3) are much smaller, and so these stars are useful as spectral standards where a redshifted feature of interest would coincide with a H^+ absorption line (such as H_2 v=1–0 S(1) 2.122 μm at $z \simeq 0.02$, coinciding with Brackett $\gamma\tilde{2}.166\,\mu$m). These stars however, display broad absorption bands of increasing strength with spectral type due to CO and H_2O molecules in their photospheres, together with narrow features due to ions of heavy elements (e.g. CaII). The choice of a particular spectral standard depends on how close any of these features might be to a (redshifted) wavelength of interest in the source spectrum. Those stars in luminosity classes III–V with intermediate spectral types (G3–G5) have the smoothest continua so provide a useful compromise if one of them can be found close in the sky to the source; in any case it is often desirable to use one late- and one early-type spectral standard to check for the presence of weak stellar features in their spectra. Representative stellar spectra in the K atmospheric window may be found in Kleinman & Hall (1986; high resolution) and Arnaud, Gilmore & Collier-Cameron (1989; low resolution). Unfortunately, no such compilations have been published yet for the J and H windows.

3.3 Wavelength calibration

This is usually the easiest part of the data reduction process, since wavelengths of points in a spectrum can be estimated from the grating equation and the optical configuration of the instrument. However a useful check is often required, and may be supplied by either a terrestial or an astronomical source. The former is usually an Argon discharge lamp, which provides a plethora of lines in the near-infrared spectral region, and whose light may be diverted into the instruments aperture. Alternatively, deep, narrow absorption features of known wavelength in the raw spectra of spectral standards, arising either in their photospheres (such as Brackett γ) or in our own atmosphere may be used. At wavelengths shorter than 2.3 μm, the spectrum of the sky background may be co-added separately to reveal large a host of of OH emission lines (see Figure 1), whose wavelengths are accurately known.

In many circumstances it is preferable to use a bright astronomical source of em

narrow (i.e. unresolved) lines, since (i) these pass through the entire optical system and (ii) they give information on the instrument's spectral Point Spread Function (PSF), which can be used for subsequent line profile fitting. Planetary nebulae are often used for this purpose; their high equivalent width, narrow lines of H^+ and He^+ are easily detectable.

For CGS2, which covers only a small range in wavelength, it was found that, to first order, only a small constant correction was necessary to calibrate the wavelength scale in this manner within a given atmospheric window. In fact, to be rigorous, the *vacuum* wavelengths of the planetary nebula lines were used to correct for the refractive index of air, which over the range 1–5 μm has the small and roughly constant value of 1.000274 (e.g. Allen 1973), or 82 km s^{-1}in velocity units. However, for the spectra presented in this thesis we have not taken the trouble to correct for the earth's orbital motion of $\simeq$30 km s^{-1} relative to the Solar System barycentre.

For our example spectrum of Markarian 463(E), which already has an estimated wavelength scale obtained from the grating equation, the final wavelength calibration was provided by the observation of the PN NGC6210 shown in Figure 5. The signal is

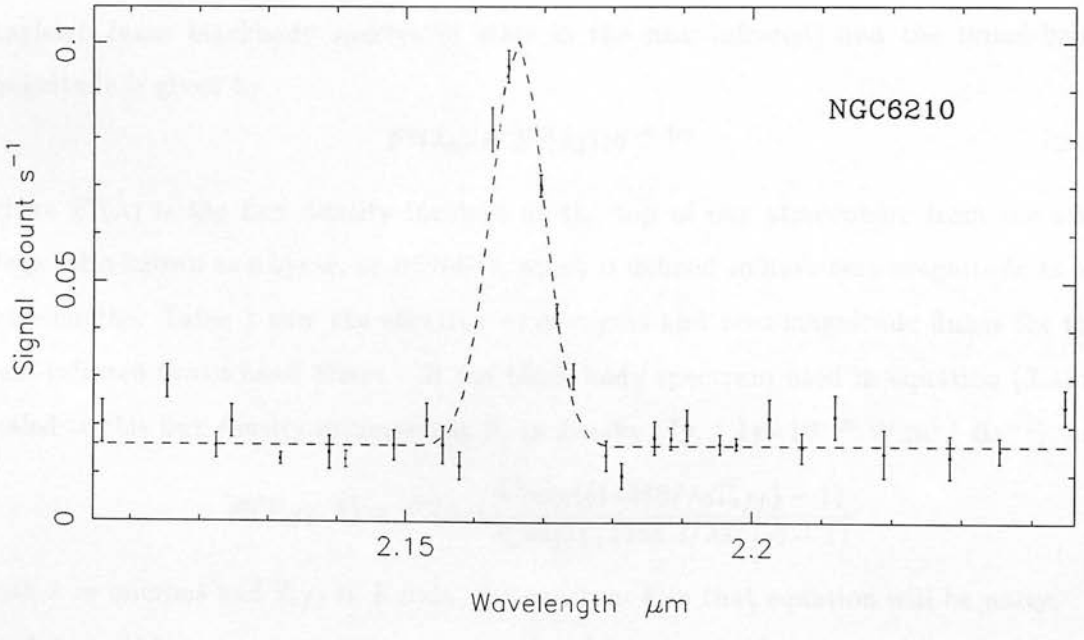

Figure 5: *Spectrum of the Brackett γ line in the planetary nebula NGC6210, which has been smoothed with a Gaussian function of FWHM=0.0035 μm. Also shown (solid line) is the fit of a Gaussian profile plus a linear continuum to these data*

strong, and the wavelength-dependent effects are negligible over this wavelength range, so the spectrum has not been ratioed. The spectrum has been smoothed for reasons described later, and the central wavelength determined from a Gaussian fit to the line profile. For this particular case the fit suggested a shift of $0.0032\,\mu$m, which has been applied to the data shown in the Figure, and a smoothed instrumental response of FWHM=$0.009\,\mu$m.

Since the planetary nebula is an extended source of line radiation, this estimate of the FWHM is likely to be an slightly higher than that applicable to a point source (such as an AGN). For the case of CGS2 it was found that the FWHM of the line decreased only slightly (by $\sim$10%) when a smaller (2.5 arcsec) entrance aperture was used to observe an extended source.

3.4 Flux calibration

The methods described above produce a spectrum of the correct intrinsic shape, but so far the normalization is arbitrary. To provide the flux calibration, the broad-band magnitude of the standard star is used. The conversion between flux density at the effective wavelength of the broad-band filter (assumed constant due to the similar Rayleigh-Jeans blackbody spectra of stars in the near-infrared) and the broad-band magnitude is given by

$$F^*(\lambda_0) = F^0(\lambda_0)10^{-0.4m} \tag{2.5}$$

where $F^0(\lambda)$ is the flux density incident at the top of our atmosphere from the star Vega (also known as αLyrae, or BS7001), which is defined to have zero magnitude at all wavelengths. Table 1 lists the effective wavelengths and zero-magnitude fluxes for the near-infrared broad-band filters. If the black-body spectrum used in equation (2.4) is scaled to this flux density expressed as F_ν in Jansky (Jy, 1 Jy=10^{-26} W m^{-2} Hz^{-1}), i.e.

$$B(T_{eff},\lambda) = F^*(\lambda_0)\frac{\lambda^3 \exp((14388/\lambda_0 T_{eff}) - 1)}{\lambda_0^3 \exp((14388.3/\lambda T_{eff}) - 1)}$$

with λ in microns and T_{eff} in Kelvin, the constant k in that equation will be unity.

Infrared photometry of bright stars is plentiful in the literature, and the compilation of Gezari, Schmitz & Mead (1987) is useful in this respect. Where photometry does not exist for a given spectral standard, the appropriate broad-band magnitude may be

Table 1: *Effective wavelengths, zero magnitude fluxes and extinction coefficients*

Band	λ_0 (μm)	F^{0} [a] (Jansky)	Extinction [b] (mag/airmass)
J	1.20	1640	0.10
H	1.64	1030	0.05
K	2.19	650	0.07
L'	3.80	250	0.09
M	4.80	170	0.15

References: [a] *Allen & Cragg (1983);* [b] *Kriscunias* et al.*(1987).*

derived from observing stars of known magnitudes on the same night. In principle, the correction for differential atmospheric extinction could be derived from multiple observations of flux standards at different zenith angles, but in practice the average extinction coefficients were mostly used. These values are also tabulated in Table 1).

The spectral standard BS5235 (G5II), has a catalogued K magnitude of 1.37 mag, and from Landölt-Bornstein (1982) we find T_{eff}=5920 for this spectral type. Figure 6 shows the ratioed, calibrated spectrum of Markarian 463(E), which has been subsequently converted to F_λ to de-emphasize the steeply-rising continuum.

3.5 Residual instrumental effects: CGS2

Although the sensitivity of the individual detectors of CGS2 varies smoothly with wavelength throughout the near-infrared, their responses *relative* to each other may differ slightly. This causes a distinctive "ripple" (of period 7 points) on the raw (unratioed) spectrum. Ideally this effect will be removed along with all the other wavelength-dependent effects by division with the ratio-ing star, but in practice a residual fixed pattern noise was seen in many of the reduced spectra, especially in conditions of good seeing. The problem arises from the different "light footprints" of the star and the galaxy on the detector surface in the *spatial* direction (i.e. perpendicular to the dispersion). The radiation from a star—a point source spread by the seeing—falls only on the central part of the detector. On the other hand, the continuum light from a galaxy is often more extended intrinsically, in addition to the larger tracking and guiding errors at the longer exposures used. Therefore the signal from a galaxy is spread more-or-less evenly over a whole detector. Since the response across a detector is variable, the division of the

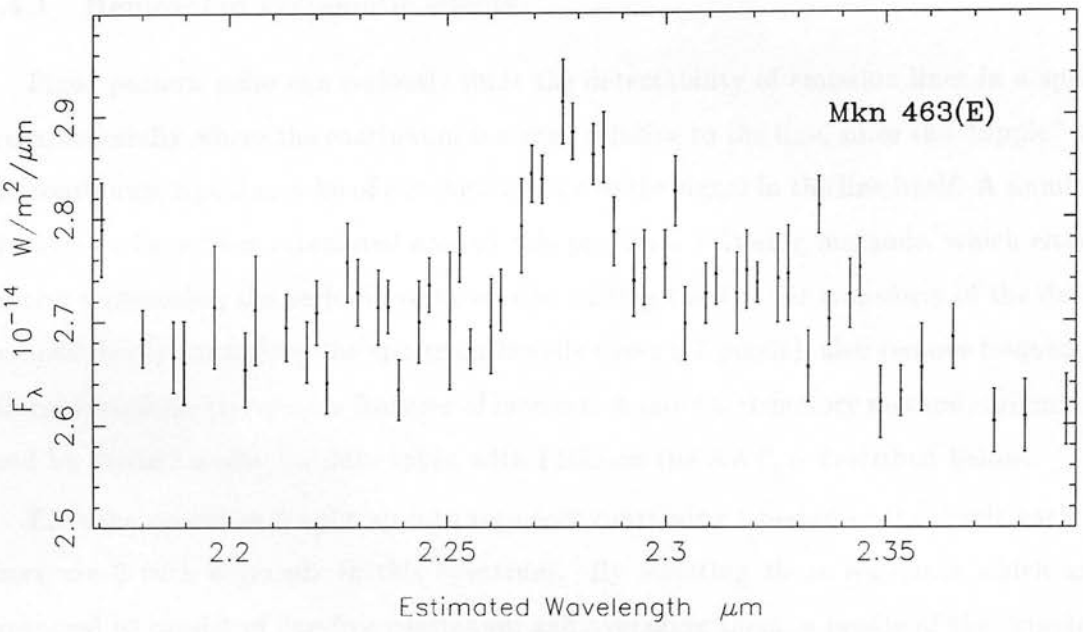

Figure 6: *Flux- and wavelength-calibrated spectrum of Markarian 463(E). The residual effects of the detectors' differential responses are visible as a "ripple" over the fully-sampled range of the spectrum.*

galaxy signal (weighted by the whole detector) by the star signal (weighted only by the central part) results in imperfect cancellation (i.e. the terms $D(\lambda)$ in the numerator and denominator of Equation (2.4) are no longer identical, which results in a fixed pattern noise "ripple" with a period of 7 detectors arising naturally from the interleaving of detector positions in a grating scan. (In our "typical" example spectrum shown in Figure 6, the period is 5 points since two detectors were not functioning).

A similar ripple effect can also occur when the seeing is poor! This arises from fluctuations in the signal reaching all the detectors at each grating position, since light is lost outside the 5 arcsec aperture of the instrument. In this case, the period of the fixed pattern noise is equal to the distance between points measured by the same detector (i.e. equal to the sampling factor). Since the sampling factor is usually 3 or 4, this is the period of the resulting pattern noise.

Fortunately the two cases described above are mutually exclusive, since poor seeing conditions cause the signal to be spread across the detectors more-or-less evenly. Otherwise if both effects were present the period of the pattern noise would be $4\times7=28$—often a large fraction of the entire spectrum.

3.5.1 Removal of systematic effects

Fixed pattern noise can seriously limit the detectability of emission lines in a spectrum, especially where the continuum is strong relative to the line, since the "ripple" on the continuum signal may be of comparable size to the signal in the line itself. A number of methods have been attempted around this problem. Filtering methods, which either involve suppressing the periodic variations by editing the Fourier transform of the data, or equivalently smoothing the spectrum heavily (over $\simeq$7 pixels), also remove frequency information from the spectra features of interest. A more satisfactory method, originally used by Jeremy Bailey for data taken with FIGS on the AAT, is described below.

First the spectrum is split up into segments containing 1 period of the ripple each—there are 8 such segments in this spectrum. By selecting those segments which are presumed to consist of line-free continuum and averaging them, a profile of the "ripple" may be built up. Repeating this pattern (normalized to a mean level of unity) across the fully-sampled range of the spectrum allows us to divide the source spectrum by this ripple, hence removing the systematic effect from the spectrum. Inspection of the result of this procedure (Figure 7) reveals a flatter continuum level and a more realistic line profile. The Fourier transform of the data (not shown) also contains less power at high sampling frequencies, where we would expect the signal transform to fall off rapidly due to the spectrometer's resolution.

While this procedure may appear successful, one must be careful not to apply it too wantonly. Since the ripple profile is determined *from the data* it reduces the number of independent variables in any subsequent fitting by (in this case) 7.

3.5.2 Removal of high frequency noise

Even where there is no obvious fixed pattern noise in a spectrum, random point-to-point variations can contribute significantly to the noise. Since a typical spectrum is sampled every 1/3 or 1/4 resolution element, fluctuations over intervals of less than 2 or 3 points (i.e. above the Nyquist sampling frequency) are unlikely to be real. By taking the Fourier transform of the data and applying an *optimal filter* high frequency components may be suppressed with little degradation of the original signal. (See Press 1989 for a clear exposition of these techniques). Equivalently, the data may be "smoothed"

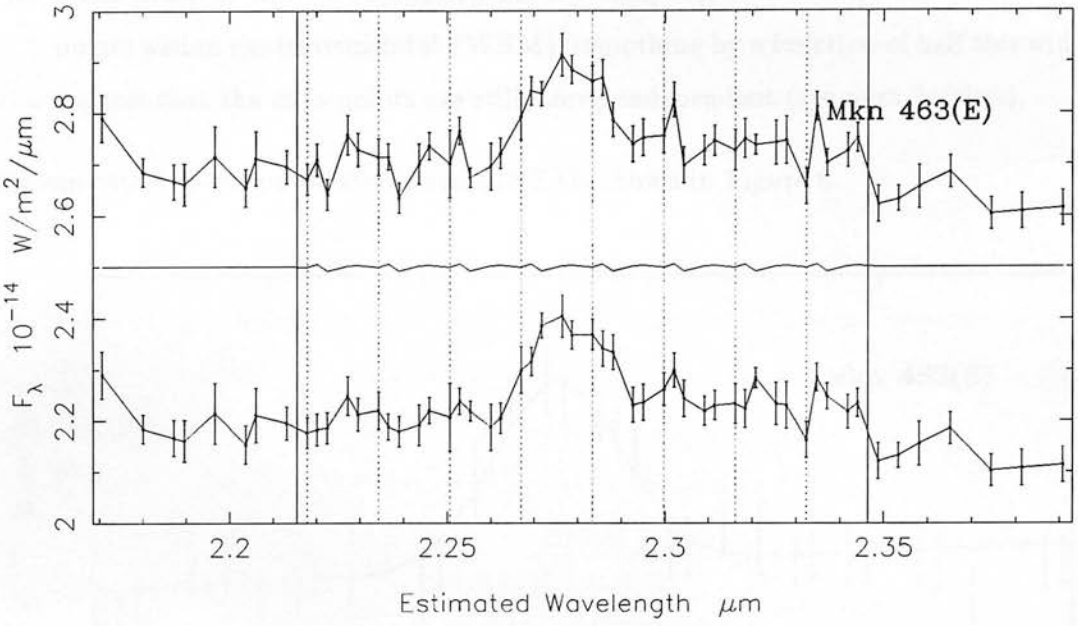

Figure 7: *Removal of periodic noise from the calibrated spectrum shown in Figure 6 (here reproduced at top). The fully-sampled portion of the spectrum has been divided into 8 segments; the line-free segments were averaged to produce the ripple profile (solid line). Division of the upper spectrum by this profile produced the lower, corrected spectrum.*

(convolved) with the Fourier transform of this filter.

The filter used in practice was a Gaussian function of Maximum (FWHM) equal to 1/2 the instrumental resolution. This was for a number of reasons–partly scientific, and partly a matter of convenience.

i. The Gaussian function falls of rapidly at abscissae greater than $\simeq 2\times$FWHM, enabling its easy application to the data set in real space. Similarly, in reciprocal space it passes low frequency components of the data but strongly suppresses frequencies above the Nyquist value.

ii. Since the Gaussian function is its own Fourier transform, successive smoothings by Gaussians of FWHM$=\Delta_i$ is equivalent to smoothing the data by a single Gaussian of FWHM$^2=\Sigma_i\Delta_i{}^2$.

iii. Smoothing by a Gaussian makes the Point Spread Function of the instrumental resolution slightly "more" Gaussian in shape. (The un-smoothed PSF of CGS2 is slightly more flat-topped than a Gaussian). Since the line parameters are found by fitting Gaussian profiles (Section 4), this is obviously desirable.

iv. Since most of the CGS2 spectra have a sampling factor of 3 or 4 (i.e. 3 or 4 points within the instrumental FWHM), smoothing by a function of half this width ensures that the data points are still *nearly* independent (see next Section).

The smoothed spectrum of Markarian 463(E) is shown in Figure 8.

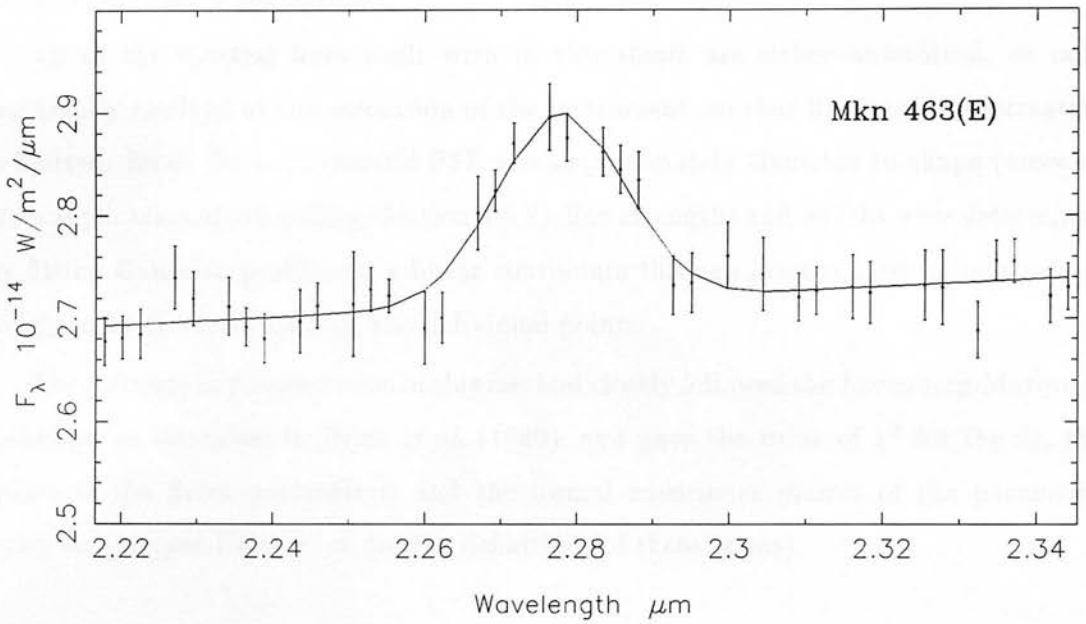

Figure 8: *Final spectrum of Markarian 463(E), which was produced from by smoothing the corrected spectrum shown in Figure 7. The solid line shows the best-fit Gaussian profile*

.

4 Data Analysis

4.1 Estimation of parameters by least squares minimization

From a spectrum consisting of many individual measurements we typically require only a handful of numbers for input into physical models. It is because the data over-determine the physical quantities in this manner that we may use maximum likelihood techniques to estimate them, and their probable uncertainties. To a good approximation, most of the spectra dealt with in this thesis consist of "lines" resulting from ionic and molecular transitions superposed on a smooth and slowly-varying "continuum".

In reality, a *stellar* continuum in the near-infrared, as in the optical, contains a

host of weak absorption features. Apart from the strong features of CO and H_2O most of them are well below the noise level of the spectra presented here, and so are not discussed further. However, the availability of more sensitive detectors in the future and the motivation to study *weak* active nuclei which do *not* dominate the stellar continua of their host galaxies will force workers in this field to take such features into account, as must be done in the optical.

All of the spectral lines dealt with in this thesis are either unresolved, or only marginally resolved at the resolution of the instrument, so that line profile information is limited. Since the instrumental PSF was approximately Gaussian in shape (more so after application of smoothing–Section 3.5.2), line strengths and widths were determined by fitting Gaussian profiles on a linear continuum through least squares minimization, weighted by the error bars on the individual points.

The software implementation of this method closely followed the Levenberg-Marquart technique as described in Press *et al.* (1989), and gave the value of χ^2 for the fit, the values of the fitted parameters, and the formal *covariance matrix* of the parameter uncertainties (see Press *et al.* for the definitions of these terms).

4.2 Independence of the data points

In order to interpret the results of a least-squares fit correctly, it is obviously necessary that the data points be *independent* measurements which, together, constrain the model. The number of independent points minus the number of fitted parameters is known as the number of *degrees of freedom* ν of the fit, and for normally-distributed data the probability of χ^2 is tabulated for different values of ν.

When the data is smoothed or re-binned a complication arises, since the errors on data points are no longer independent. We may, however, still use least squares minimization to estimate the line parameters, but the distribution of χ^2 is no longer known. Monte-Carlo simulations are the only rigorous way of establishing confidence intervals, but a simple rule-of-thumb, which can at least be partially justified, was used here. Consider a measurement of a constant continuum level, comprising N_x points each with error $\sigma(\lambda)$. Smoothing this by a Gaussian will reduce the apparent size of the error bars, and hence the magnitude of the error on the fitted continuum

level. For a Gaussian of FWHM$\simeq$2 points this reduction factor is about 1.3. Assuming that other parameters in the same spectrum (describing a line profile, for instance) are also approximately linear in the region of best fit, we may multiply our formal errors by this factor. For the record, the fit of a Gaussian to our final spectrum of Markarian 463(E) yielded a flux of $3.9\pm0.5\times10^{-17}$ W m^{-2}, with an intrinsic (resolution-corrected) FWHM=$0.017\pm0.002\,\mu$m, or $\simeq$2250 km s^{-1}. The new data presented in Chapter 5 reveal the more complex situation which we have modelled simply here.

4.3 Confidence intervals in more than 1 parameter

The parameters describing a line in a spectrum (flux, central wavelength, FWHM velocity) are related to each other through the data. For example, positive errors in the line width tend to include more flux under the line profile, resulting in an overestimate of the line flux. Similarly, an estimated continuum level below the "real" value will cause us to over-estimate both the line width *and* flux.[2] For normally-distributed errors, contours of constant χ^2 describe boundaries of *confidence regions* in parameter space (see Press *et al.* 1989). For small deviations from the minimum value, this boundary can be approximated by an ellipse, with an equation given by the coefficients of the covariance matrix, but for larger deviations from χ^2 with a non-linear model the boundary, or its projection onto a smaller number of parameters, has to be evaluated explicitly. An extreme example of this is shown in Figure 9. The data and the model are taken from Chapter 5, Figure 3. In the Figure we show the boundaries of constant χ^2 enclosing regions of different confidence levels for two parameters of interest— the [SiVI] line width, and its flux. All the other parameters in the fit were left free in this evaluation of χ^2. As might be expected, the fitted flux in the line increases if the line width is held fixed at increasing values, and *vice versa*. The curious *finite* flux at zero line width merely reflects the instrumental resolution of CGS2, and corresponds to an unresolved line, which is just consistent with the data at the 99% contour. However, from the Figure it can be seen that the line width is greater than than 550 km s^{-1}(the width of the Balmer and Paschen lines in Cygnus A) at the 95% confidence level, hence the claim in Chapter 5 that the [SiVI] line in Cygnus A is "probably" broad (since the apparent

[2] "Where do I draw the continuum?" is the Fundamental Question of astronomical spectroscopy.

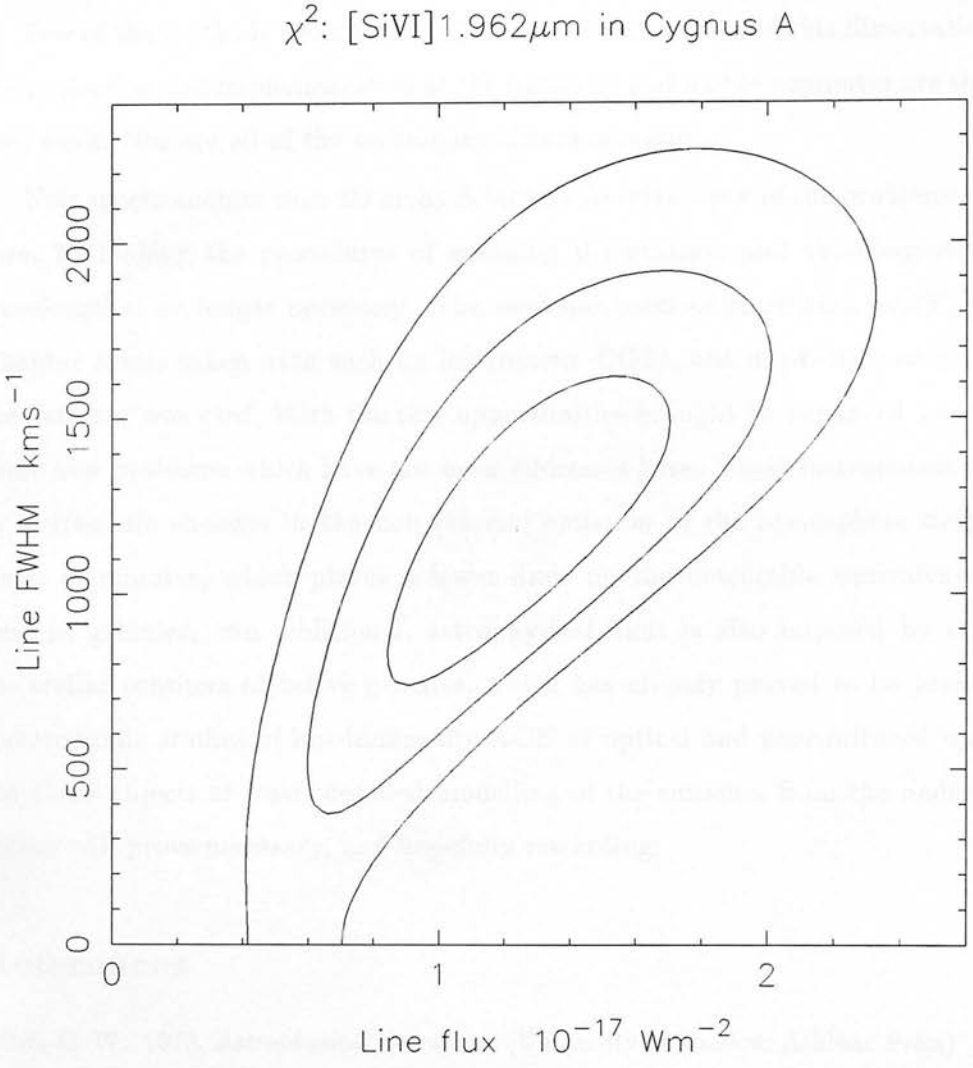

Figure 9*: Joint confidence regions for the flux and width of the [SiVI]1.962μm line in Cygnus A, as determined from the spectrum shown in Figure 2 of Chapter 4. The coordinates of the minimum point (χ^2=40.28 for 48 degrees of freedom) correspond to the values given in Table 2 of that chapter. Contours are shown at the 68%, 90%, 95% and 99.7% confidence boundaries. A finite flux of "zero" width corresponds to an unresolved [SiVI] line, which falls within the 99% confidence interval*

.

width may still be largely the result of systematic changes in atmospheric transmission).

5 Conclusions

Few of the methods described in this chapter are original to this dissertation, though their selection and implementation at the telescope and on the computer are the author's own work. Nor are all of the techniques always necessary.

New spectrometers with 2D array detectors do solve a few of the problems confronted here, by making the procedures of scanning the grating, and sky-chopping (at short wavelengths) no longer necessary. The new spectrum of Markarian 463(E) utilized in Chapter 5 was taken with such an instrument–CGS4, but in practice only one row of the detector was used, With the new opportunities brought by enhanced sensitivity will come new problems which have not been addresses here. These instruments are limited by systematic changes in the non-thermal emission of the atmosphere over exposure times of minutes, which places a lower limit on the detectable equivalent widths of lines in galaxies. An additional, astrophysical limit is also imposed by structure in the stellar continua of active galaxies, which has already proved to be problematic in spectroscopic studies of low-luminosity AGN at optical and near-infrared wavelengths. For these objects at least, detailed modelling of the emission from the underlying host galaxy will prove necessary, and hopefully rewarding.

References

Allen, C. W., 1973. *Astrophysical Quantities* (University of London: Athlone Press)

Allen, D. A. & Cragg, T., 1983. *Mon. Not. R. astr. Soc.*, **203**, 777.

Arnaud, K. A., Gilmore, G. & Collier Cameron, A., 1989. *Mon. Not. R. astr. Soc.*, **237**, 495.

Chapman, R., Beard, S. M., Mountain, M., Pettie, D., Pickup, D. & Wade, R., 1990. in *Astronomical Telescopes and Instrumentation for the 21st Century*, SPIE **1235**, 25.

Gezari, D. Y., Schmitz, M. & Mead, J., 1987. *Catalog of Infrared Observations, Part I—Data*, NASA RP–1196.

Hoffleit, D. & Jaschek, C., 1982. *The Bright Star Catalogue* (Yale University Observatory).

Kleinman, S. G. & Hall, D. N. B., 1986. *Astrophys. J. Suppl. Ser.*, **62**, 501.

Kriscunias, K. *et al.*, 1987. *Publs astr. Soc. Pacific*, **99**, 887.

Landölt-Bornstein, 1982.

Press, W. H., Flannery, B. P., Teukolsky, S. A. & Vetterling, W. T., 1986. *Numerical Recipes* (Cambridge University Press).

Chapter 3

Broad infrared line emission from the nuclei of X-ray-selected Seyfert 2 galaxies

Prologue: In the 1970s and '80s space-borne observatories revealed that Seyfert 1 galaxies and quasars are strong sources of X-rays. However, the distinction between the optical classifications Seyfert type 1 and type 2 appeared to apply at these energies; Seyfert 1s were generally strong X-ray emitters, Seyfert 2s were not, apart from a handful of intermediate objects which became known as Narrow Line X-ray Galaxies. In the current "unified model" of Seyfert galaxies, these objects form part of a continuous sequence of Seyfert types with increasing line-of-sight extinction. In order to test this hypothesis we observed the Paschen β infrared recombination line to search for broad wings from an (optically-obscured) BLR, and thereby examine any intrinsic differences between these and Seyfert 1 AGNs. This research was carried out in collaboration with Martin Ward and Gillian Wright, and has been published in *Monthly Notices of the Royal Astronomical Society* (Blanco, Ward & Wright 1990).

Summary

We report spectroscopic observations at a resolution of $\lambda/\delta\lambda \simeq 300$ of the Paschen β hydrogen recombination line in the Narrow-line X-ray Galaxies NGC5506 and A0945-30 (=MCG-5-23-16), and in the Seyfert 2 galaxy NGC4388. The line profiles of NGC5506 and A0945-30 are both found to possess broad components of FWHM>1500 km s^{-1}; this removes the previous controversy concerning the presence of broad line components in their Hα line profiles. We use optical, X-ray and mid-infrared data to estimate the extinction towards the line and continuum sources in these objects in order to test the hypothesis that they are in fact moderately obscured Seyfert 1 nuclei.

Our non-detection of a broad Paschen β line profile in NGC4388 is consistent with a scattered (as opposed to a transmitted) origin for the observed off-nuclear broad Hα emission, in agreement with models of the optical emission line geometry in this galaxy.

1 Introduction

There is increasing evidence that the diversity of spectral shapes of Seyfert Active Galactic Nuclei (AGN) from infrared to X-ray frequencies is due at least in part to the effects of obscuring material along the line of sight (Lawrence & Elvis 1982, Ward *et al.* 1987). In particular, observations at X-ray energies have revealed that a subset of those AGN which have narrow lines of hydrogen and helium in their optical spectra (and are hence classified as Seyfert 2s, Weedman 1977) emit hard X-rays at luminosities characteristic of Seyfert 1 nuclei. This is despite the fact that at lower X-ray energies, Seyfert 2s are roughly one hundred times less luminous than Seyfert 1s (Kriss, Canizares & Ricker 1980). A step towards understanding these so-called *Narrow Line X-ray Galaxies* resulted from a study of the archetypal Seyfert 2 galaxy NGC1068 by Antonucci & Miller (1985). Using spectropolarimetry they discovered a polarized (scattered) broad line component to the optical permitted lines, which implies that the true Seyfert 1 nucleus is hidden by a very large column of obscuring material. The amount of dust and gas is so great (eg. A_V>100 mag, Depoy 1987), that even the hard X-rays are extinguished.

It has been suggested that the nuclei of many Seyfert 2 galaxies harbour a Broad Line Region (*BLR*), which together with the powerful Seyfert 1 ionizing continuum source is hidden from direct view by intervening gas and dust; the much larger Narrow Line Region (*NLR*) would then extend beyond this 'blocking' material (eg. Krolik & Begelman 1986). The geometry of this obscuring matter is, however, not well known. If it is in the form of a simple torus, then the column of material intercepted by our line of sight will depend on its inclination. An alternative possibility is that the active nucleus is completely enshrouded by dust (i.e. a covering factor of unity). However, this seems unlikely in those AGN where there is strong narrow line emission from HeII, [FeVII] and [NeV], which requires a hard, unreddened ultraviolet continuum for excitation. Since the spectra of Seyfert 2 nuclei often display lines of such high excitation species (Koski 1978), the detection of heavily reddened BLRs in them provides a test for models involving collimation of the ionizing continuum. This may be produced either by intrinsic physical processes, or simply by angle-dependent absorption ('shadowing') of the continuum source.

The extinction along our line of sight to the BLR in a Seyfert nucleus will of course be a variable parameter from object to object. This is supported by the existence of an intermediate class of Seyfert galaxy—Seyfert 1.9 (Osterbrock 1981). The optical spectra of these AGN display weak broad wings on the Hα line, whereas this component is almost undetectable at shorter wavelengths due to the differential extinction of dust grains. The extinction towards the BLRs in these galaxies must be $A_V \lesssim 5$ mag for the broad Hα line components to be visible at all. This leads us to expect that there may be many AGN in which the BLR is obscured in the visible by more than this (resulting in their classification as Seyfert 2s), but which emit broad line radiation directly observable in the near-infrared (1–4 μm), where the extinction due to intervening dust is much less.

We report here observations of the 1.282 μm Paschen β line in three Seyfert 2 galaxies. The extinction due to dust at this wavelength is related to that in the optical by $A_{1.28\mu m} \simeq 0.3 A_V$, i.e. the line is attenuated only by a factor of 4 for a visual extinction of 5 mag. The achievable limit in practice for detecting broad lines depends of course on the signal-to-noise ratio of the spectrum and the equivalent widths of the broad and narrow line components.

2 Observations and reduction

The spectra presented in Figure 1 were taken at the United Kingdom Infrared Telescope (UKIRT) in 1989 February with the cooled grating spectrometer CGS2, using a 637 lines/mm grating in first order and a circular aperture 5.0 arcsec in diameter. The resolution of the instrument is fixed by the finite size of the detector elements. The aperture was centred on the optical nuclei of NGC5506 and A0945-30, and a position 3 arcsec N, 4 arcsec E of the optical nucleus of NGC4388 for reasons described later (Section 3.1). The grating was stepped successively so that adjacent points in the spectrum were spaced by one quarter of a detector width. Standard chopping and beamswitching procedures were followed to subtract the background emission, and atmospheric absorption features were removed by dividing each galaxy spectrum by that of a late type star close in the sky. Although conditions were not photometric, on both nights the cancellation of telluric absorption features was excellent (remaining features are at less than 3 per cent of the continuum level). An approximate flux calibration of 15–20 per cent

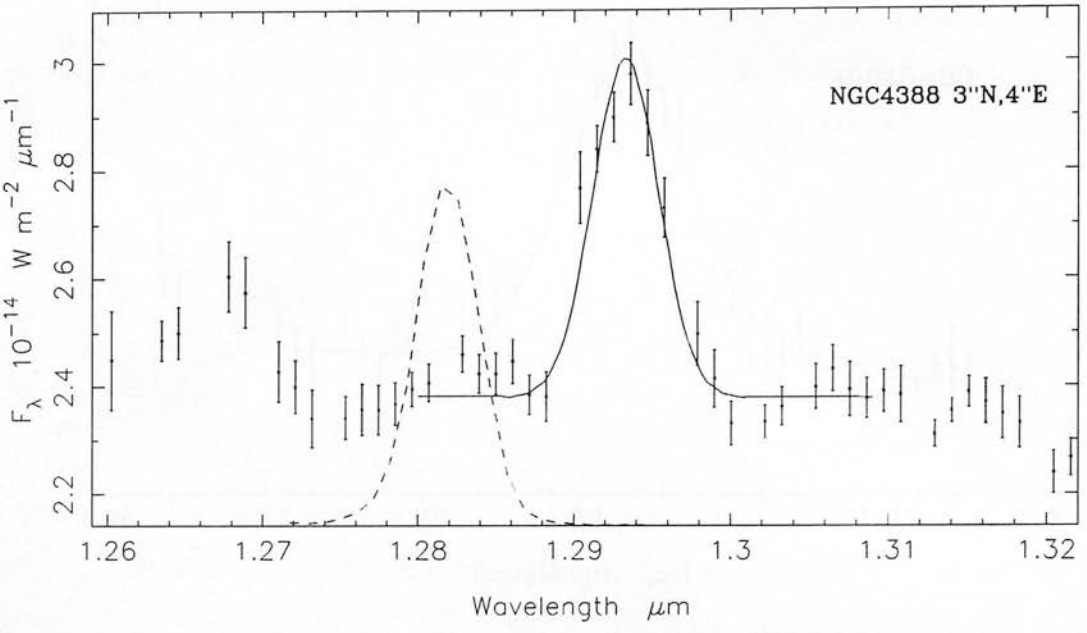

Figure 1: *Near-infrared spectrum of the Seyfert 2 galaxy NGC4388 (at a position 3 arcsec N, 4 arcsec E of the optical nucleus). The spectrum has been smoothed with a Gaussian of FWHM equal to half of that of the instrumental profile. Also shown for each spectrum is the model fit to the Paschen β profile (solid line), and the smoothed instrumental resolution (broken line) which was derived from spectra of planetary nebulae, and which has a FWHM of 1100 km s^{-1}.*

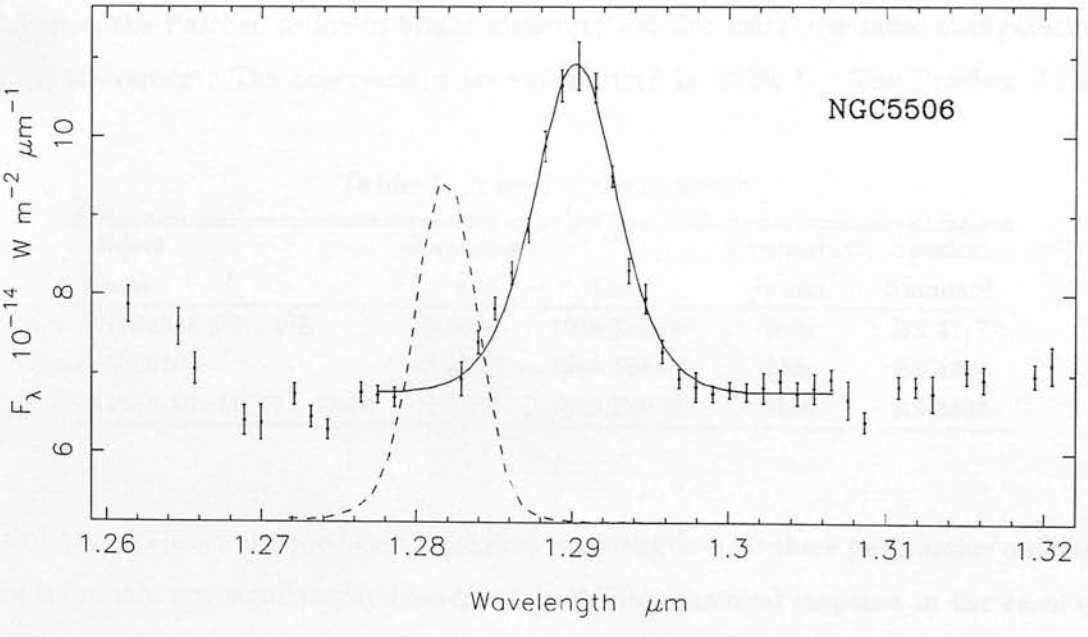

Figure 2: *Near-infrared spectrum of the nucleus of NGC5506. Details as for Figure 1.*

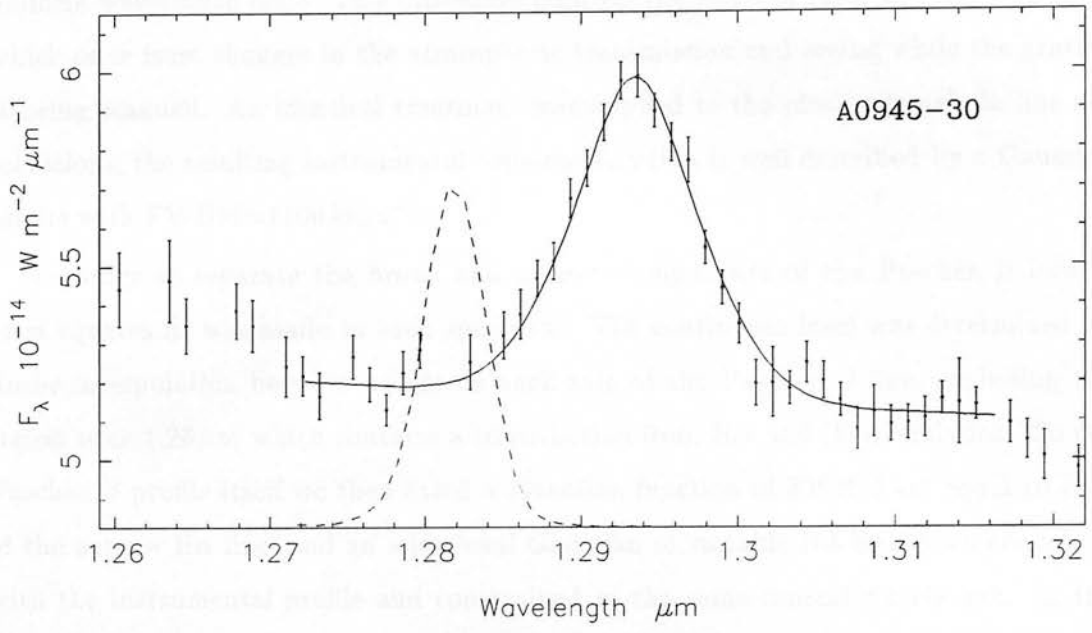

Figure 3: *Near-infrared spectrum of the nucleus of A0945-30=MCG-5-23-16. Details as for Figure 1.*

accuracy was obtained by observing standard stars at similar airmasses. For NGC5506 the flux calibration is accurate to within 10%, because we were able to calibrate the peak line flux from an earlier, lower signal-to-noise spectrum taken in photometric conditions. Wavelength calibration and determination of the instrumental profile were performed by observing the Paschen β line in bright planetary nebulae using the same configuration of the instrument. The observations are summarized in Table 1. The Paschen β line

Table 1: *Journal of Observations*

Object Name	Recession z	UT Date	Integration /point	Spectral Standard
NGC4388 3″N, 4″E	0.0084	1989 Feb 25	140s	BS 4777
NGC5506	0.0059	1989 Feb 26	220s	BS 5384
A0945-30=MCG-5-23-16	0.0086	1989 Feb 26	310s	BS 3833

was detected close to its predicted redshifted wavelength in all three programme objects, and its profile was significantly broader than the instrumental response in the cases of NGC5506 and A0945-30. The divided spectra were smoothed with a Gaussian function of FWHM=0.00215 μm (equal to one half of a detector width), and then re-binned onto a

uniform wavelength scale. This procedure removes the worst of pixel-to-pixel variations which arise from changes in the atmospheric transmission and seeing while the grating is being scanned. An identical treatment was applied to the planetary nebula line observations; the resulting instrumental response function is well described by a Gaussian profile with FWHM=1100 km s^{-1}.

In order to separate the broad and narrow components of the Paschen β lines a least squares fit was made to each spectrum. The continuum level was determined by linear interpolation between points on each side of the Paschen β line, excluding the region near 1.26 μm which contains a contribution from HeI and [FeII] emission. To the Paschen β profile itself we then fitted a Gaussian function of FWHM set equal to that of the narrow Hα line, and an additional Gaussian of variable FWHM, both convolved with the instrumental profile and constrained to the same central wavelength. In the case of NGC4388 the inclusion of a Gaussian profile broader than the narrow line width did not improve the fit significantly. The results of the fitting procedure for each object are presented in Table 2.

Table 2: *Fitted Paschen β line widths and fluxes*

	Narrow Line		Broad Line		Continuum
Object	FWHM	Flux	FWHM	Flux	F_λ (1.29 μm)
NGC4388	230 [a]	3.3±0.2	2000 [a]	<1.5 (3σ)	2.4 (15%)
NGC5506	370 [b]	11±3	1550±300	18±3	6.8 (10%)
A0945-30	270 [c]	<2.5 (3σ)	2150±250	7.5±0.7	5.2 (20%)

Notes:

1. Line fluxes are in units of 10^{-17} W m^{-2}; line widths (corrected for the instrumental profile) are in km s^{-1}. The errors given for these are the formal 1σ uncertainties obtained from the fitting procedure.

2. The continuum flux densities at 1.29 μm are given in units of 10^{-14} W m^{-2} μm^{-1}. The quoted percentage errors reflect the uncertainty in the absolute *flux calibration.*

References: [a] Shields & Filippenko (1988); [b] Shuder (1980); [c] Wilson, Baldwin & Ulvestad (1985).

3 Comparison with existing data

All three objects observed have been extensively studied at optical wavelengths and show different degrees of evidence for broad line components on the Hα line. We discuss each galaxy in order of increasing hard X-ray (2-10 keV) luminosity. By combining the measured Paschen β fluxes with optical spectroscopy it is possible to derive the extinction towards the line emitting regions in these objects. We use the interstellar dust extinction law as interpolated from Mathis (1990) and make the assumption that the intrinsic Hα/Pa β line ratio is close to its "case B" value of 17.6. For NGC5506 and A0945-30 we may compare these extinction estimates with the obscuration towards their nuclear continuum sources as derived from X-ray and mid-infrared data.

3.1 NGC4388

Despite being the nearest of the three Seyferts discussed in this chapter (taking the distance of the Virgo cluster to be 18 Mpc), NGC4388 was the last of these AGN to be reported as a detection in hard X-rays, mainly due to the presence of contaminating emission from M87 nearby, and partly due to the high absorbing column N_H=2.7×10^{23} cm^{-2} (Hansen *et al.* 1990).

This edge-on galaxy was the subject of an extensive Hα line imaging study by Shields & Filippenko (1988) who found broad wings on this line at a number of positions close to the optical nucleus. The infrared spectrum shown in Figure 1 was taken at the peak of the broad Hα emission reported by these authors, which they gave as 3 arcsec N, 4 arcsec E of the optical nucleus. It can be seen from the spectrum that there are no detectable broad wings on the Paschen β line. Although a smaller aperture was used for the optical observations, and our 5-arcsec beam averages the line emission over a region of non-uniform broad Hα emission, we can at least be certain from our upper limit for the corresponding broad component of Paschen β (Table 2) that the average extinction suffered by the broad line emission at this position in NGC4388 is A_V<6.5 mag.

Pogge (1988) compares the optical emission line geometry of this galaxy to that of NGC1068, in which the radiation from the BLR is believed to be scattered into our line of sight, either by electrons or perhaps by dust grains. In both NGC1068 and NGC4388 the high excitation gas (as defined by the ratio of [OIII] to Hα emission) has a

cone-like morphology. In terms of the "obscured Seyfert 1" hypothesis described in the Introduction, the large column of gas prevents us from observing hard X-rays directly from the active nucleus, while the associated dust blocks the direct (transmitted) broad line emission even in the near-infrared. The *scattered* off-nuclear broad line emission, on the other hand, is not expected to be highly reddened, since the scattering region 'mirrors' its less obscured view of the BLR. Our non-detection of broad Paschen β is consistent with this origin of the broad Hα emission in NGC4388, as it rules out transmitted broad line radiation from a highly reddened source. However, as noted by Shields & Filippenko (1988), spectro-polarimetry of the optical permitted lines at a number of off-nuclear positions is essential to confirm this picture.

3.2 NGC5506

This edge-on galaxy is noted for its rapid X-ray variability and high 2–10 keV luminosity (Turner & Pounds 1989). Although these properties are characteristic of Seyfert 1 activity, the optical spectrum of this galaxy is that of a Seyfert 2 with permitted lines of FWHM=370 km s^{-1} (Shuder 1980). The Paschen β spectrum shown in Figure 2 displays an additional broad line component of FWHM=1550 km s^{-1}, providing unambiguous evidence of an obscured BLR in this galaxy.

Traditionally, studies of reddened Seyfert nuclei have concentrated on searches for broad wings on the Hα line (eg. Véron *et al.* 1980). The blending of this line with emission from [NII] and uncertainty over the intrinsic profile of the narrow component have meant that different workers have arrived at discrepant results for the case of NGC5506 (eg. Whittle 1985, Boisson & Durret 1986). Fortunately, though, there is a secondary indicator of Seyfert 1 activity in the optical, provided that the extinction towards the BLR is not too great. Line emission from OI at 844.6 nm is believed to arise from Lyman β fluorescence in high optical depth, high density clouds (Grandi 1980). This line was detected in NGC5506 and NGC7314 by Morris & Ward (1985), who suggested that its presence is closely related to the Seyfert 1 phenomenon. Taking the sample of unobscured Seyfert 1s with fluxes reported for this line (Grandi 1980, Morris & Ward 1988) we find that the median value of the line flux ratio (OI 844.6 nm/Hα) is approximately 0.038, which implies an intrinsic (OI 844.6 nm /broad Paβ) line ratio

of $\simeq$1.5. Comparing this characteristic value for Seyfert 1s with the ratio observed for NGC5506 (Morris & Ward 1985,1988) implies $A_V \simeq 6$ mag for the BLR gas. Similarly, if we take the broad Hα flux reported by Durret & Bergeron (1988) we obtain $A_V = 5.0 \pm 0.5$ mag from the broad (Hα/Paβ) ratio.

From the low energy cutoff in the X-ray spectrum of NGC5506 Turner & Pounds (1989) derive a gas column density of $N_H = 2.8 \pm 0.5 \times 10^{22}$ cm^{-2} towards the hard X-ray source. Note that the BLR visual extinction determined above implies that a column of approximately 1.7×10^{22} cm^{-2} of this gas is situated between the BLR and the hard X-ray source, assuming that a standard dust-to-gas ratio of $A_V = 4.5 \times 10^{-22} N_H$ applies exterior to the BLR.

An estimate of the dust extinction towards the infrared continuum emission is provided by the 8–13 μm spectrum of Roche *et al.* (1984). From the optical depth of the 9.7 μm silicate feature they derive an equivalent visual extinction of 20 ± 2 mag to the 10 μm source (taking $A_V = 15 \tau_{9.7}$). If this is correct, our estimate of the BLR extinction above would imply that a large amount of silicate dust exists between the non-thermal source and the BLR, a situation we consider unlikely since the grains could not survive so close to the source of the ultraviolet photons(e.g. Barvainis 1987). Noting this difference, we adopt an extinction to the BLR gas of $A_V = 5.7 \pm 1$ mag, which is consistent with the optical observations within the uncertainties.

3.3 A0945-30=MCG-5-23-16

Slightly more luminous at hard X-ray energies than NGC5506 (Turner & Pounds 1989), A0945-30 has also been optically classified as a Seyfert 2, with permitted recombination lines of FWHM 270 km s^{-1} (Wilson, Baldwin & Ulvestad 1985). Véron *et al.* (1980) tentatively fitted a broad component to the Hα line profile, while more recently Durret & Bergeron (1988) reported a broad line flux an order of magnitude higher from their line profile fitting. In the spectrum shown in Figure 3, it can be seen that the broad line emission (FWHM=2150km s^{-1}) dominates the total line profile. Combining the measured flux in this component (Table 2) with the broad Hα flux reported by Durret & Bergeron (1988) gives a BLR extinction of $A_V = 4.0 \pm 0.7$ mag. Following the same arguments as for NGC5506 above, we find that this extinction value is just consistent

with the observed upper limit on the OI 844.6 nm line flux (Morris & Ward 1989), which yields A_V>6 mag.

The gas column density towards the hard X-ray source of N_H=1.06±0.4 × 10^{22} cm^{-2} reported by Turner & Pounds (1989) would imply a similar visual extinction of 4.8±2.5 mag for a standard Galactic dust abundance. For the purpose of this chapter we therefore adopt a broad line extinction of A_V=5.0±1.5 mag. Finally we note that Aitken & Roche (1985) determined an extinction of A_V=6±1.5 mag to the 10 μm source from the depth of the 9.7 μm silicate feature, which in this case is in agreement with the other extinction estimates.

4 NGC5506 & A0945-30: obscured Seyfert 1 nuclei

We have detected broad Paschen β line emission from both NGC5506 and A0945-30, but it still remains to be shown that they are indeed moderately obscured, but otherwise typical, Seyfert 1 nuclei. (It is conceivable, for instance, that this class of AGN could have an intrinsically under-luminous BLR, which escapes detection in the optical without the need for significant obscuration.)

For relatively unobscured Seyfert 1 AGN there exists a well-established correlation between broad Hα and 2-10 keV luminosity (eg. Ward *et al.*1988). By correcting the broad Paschen β fluxes for A0945-30 and NGC5506 (Table 2) for the BLR extinction values adopted in Section 3, we can estimate the intrinsic (i.e. de-reddened) broad Hα luminosity L(Hα) for each object. The results of this procedure are presented in Table 3. On a plot of L(2-10keV) vs. L(Hα) (eg. as presented in fig. 5 of Ward *et al.* 1988; note that they use c.g.s. units), we find that both NGC5506 and A0945-30 lie close to the correlation line for X-ray selected Seyfert 1 nuclei, once this correction for extinction has been made. Hence our observations provide direct support for the Seyfert 1 nature of the active nuclei in these two galaxies.

It should be noted that for each of the methods used above to determine the extinction towards the BLRs of NGC5506 and A0945-30, no information can be obtained as to the location of the obscuring matter along the line of sight. However, some indirect arguments can be made. NGC5506 appears on photographs as a dusty edge-on disk galaxy. One can reasonably assume that most of the BLR extinction takes place in

Table 3: *Derived extinctions and intrinsic luminosities*

	A_V	Log_{10} L (Watt)	
Object	(mag) [a]	broad Hα [a]	2–10 keV [b]
NGC5506	5.7±1.0	35.3±0.1	36.1
A0945-30	5.0±1.5	35.1±0.4	36.3

Note: We take H_o*=50 km* $s^{-1}Mpc^{-1}$ *and assume isotropic emission.*
References: [a]see Section 3 of the text; [b]Turner & Pounds (1989)

the interstellar medium of the disk over several kiloparsec. On the other hand, the host galaxy of A0945-30 appears to be of type S0. Based on the optical narrow line ratios (Durret & Bergeron 1988) and the upper limit we find for the flux of the narrow component of Paschen β (Table 2), the NLR gas is obscured by only $A_V \simeq 2.5$ mag, so in this case a large fraction of the nuclear extinction takes place within, or more likely just outside, the BLR of this active nucleus.

5 Discussion

In attempts to unify the classification of AGN it is often proposed that at least some Seyfert 2 galaxies possess obscured Seyfert 1 nuclei (eg. Lawrence 1987). NGC5506 and A0945-30 represent an extension of the Seyfert 1.9 class; their broad Hα emission is barely detectable, and has thus been the subject of previous controversy.

Observations of the Paschen β line are sensitive to extinctions in the range $5 \lesssim A_V \lesssim 10$ mag. This is because if the BLR extinction is less, we would detect clear broad components on the Hα line, but for values much more than this the broad Paschen β components would also be extinguished. This is probably the case for NGC4388 and NGC1068, which display scattered off-nuclear broad line emission. However, a detailed search for transmitted broad line emission from these nuclei, perhaps slightly offset from the peaks of their continuum emission, is necessary to confirm this.

All three galaxies discussed in this chapter contain large quantities of extended high excitation narrow line gas (NGC5506 & A0945-30–Wilson, Baldwin & Ulvestad 1985; NGC4388– Pogge 1988). It follows that this gas must be exposed to a less obscured view of the active nucleus in comparison to our own particular line of sight, otherwise there would be far too few ultraviolet photons to produce the observed line strengths.

This provides an indirect argument for an anisotropic continuum emission mechanism in these objects (e.g. Wilson, Ward & Haniff 1988), in which the obscuring material along our line of sight also serves to collimate the ionizing continuum.

6 Conclusions

We have detected broad (FWHM>1500 km s^{-1}) components in the Paschen β line of NGC5506 and A0945-30, removing the previous controversy over the existence of an obscured BLR in these objects. In NGC4388 the upper limit we find for the broad Paschen β flux at the peak of broad Hα emission is consistent with the scattered broad emission line geometry proposed for this and other Seyfert 2 galaxies.

We also find that the strength of the OI 844.6nm line in NGC5506, and the upper limit reported for A0945-30, are consistent with other estimates of the BLR reddening in these objects. On the basis of our results for this line we predict that NGC7314 should display broad Paschen β emission of similar strength to A0945-30.

With the recent increase in the performance of ground-based infrared spectroscopy it is now becoming possible to detect (or set stringent upper limits on) dust-obscured broad line emission in Seyfert 2 galaxies. Resolved spectroscopy of the 2.17 μm Brackett γ line ($A_{2.17\mu m} \simeq 0.1\ A_V$) and the 4.05 μm Brackett α line ($A_{4.05\mu m} \simeq 0.05\ A_V$) will be able to explore the highly extinguished regions of AGN to greater dust optical depths than is possible with the Paschen β line utilized here. Unfortunately the increased thermal background radiation at these wavelengths, combined with the steeply rising 1–10 μm continua of Seyfert galaxies and the correspondingly small equivalent widths of the Brackett lines, make these observations much more difficult in practice. However, further observations of infrared recombination lines in a sample of Seyfert 2 galaxies *not* known to be strong emitters of hard X-rays are needed in order to establish their relationship, if any, to luminous Seyfert 1 nuclei.

Subsequent work

Since this research was completed, observations of the Paschen β line in NGC5506 at higher signal-to-noise have confirmed the presence of a broad component to this line. Two independent measurements of the Brackett α line, however, are in apparent dis-

agreement (Moorwood & Oliva 1988; Kawara, Nishida & Gregory 1990). A possible explanation may be the different resolutions employed by these groups; the lower resolutions observations of the latter authors may be sampling the underlying broad line emission, whereas this component is unrecognizable in the spectrum presented by Moorwood & Oliva. Given this discrepancy and the large silicate optical depth observed in NGC5506, it is important to re-observe the Brackett α line to confirm unambiguously the broad line extinction estimated here.

Ackowledgements

It is a pleasure to thank Tom Geballe, Phil Puxley and Dolores Walther for their assistance at the telescope. We would also like to acknowledge the UKIRT Service observing programme for obtaining the initial spectrum of NGC5506 which prompted this work. Pat Roche contributed valuable advice and encouragement during the analysis of the data. These observations were made possible by the technical skill of Rosemary Chapman and the other members of the CGS2 upgrade team in Edinburgh and in Hilo, to whom we are indebted for the improvements made to the instrument shortly before our observing run.

References

Aitken, D. K. & Roche, P. F., 1985. *Mon. Not. R. astr. Soc.*, **213**, 777.

Antonucci, R. R. J. & Miller, J. S., 1985. *Astrophys. J.*, **297**, 621.

Barvainis, R., 1987. *Astrophys. J.*, **320**, 537.

Blanco, P. R., Ward, M. J. & Wright, G. S., 1990. *Mon. Not. R. astr. Soc.*, **242**, 4P.

Boisson, C. & Durret, F., 1986. *Astr. Astrophys.*, **168**, 32.

Depoy, D. L., 1987, in *Infrared Astronomy with Arrays*, eds C. G. Wynn-Williams & E. E. Becklin (Honolulu: University of Hawaii press), p. 426.

Durret, F. & Bergeron, J., 1988. *Astr. Astrophys. Suppl.*, **75**, 273. (*DB88*)

Grandi, S. A., 1980. *Astrophys. J.*, **238**, 10.

Green, P. J., Ward, M. J., Anderson, S. F., Margon, B., de Grijp, M. H. K. & Miley, G. K., 1989. *Astrophys. J.*, **339**, 93.

Hansen, C. G., Skinner, G. K., Eyles, C. J. & Willmore, A. P., 1990. *Mon. Not. R. astr. Soc.*, **242**, 262.

Kawara, K., Nishida, M. & Gregory, B., 1990. *Astrophys. J.*, **352**, 433.

Koski, A. T., 1978. *Astrophys. J.*, **223**, 56.

Kriss, G. A., Canizares, C. R. & Ricker, G. R., 1980. *Astrophys. J.*, **242**, 492.

Krolik, J. H. & Begelman, M. C., 1986. *Astrophys. J. Lett.*, **308**, L55.

Lawrence, A., 1987. *Publs astr. Soc. Pacific*, **99**, 309.

Lawrence, A. & Elvis, M., 1982. *Astrophys. J.*, **256**, 410.

Mathis, J. S., 1990. *Ann. Rev. Astr. Astrophys.*, **28**, 37.

Moorwood, A. F. M. & Oliva, E., 1988. *Astr. Astrophys.*, **203**, 278.

Morris, S. L. & Ward, M. J., 1985. *Mon. Not. R. astr. Soc.*, **215**, 57P.

Morris, S. L. & Ward, M. J., 1988. *Mon. Not. R. astr. Soc.*, **230**, 639.

Morris, S. L. & Ward, M. J., 1989. *Astrophys. J.*, **340**, 713.

Pogge, R. W., 1988. *Astrophys. J.*, **332**, 702.

Osterbrock, D. E., 1981. *Astrophys. J.*, **249**, 462.

Rix, H-W., Carleton, N. P., Rieke, G. & Rieke, M., 1990. *Astrophys. J.*, **363**, 480.

Roche, P. F., Aitken, D. K., Phillips, M. M. & Whitmore, B., 1984. *Mon. Not. R. astr. Soc.*, **207**, 35.

Shields, J. C. & Filippenko, A. V., 1988. *Astrophys. J. Lett.*, **332**, L55.

Shuder, J. M., 1980. *Astrophys. J.*, **240**, 32.

Turner, T. J. & Pounds, K. A., 1989. *Mon. Not. R. astr. Soc.*, **240**, 833.

Véron, P., Lindblad, P. O., Zuiderwyk, E. J., Véron, M. P. & Adam, G., 1980. *Astr. Astrophys.*, **87**, 245.

Ward, M. J., Done, C., Fabian, A. C., Tennant, A. F. & Shafer, R. A., 1988. *Astrophys. J.*, **324**, 767.

Ward, M. J., Elvis, M., Fabbiano, G., Carleton, N. P., Willner, S. P. & Lawrence, A., 1987. *Astrophys. J.*, **315**, 74.

Weedman, D. W., 1977. *Ann. Rev. Astr. Astrophys.*, **15**, 69.

Whittle, M., 1985. *Mon. Not. R. astr. Soc.*, **216**, 817.

Wilson, A. S., Baldwin, J. A. & Ulvestad J. S., 1985. *Astrophys. J.*, **291**, 627.

Wilson, A. S., Ward, M. J. & Haniff, C. A., 1988.*Astrophys. J.*, **334**, 121.

Chapter 4

Infrared spectroscopy of Cygnus A: implications for the obscured active nucleus

Prologue: A "unified scheme", parallel to that already discussed for radio-quiet Seyfert galaxies, has also been proposed for those emission-line galaxies which possess extended, double lobes of radio emission. The narrow-line radio galaxy Cygnus A was one of the first of this class to be identified due to its proximity and high radio power. Near-infrared spectra of Cygnus A were obtained in 1990 in an attempt to penetrate the foreground dust and reveal optically-obscured broad line emission from a quasar nucleus, and to search for evidence of excited molecular gas. Part of this research was carried out in collaboration with Martin Ward, Andrew Wilson and Minoru Nishida, and has been accepted for publication by *Astrophysical Journal* (Ward, Blanco, Wilson & Nishida, 1991).

Summary

We present near-infrared spectroscopic observations of the central regions of the luminous radio galaxy Cygnus A (3C 405), and interpret these results in terms of an obscured quasar nucleus. We have detected strong emission in the molecular hydrogen lines v=1–0 S(1) and v=1–0 S(3), the strengths of which are plausibly accounted for through heating by the nuclear hard X-ray source. Assuming that Cygnus A obeys the good correlations between hard X-ray, broad hydrogen line and near-infrared continuum luminosities established for quasars with little reddening, the intrinsic strengths of broad Paschen α and the 2.2 μm continuum may be estimated empirically. Our observed upper limit to the flux of broad Paschen α then implies an extinction to the putative broad line region A_V(BL) of at least 24 mag, and the observed continuum intensities of the nuclear point source in the near-infrared (Djorgovski *et al.* 1991) give an extinction A_V(NC)=37±6 mag towards the optical–infrared continuum. These extinction estimates are consistent with the gas column density inferred from the low-energy X-ray cut-off.

We argue that the small-aperture near-infrared colours of Cygnus A are due to a combination of starlight from the host galaxy, and an electron-scattered nuclear continuum. Using our estimate above for the intrinsic near-infrared luminosity we then find that these electrons scatter a fraction $f \sim 0.05$ of this luminosity towards us. Applying this fraction to the non-stellar optical radiation we find that the intrinsic optical luminosity of Cygnus A is that of a medium-luminosity quasar. This inferred luminosity is sufficient to power the far-infrared excess in Cygnus A through heating of interstellar dust grains by the active nucleus.

We also report strong, broad [SiVI]1.962μm line emission from Cygnus A, the first such detection in a radio galaxy, at a level consistent with photo-ionization by the nuclear hard ultraviolet continuum.

1 Introduction

The so-called *unified model* of Seyfert galaxies is one in which the inclination angle at which we view the Active Galactic Nucleus (*AGN*) is a crucial parameter. This angle will determine whether we can see the AGN relatively free of obscuring material, and hence observe the Broad Line Region (*BLR*) and non-stellar continuum directly, or whether these components are hidden at optical wavelengths. In the latter case, we see only the extra-nuclear signatures of activity, such as extended high ionization line emission and scattered nuclear light. For moderate amounts of foreground extinction, however, infrared radiation from the BLR and continuum source may still be able to penetrate the dust. Moreover, if the optically thick material is associated with molecular gas (possibly in the form of a disk or torus), it may be subjected to significant heating effects by high energy photons from the nucleus, which would enhance the strength of line emission from molecular species such as H_2.

These ideas stemmed primarily from the discovery by Antonucci & Miller (1985) of broad polarized components to the Hα and Hβ lines in the type 2 Seyfert galaxy NGC1068. Since then much observational and theoretical effort has been directed towards explaining the properties of Seyfert 2s in terms of obscured Seyfert 1 nuclei. The idea that powerful radio galaxies are mis-directed quasars is an extension of this general concept (e.g. Barthel 1989). There are sub-classes of radio galaxy with, respectively,

strong broad permitted lines (*BLRGs*), and strong narrow permitted lines (*NLRGs*) in their optical spectra. It has been pointed out by many workers that spectroscopically these classes represent the radio-loud analogues of Seyfert 1s and 2s. It is, therefore, important to confirm this hypothesis by means of observational tests. Cygnus A (3C405) is an obvious choice for study. The observed optical continuum is weak compared to BLRGs, but the emission lines from the Narrow Line Region (*NLR*) are very strong (Osterbrock 1983). The optical emission line spectrum, which includes both high excitation lines of [NeV]342.6 nm and HeII468.6 nm, and strong lines of neutral species such as [OI]630.0 nm, 636.3 nm, and [NI]519.9 nm, indicates that the gas in Cygnus A is photoionized by an active nucleus (Osterbrock & Miller 1975). In most respects, then, the optical spectrum of Cygnus A resembles that of a Seyfert 2 nucleus. This makes it an ideal candidate to search for broad wings to the profiles of the near-infrared hydrogen recombination lines, and for evidence of excited molecular gas.

The subject of this chapter is infrared spectroscopy of Cygnus A. In particular we report detections of the hydrogen recombination lines Paschen α and Brackett γ, the v=1–0 S(1) and v=1–0 S(3) quadrupole transitions of molecular hydrogen, and the high ionization line of [SiVI] at rest wavelength 1.9615 μm. Utilizing these new observations in conjunction with existing data at X-ray and infrared frequencies, we show that we are able to account for the properties of Cygnus A in terms of a quasar nucleus which is heavily obscured along our line of sight, and give estimates for the extinction towards its line and continuum emitting regions. Extending these arguments to the small-aperture optical/near-infrared fluxes from the nuclear regions, we argue that the non-stellar radiation is due to wavelength-independent scattering of a quasar nuclear continuum, and show that the inferred optical/UV luminosity of Cygnus A is sufficient to power the far-infrared excess through absorption and subsequent emission by dust grains.

A redshift cz=16950 km s^{-1} and a Hubble constant H_0=50 km s^{-1} Mpc^{-1} have been used throughout this chapter.

2 Observations

The spectra presented in Figure 1 were obtained at the f/35 Cassegrain focus of the U. K. Infrared Telescope using the 7-element grating spectrometer CGS2 with a 637

lines/mm grating in first order.

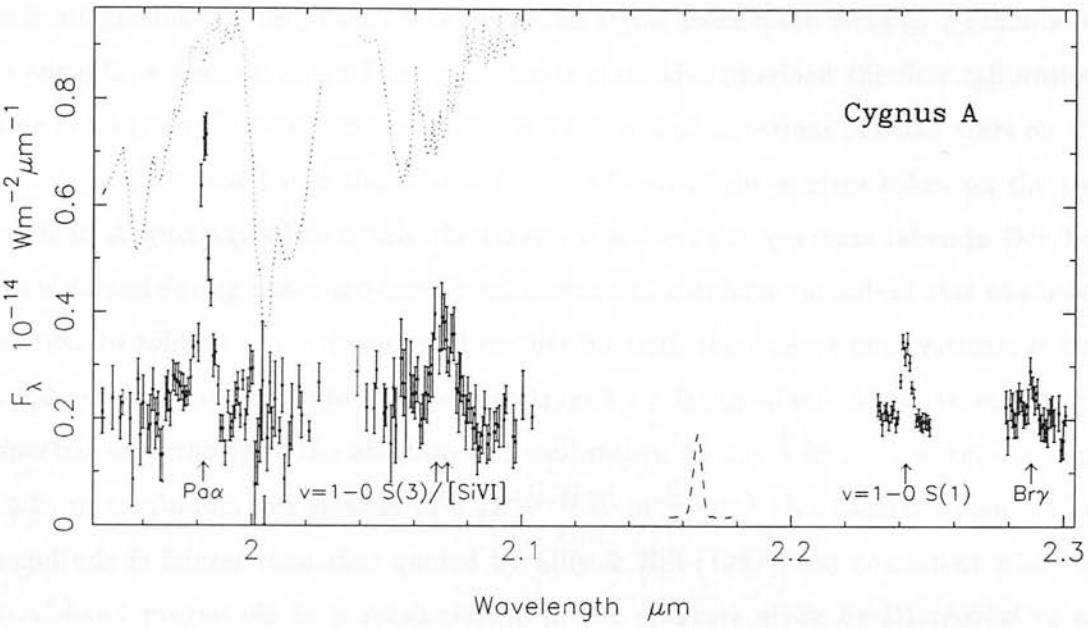

Figure 1: *Composite near-infrared spectrum of Cygnus A. The resolution of the instrument at 2.166μm is given by the profile of Brackett γ in the planetary nebula NGC7027 (dashed line), shown scaled to the same strength as H_2 v=1-0 S(1). Also displayed (dotted) are the relative signals of the standard stars which are modified by the atmospheric transmission as a function of wavelength.*

A circular aperture of diameter 5.0 arcsec was centered on the nucleus of Cygnus A by offsetting from the position of peak infrared emission of a nearby star. To provide adequate sampling of the spectral resolution, the grating was stepped in increments of 1/4 detector width. The journal of observations is presented in Table 1. Standard

Table 1: *Journal of observations*

UT Date	$\lambda - \lambda$ (μm)	Integration time per point (s)	Standard star
1990 Aug 23	1.945–2.025	260	BS 7178
1990 Aug 23	2.232–2.252	1080	BS 7178
1990 Aug 24	2.279–2.301	360	BS 7178
1990 Oct 1	2.039–2.104	180	BS 7796

chopping and beamswitching procedures were followed to subtract the sky background.

The effects of telluric absorption, which can be severe at wavelengths less than 2.1 μm, were removed by observing standard stars close to Cygnus A on the sky before and after each integration on the galaxy. The measured signal from these stars as a function of wavelength is also shown in Figure 1. These stars also provided the flux calibration; their catalogued K magnitudes were checked through observations of other stars on the same nights. It was found that the continuum levels of the spectra taken on the two nights in August agreed to within the errors. However, the spectrum taken in October was obtained during non-photometric conditions and a different standard star was used. In order to achieve a continuum level compatible with the August observations, it was found necessary to scale the October spectrum by a factor of 0.9, which is within the expected uncertainty of the absolute flux calibration. In our 5 arcsec aperture we find a 2.2 μm continuum flux density of 0.2×10^{-14} W m^{-2} μm^{-1} (K=13.2$\pm$0.1 mag). This magnitude is fainter than that quoted by Lilly & Hill (1987), but consistent with the broad-band magnitude in a synthesized 3 arcsec aperture given by Djorgovski *et al.* (1991).

The instrumental line profile was determined by observations of the 2.166 μm Brackett γ line in the planetary nebula NGC7027, giving a FWHM resolution at this wavelength of 490 km s^{-1}. The resolution at other wavelengths was calculated from this measurement and the known properties of CGS2, and varies from 570 to 450 km s^{-1} over the observed wavelength interval. Wavelength calibration was achieved by using the Brackett γ line in NGC7027 together with narrow atmospheric absorption features observed in the raw spectra of the standard stars (see Figure 1), and is believed to be accurate to within 6×10^{-4} μm.

3 Results

We have clearly detected Paschen α, Brackett γ, H_2 v=1–0 S(1) and a blend of the H_2 v=1–0 S(3) and [SiVI]1.962 μm lines close to their expected wavelengths at a redshift of 0.0565 (Figure 1). Line fluxes and widths were determined by finding the least-squares fit of a Gaussian profile to the feature of interest. The blend of [SiVI] and H_2 v=1–0 S(3) lines was separated by fixing the intrinsic width of the v=1–0 S(3) line to that determined from the higher signal-to-noise observation of H_2 v=1–0 S(1) (see Figure 2).

The results of the fitting procedure for all the lines are presented in Table 2. Unlike

Table 2: *Fitted line fluxes for Cygnus A*

λ_{obs} (μm)	Line	Flux
1.9821	Pa α (narrow)	2.6 $\pm$0.2
1.9821	Pa α (broad)	<1.2 (3σ)
2.0550	Br δ	<0.6 (3σ)
2.0682	H_2 v=1–0 S(3)	0.4 $\pm$0.16
2.0724	[SiVI]1.962μm	1.2 $\pm$0.3
2.2422	H_2 v=1–0 S(1)	0.60$\pm$0.05
2.2881	Br γ	0.26$\pm$0.08

Note:
Line fluxes are given in units of 10^{-17} *W* m^{-2}. *The quoted errors are the formal* 1σ *uncertainties obtained from the fitting procedure.*

the near-infrared lines measured in most other AGN, the equivalent widths of the lines in Cygnus A are high. We shall examine each line individually.

3.1 Paschen α and the Brackett lines

Paschen α has been previously detected in Cygnus A by Lilly & Hill (1987). However, the present observations represent a dramatic improvement in signal-to-noise ratio over these earlier data. Our measured line flux is about 20% less than that reported by Lilly & Hill, mainly due to the different absolute flux calibration. The resolution-corrected FWHM velocity of 510$\pm$60 km s^{-1} agrees well with the Balmer line widths reported by Osterbrock & Miller (1975). More importantly, we are able to set a stringent upper limit to the flux of a broad (FWHM$\simeq$3000 km s^{-1}) line component (Table 2), which is a factor of 2 less than the upper limit given by Lilly & Hill.

We have also detected Brackett γ in Cygnus A at the 3-σ level, but Brackett δ (rest wavelength 1.9451μm), which is expected to be roughly two thirds the strength of Brackett γ, is not detected due to the lower signal-to-noise ratio of our data at this wavelength.

3.2 The v=1–0 molecular hydrogen lines

The H_2 v=1–0 S(1) line is exceptionally strong in Cygnus A, with a high equivalent width of nearly 3.0 nm. The line is not spectrally resolved by our observations (FWHM$\leq$400 km s^{-1}). The measured flux ratio F(v=1–0 S(1))/F(Brγ) has a high value of 2.3$\pm$0.7. The error in this ratio is dominated by the uncertain flux of Brackett γ; if instead this flux is calculated from the Paschen α flux, assuming the "case B" line ratio and neglecting the small differential extinction (Section 4), we find F(v=1–0 (1))/F(Brγ)=2.6$\pm$0.3. This value is only clearly exceeded by very few galaxies, such as NGC6240 and the Circinus galaxy (Mouri *et al.* 1989, Moorwood & Oliva 1990).

We have also detected the H_2 v=1–0 S(3) line (rest wavelength 1.9576 μm) blended with [SiVI]1.9615 μm. With the valid assumption of identical profiles for the v=1–0 S(1) and S(3) lines we find the flux ratio F(v=1–0 S(3))/F(v=1–0 S(1))=0.7$\pm$0.3. The larger uncertainty in the flux of v=1–0 S(3) is partly due to blending with [SiVI] and partly due to the lower signal-to-noise of the spectrum over this range.

3.3 [SiVI]1.962 μm

[SiVI]1.962 μm has been observed previously in the spectrum of the Seyfert galaxy NGC1068 by Oliva & Moorwood (1990), but this is the first detection in a radio galaxy. The line is blended with H_2 v=1–0 S(3), but the good signal-to-noise measurement of the v=1–0 S(1) profile allows us to separate the blend as described above and shown in Figure 2. We note that the best-fitting [SiVI] line profile is broader (FWHM=1200$\pm$300 km s^{-1}) than the hydrogen lines. Although the corrections for atmospheric absorption are believed to be accurate, and the resultant measured flux ratio F(v=1–0 S(3))/F(v=1–0 S(1)) after deblending is reasonable (Section 5.2), the larger width of the [SiVI] line may be a result of systematic errors due to the non-photometric conditions. It is important, therefore, to check the profile of the [SiVI] line by observing at higher spectral resolution and sensitivity.

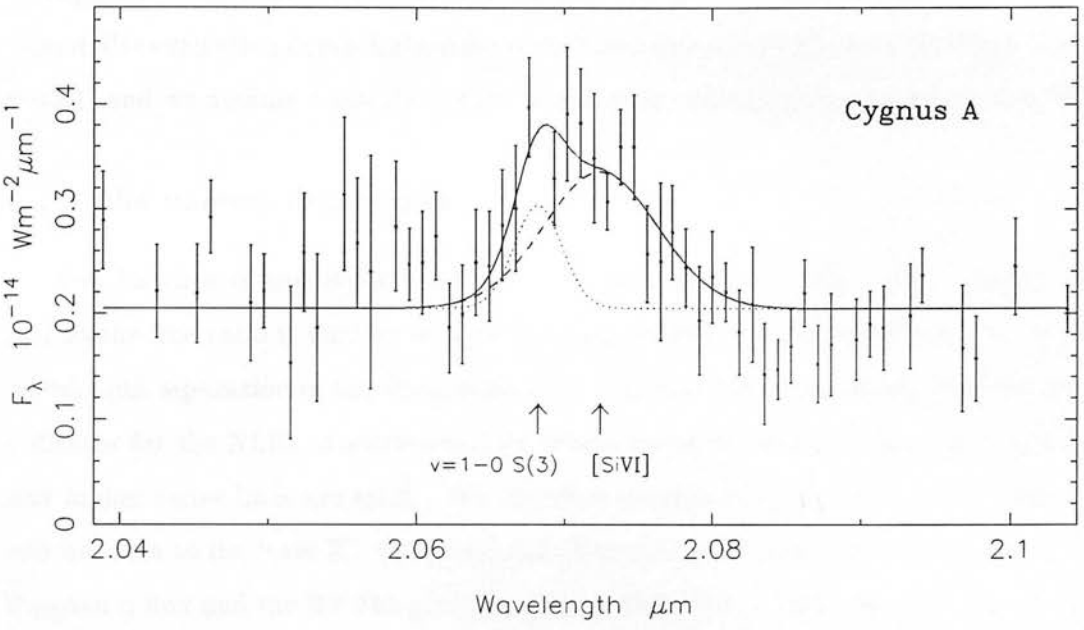

Figure 2: *Part of the spectrum displayed in Figure 1 covering the blend of [SiVI]1.962μm with H_2 v=1–0 S(3)1.9576μm. The best-fit model spectrum (solid line) is the sum of the individual components of [SiVI] (dashed) and H_2 v=1–0 S(3) H_2 (dotted).*

4 The obscuration towards Cygnus A

A number of estimates can be made of the extinction appropriate to the different line and continuum emitting regions within Cygnus A. These values are summarized in Table 3, and their derivations are given below. Note that these estimates do *not* include

Table 3: *Extinction estimates (A_V) for Cygnus A*

Extinction (mag)	Component	Measurements
A_V(Gal)=1.2 [a]	Galactic foreground	host galaxy E(B−V), N_H(Gal)
A_V(NL)=1.2±0.15	Narrow lines	narrow Paschen α [b], Balmer lines [c]
A_V(BL)>24	Broad lines	broad Paschen α [b], X-rays [d]
A_V(NC)=37±6	Nuclear continuum	near-IR point source [e], X-rays [d]

Note: The contribution of the foreground extinction in our Galaxy (A_V(Gal) =1.2 mag) is not included in the values quoted for A_V(NL), A_V(BL), and A_V(NC).
References: [a] Adopted value (see Djorgovski et al. *1991, and references therein); [b] this work; [c] Lilly & Hill (1987); [d] Arnaud* et al. *(1987); [e] Djorgovski* et al. *(1991).*

the extinction due to dust in our own Galaxy, for which we adopt A_V(Gal)=1.2 mag

(Djorgovski *et al.* 1991, and references therein). In the following calculations we use an interstellar extinction curve derived from the tabulated values given by Mathis (1990) for R=3.1, and we assume a standard dust-to-gas ratio corresponding to $A_V=5\times10^{-22}N_H$.

4.1 The narrow line region

The Paschen α and Hβ transitions of HI arise from the same upper energy level, and so the line ratio is unaffected by collisional excitation. This property, and the long wavelength separation of the lines, makes the Paα/Hβ flux ratio an excellent reddening indicator for the NLRs of active galaxies, where radiative transfer effects in the Balmer and higher series lines are small. We therefore assume that the intrinsic line flux ratio will be close to its "case B" value of 0.332 (Hummer & Storey 1987). From our narrow Paschen α flux and the Hβ flux given by Lilly & Hill (1987), both corrected for A_V(Gal), we derive a foreground narrow line extinction A_V(NL)=1.2±0.15 mag.

This estimate for A_V(NL) is in good agreement with the value of 1.05±0.15 mag which we derive similarly from the Balmer decrement quoted by Lilly & Hill (1987), assuming an intrinsic line flux ratio of 3.0 appropriate to the NLR (Gaskell & Ferland 1984). Our observed Brackett γ line flux and Brackett δ upper limit are consistent with "case B" excitation conditions and A_V(NL)=1.2 mag. Similar estimates for the foreground extinction were derived by Malkan (1983) using the optical [OII] and [SII] line flux ratios.

If this dust extinction takes place *within* the NLR, we would expect the Paschen α flux to be enhanced relative to the Balmer lines for a given Balmer decrement. Unfortunately this effect is sensitive to our adopted values for A_V(Gal) and the intrinsic NLR Balmer decrement (cf. Binette *et al.* 1990), and so cannot be distinguished from foreground extinction with the observations currently available. If such internal extinction were to dominate, however, a dust column of *at least* $A_V\sim10$ mag would be necessary to account for the high Paα/Hβ ratio.

It should also be noted that the Balmer decrement is known exhibit spatial variations within the region enclosed by our aperture (Pierce & Stockton 1986), so in this sense our value for A_V(NL) is a flux-weighted average over the central 5 arcsec.

4.2 The hypothetical broad line region

Our upper limit to the broad component of Paschen α may be combined with a prediction of the intrinsic broad line flux to provide an estimate of the minimum extinction to the broad line region A_V(BL).

It has long been known that a good correlation exists between the hard X-ray and the broad Hα luminosities of relatively unobscured AGN (for a recent compilation of data see Ward *et al.* 1988). Although hard X-ray emission has been detected from the vicinity of Cygnus A, this emission is believed to be a blend of two components, one associated with hot intracluster gas and the other with the active nucleus. A detailed decomposition has been carried out by Arnaud *et al.* (1987), who determined the intrinsic 2–10 keV luminosity L_X of the nucleus of Cygnus A to be 5.3×10^{37} W. This value is similar to that observed from the BLRGs 3C390.3, 3C382 and 3C445 (e.g. Ward *et al.* 1988, and references therein).

Using the relationship between L_X and broad Hα luminosity and assuming an intrinsic broad line flux ratio F(Paα)/F(Hα)=0.10 (cf. Yates & Garden 1989), we predict F(Paα)$\simeq3\times10^{-16}$ W m^{-2} in the absence of extinction. Reduction of this predicted value below our observed upper limit (Table 2) corrected for A_V(Gal) requires A_V(BL)>24 mag. For a normal gas-to-dust ratio, this limit on A_V(BL) corresponds to a hydrogen column density $N_H>4.8\times10^{22}$ cm^{-2} and hence a rest-frame low-energy cut-off in the nuclear X-ray spectrum at an energy above 2.6 keV (Morrison & McCammon 1983). Such a column is consistent with the range of values of N_H towards the compact component in the composite model of Arnaud *et al.* (1987), and with the fact that no unresolved source was detected by the low-energy *Einstein* HRI experiment (Arnaud *et al.*1984). The lower limit to A_V(BL) derived above is more than enough to hide any broad optical lines and the associated non-thermal optical continuum from direct view.

The intrinsic broad Hα flux derived from the nuclear X-ray luminosity corresponds to a broad Hβ flux of 8.6×10^{-16} W m^{-2}, assuming F(Hα)/F(Hβ)=3.5 in the BLR (e.g. Yates & Garden 1989). Correcting the [OIII]500.7 nm and narrow Hβ fluxes reported by Osterbrock & Miller (1975) for A_V(Gal) and A_V(NL)=1.2 mag (Section 4.1), we obtain an estimate of the intrinsic flux ratio F([OIII]500.7 nm)/F(Hβ total)$\simeq$1.7, where F(Hβ total) represents the sum of the intrinsic broad and narrow line fluxes of Hβ. This

ratio is well within the range observed for BLRGs (Rudy 1984), and hence provides a consistency check on our method.

4.3 The optical–infrared nuclear continuum

We may apply a similar method to that used above for Paschen α in estimating the extinction A_V(NC) towards the nuclear continuum source. A measurement of the observed nuclear continuum at any wavelength combined with an independent estimate of its intrinsic level would enable us to calculate the obscuration towards this component.

Djorgovski *et al.* (1991) have recently presented near-infrared images of Cygnus A showing a faint point source at 2.2 μm which is probably direct radiation from the quasar nucleus. By comparing the observed nuclear fluxes of Cygnus A with assumed analytic forms of the quasar's intrinsic spectral energy distribution, they were able to estimate the extinction suffered by the continuum radiation. However, since the observed data could be reconciled with a wide range of possible intrinsic spectral shapes, their estimate A_V(NC)=50±30 mag has a large uncertainty.

We employ here an alternative, empirical technique for estimating A_V(NC). This method makes use of the good correlation between the near-infrared and low energy X-ray continuum luminosities established for those quasars observed by *Einstein* (Kriss 1988). For Cygnus A we may calculate the 0.5–4.5 keV luminosity from the absorption-corrected 2–10 keV flux reported by Arnaud *et al.* (1987) using their spectral index of $\simeq -0.7$. Then from the X-ray/near-infrared correlation established for radio-loud quasars (Figure 8 of Kriss 1988), we find an intrinsic 1 μm luminosity $L_\nu(1\,\mu\mathrm{m})=1.6\times10^{23}\,\mathrm{W\,Hz^{-1}}$ for Cygnus A, uncertain by about 0.2 in the logarithm.

We infer the *extinguished* luminosities $L_\nu^{ext}(\lambda)$ from the observed 1.65, 2.2 and 3.8 μm nuclear fluxes reported by Djorgovski *et al.* (1991), corrected for A_V(Gal). This observed continuum may be represented as a power-law nuclear continuum of spectral index α ($L_\nu \propto \nu^\alpha$) transmitted through a dust column A_V(NC), such that the difference between the extinguished luminosities and the intrinsic value at 1.0 μm is given by:

$$\log L_\nu^{ext}(\lambda) = \log L_\nu(1\,\mu\mathrm{m}) - \alpha \log(\lambda/1\,\mu\mathrm{m}) - 0.4 A_V(\mathrm{NC}) A(\lambda)/A_V$$

where $A(\lambda)/A_V$ is calculated from the extinction law of Mathis (1990).

Fitting this model to the data for Cygnus A, weighted by their errors and using our derived value of $L_\nu(1\,\mu\mathrm{m})$ above, we find the optimum values $A_V(\mathrm{NC})=37\pm6$ mag and $\alpha = -0.3\pm0.5$ ($\chi^2_{min}=0.85$ for 1 degree of freedom).

The best-fit value for the spectral index α is marginally flatter than the range of values -1 to -2 found for the PG quasars by Neugebauer *et al.* (1987); fixing the spectral index at -1.0 does not, however, change the reduced χ^2 or $A_V(\mathrm{NC})$ significantly. More important, our estimate for $A_V(\mathrm{NC})$ is in excellent agreement with that expected from the X-ray absorbing column reported by Arnaud *et al.* (1987)—$A_V(\mathrm{NC})=41^{+50}_{15}$ mag (90% confidence interval)—but has a much smaller uncertainty; the contribution to the probable error on $A_V(\mathrm{NC})$ is shared equally by the scatter in the Kriss (1988) correlation and the measurement uncertainties of Djorgovski *et al.*'s observations. This error is, of course, the width of the 67% confidence interval containing $A_V(\mathrm{NC})$ only if our *a priori* assumptions hold true. The most important of these may be summarized as follows (the list is not exhaustive):

i. *Cygnus A obeys the X-ray/near-infrared continuum correlation established for radio-loud quasars.* (Even if Cygnus A is a buried quasar, this might not hold if the X-ray/near-infrared luminosity ratio is itself a function of viewing angle. For instance, if the near-infrared radiation is beamed along the radio axis, our estimate for $L_\nu(1\,\mu\mathrm{m})$ will be too high for the case of Cygnus A, causing us to overestimate the nuclear extinction.)

ii. *The quasar continuum is extinguished by foreground interstellar dust with a filling factor of unity* (i.e. the dust is assumed to cover all our direct lines-of-sight to the continuum source). Note that if the obscuring dust is also a *source* of the "nuclear" near-infrared continuum through emission from grains at $\simeq$1500 K (e.g. Barvainis 1987) then our derived dust column (in terms of A_V) will be a lower limit, and the fitted spectral index will be in error. The existing data does not warrant a more complex model taking this into account.

iii. *The near-infrared extinction law in Cygnus A is similar to that of our Galaxy.* Although the response of small dust grains to different radiation environments (from molecular clouds to the emission-line regions of AGN) leads to wide variations in optical/UV reddening, the larger grains responsible for the near-infrared extinction

appear to obey a "standard" extinction law, so this assumption may only affect our normalization of the fitted near-infrared extinction by A_V(NC) (see the review by Mathis 1990 for a thorough discussion of these issues).

iv. *Djorgovski* et al.*'s nuclear fluxes are due solely to direct nuclear radiation transmitted through the obscuring material.* We have assumed that they include no contribution from starlight or scattered radiation. This may not be the case for the L′ flux (Section 6).

5 The observed continuum from the nuclear regions of Cygnus A

In Figure 3 we present the observed continuum Spectral Energy Distribution (*SED*) of the nucleus of Cygnus A, together with some of the results derived in this chapter. The extinguished power-law continuum fitted to the near-infrared nuclear fluxes (Section 4.3) is shown as a dashed line, extrapolated to a rest wavelength of 1.0 μm. Open symbols represent small-aperture fluxes from the central few arcsec of Cygnus A; as we shall see below, these fluxes include direct radiation from the nuclear source, scattered radiation from this source, and starlight from the host galaxy. This SED is plotted logarithmically as λF_λ vs wavelength λ (see Djorgovski *et al.* 1991 for Cygnus A's SED plotted as F_ν vs ν). Thus the "flat" radio core spectrum (spectral index$\simeq$0) has a gradient of unity in this plot, while a power-law of spectral index -1 would appear as a horizontal line. The values of λF_λ at different wavelengths may be interpreted as measures of the flux received over over a fixed logarithmic wavelength (i.e. velocity) interval. It can readily be seen, for instance, that despite the "radio-loud" nature of Cygnus A, the bulk of its power is emitted in the far-infrared.

6 Scattering of nuclear radiation in Cygnus A

The so-called featureless optical continuum identified by Osterbrock (1983) and imaged by Pierce & Stockton (1986) cannot possibly be the quasar continuum transmitted through A_V(NC)$\simeq$37 mag. Tadhunter, Scarrott & Rolph (1990) have found that the optical light on the scale of a few arcseconds (comparable to the apertures used by us

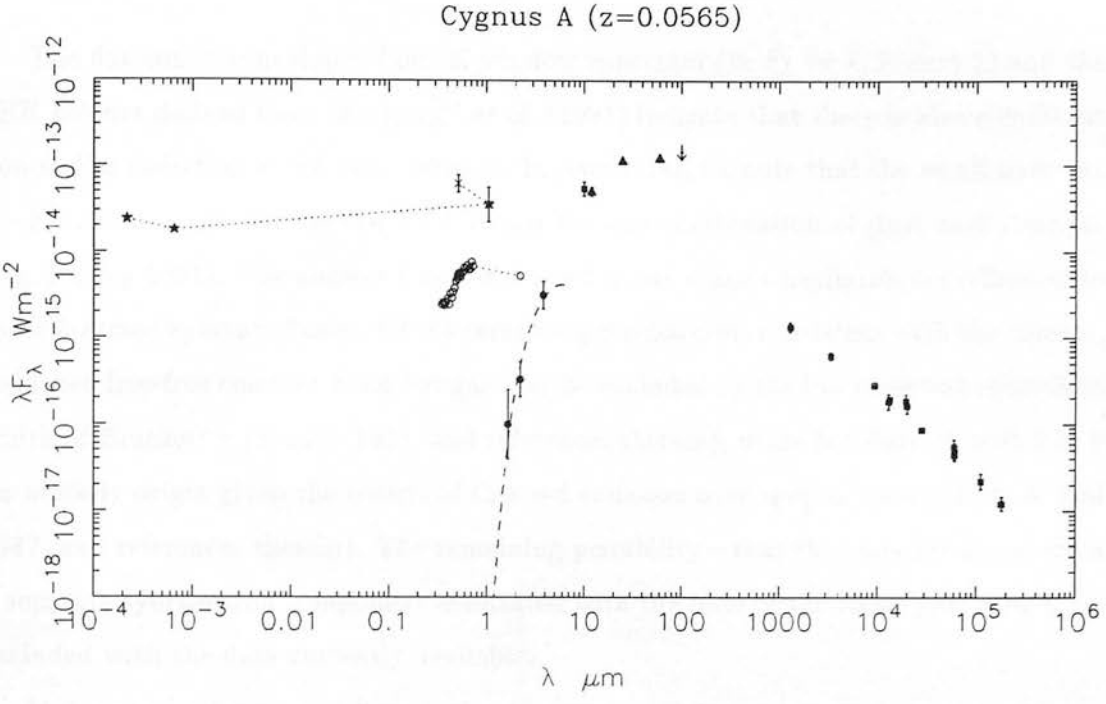

Figure 3: *Spectral Energy Distribution of the nuclear regions of Cygnus A. Dotted line segments merely connect related spectral components, and are not intended to interpolate between them. Fluxes between 300.0 nm and 3.8 μm have been corrected for* A_V*(Gal)=1.2 mag. Symbols are as follows: filled squares—radio and 10 μm fluxes (Salter* et al. *1989, and references therein, Rieke & Low 1972); filled triangles and upper limit—IRAS data from Knapp, Bies & van Gorkum (1990); •—nuclear point source fluxes at 1.65, 2.2 & 3.8 μm (Djorgovski* et al. *1991), to which has been fitted an extinguished power-law continuum (dashed line, see Section 4.3); ⋆—absorption-corrected hard X-ray continuum (Arnaud* et al. *1987), together with the inferred intrinsic nuclear continuum fluxes at 2.0/(1+z) keV and 1.0(1+z) μm (see Section 4.3); ×—estimate of intrinsic nuclear flux at 486.1(1+z) nm, the associated error bar refers only to the 486.1 nm/1.0 μm flux ratio (see Section 5.2); ○—small-aperture continuum fluxes of the central regions, in the optical (Osterbrock & Miller 1975: 4.0×2.5 arcsec aperture), and near-infrared (this work: 5 arcsec circular aperture).*

and Osterbrock 1983) displays a polarization pattern reminiscent of a bipolar reflection nebula. This result supports the notion that the nuclear point source itself is highly obscured along our line of sight, and that the featureless optical continuum is seen only after scattering.

6.1 Near-infrared emission components in Cygnus A

The flat continuum slope of our K-window spectrum (in F_λ vs λ, Figure 1) and the JHK colours derived from Djorgovski *et al.* (1991) indicate that there is also significant non-stellar radiation in the near-infrared. In particular, we note that the small-aperture H−K colour is too red for the J−H colour for any combination of dust and starlight (e.g. Puxley 1991). The nuclear fluxes discussed above make a negligible contribution to these 3-arcsec-aperture fluxes. Of the remaining mechanisms consistent with the colours, reddened free-free emission from hot gas may be excluded by the low observed equivalent width of Brackett γ (Puxley 1991, and references therein), while hot dust at $\simeq$1000 K is an unlikely origin given the extent of this red emission over several arcsec (Lilly & Hill 1987, and references therein). The remaining possibility—that the emission arises from a separate synchrotron component associated with the base of the radio jets, cannot be excluded with the data currently available.

If the non-stellar optical light is due to wavelength-independent electron scattering of a canonical quasar continuum (Sanders *et al.* 1989), it may contribute significantly to the near-infrared fluxes. Taking the JHK colours of the host galaxy from M$^{\rm c}$Alary & Rieke (1988) (for a deVaucouleurs morphological type of $T = -5$) and correcting all fluxes for A_V(Gal), we model the near-infrared fluxes given by Djorgovski *et al.* (1991) as the sum of starlight and a power law of index -1.5 ± 0.25. The best-fit decomposition is listed in Table 4, and corresponds to a stellar fraction in the J-band continuum of $55\pm15\%$. From our fitted stellar component at 1.25 μm we predict an extinction-corrected stellar continuum strength of $F_\nu \simeq 0.21$ mJy at 550.0 nm for a reasonable value of the host galaxy V−J colour (M$^{\rm c}$Alary & Rieke 1988). This is only $\sim$1/2 of the stellar flux determined spectroscopically at 513.5 nm by Osterbrock (1983), but the discrepancy becomes less significant when one considers the effects of different aperture sizes, centring and extinction.

We have shown that the J, H and K-band fluxes measured in small apertures are well described by a sum of starlight from the host galaxy and electron-scattered radiation from the nuclear source. However, in extrapolating this model to 3.8 μm, we find that a significant fraction of the L′ flux quoted by Djorgovski *et al.* would then be supplied by this scattered nuclear power law (Table 4). Although its spatial extent over the central

Table 4: *Fitted stellar and scattered fluxes in the central 3 arcsec of Cygnus A* [1]

$\lambda_{obs}(\mu m)$	F_ν(Stellar)	$F_\nu=0.471\lambda^{1.5}$	Total	Observed [a]
1.25	0.803	0.659	1.462	1.468±0.09
1.65	0.952	0.999	1.951	1.945±0.10
2.2	0.706	1.539	2.244	2.254±0.14
3.8	0.377	3.489	3.866	<3.96 ±40% [2]

Notes:

1. All flux densities are given in units of mJy and have been corrected for A_V*(Gal)=1.2 mag.*

2. The quoted 3.8 μ*m flux may include significant direct radiation from the active nucleus, and hence is given here as an upper limit.*

Reference: [a] *Djorgovski* et al. *(1991, synthesized 3 arcsec circular aperture).*

few arcsec would render this component undetectable in their L′ image, it may nevertheless contaminate the reported nuclear flux estimate at this wavelength. Fortunately, we find that excluding this flux from our calculation of A_V(NC) above does not change our estimate significantly (Figure 3).

6.2 An estimate of the optical luminosity of Cygnus A

From the power-law scattered component fitted above we may calculate the scattered 1 μm luminosity of Cygnus A (in WHz^{-1}), which is given by $\log L_\nu^{scat}(1\,\mu\mathrm{m})\simeq 21.86$, with an uncertainty in the log of $\simeq 0.1$ depending on the adopted spectral index. Comparing this with our estimate of the intrinsic nuclear luminosity $L_\nu(1\,\mu\mathrm{m})$ above we therefore find that a fraction $f \simeq 10^{-1.34\pm0.3}$, or ~ 0.05, of the quasar's near-infrared continuum is scattered towards us. Applying this same efficiency factor to Osterbrock's (1983) measurement of the non-stellar flux at 513.5 nm corrected for A_V(Gal), we estimate that the intrinsic luminosity of Cygnus A at 486.1 nm (in WHz^{-1}) is given by $\log L_\nu(0.4681\,\mu\mathrm{m})=23.2\pm0.32$, as seen by the scattering medium. To arrive at this estimate we have assumed that (i) the emission is isotropic, (ii) the non-stellar radiation in the near-infrared and optical arises from scattering of a quasar continuum. We note from our estimate that Cygnus A would appear visually as a typical quasar when viewed along the scattering axis, with the host galaxy barely detectable in contrast to the nuclear source.

The actual value of $L_\nu(0.4861\,\mu\mathrm{m})$ which we derive above is of course sensitive to the assumed quasar spectral index, as well as aperture effects. These latter systematic effects could be reduced by using the existing multi-band imaging of Djorgovski *et al.* (1991). The result does at least demonstrate the potential of multifrequency data to estimate the visual luminosity of an object obscured by $\simeq$40 mag of extinction!

7 Implications for the far-infrared continuum

Cygnus A has been detected as a point source by *IRAS* at 12, 25 and 60 μm, but not at 100 μm due to foreground "cirrus" emission in the plane of our Galaxy (Knapp, Bies & van Gorkum 1990). Whilst the far-infrared emission lies well above the extrapolated radio continuum level and the near-infrared luminosity derived above (Section 4.3 and Figure 3), it is not unusual for an AGN of this bolometric power. Ward *et al.* (1988) presented a rough correlation between far-infrared (25–60 μm) and hard X-ray (2–10 keV) luminosities for broad line AGN. Taking *IRAS* fluxes for Cygnus A from Knapp, Bies & van Gorkum (1990), and L_X as before above we find that the 25–60 μm luminosity of Cygnus A (L_{IR}(25-60)=3.5$\times10^{38}$ W) is well within the range of expected values from this correlation, and hence can be accounted for without the presence of a "radio-loud" component.

The nature of the dominant emission mechanism ("thermal vs non-thermal") in the far-infrared spectra of active galaxies is a still a point of controversy (see Carleton *et al.* 1987, Barvainis 1990). Nonetheless, our estimate of the intrinsic near-infrared luminosity of Cygnus A (Section 4.3) allows us to investigate *possible* contributions from different components more reliably than previously.

7.1 Non-thermal components

In their attempts to separate the far-infrared SEDs of X-ray-selected AGN into thermal and non-thermal emission components, Carleton *et al.* (1987) invoked a hypothetical X-ray–near-infrared power law (of index ~ -1.2) extending to 100 μm. Following their method, and using the (absorption-corrected) X-ray and 1 μm continuum luminosities of Cygnus A (Section 4), we find that such a component would dominate the energy output of Cygnus A at 10 and 100 μm, and would have to turn over at $\lesssim$100 μm if there

is continuity with the radio continuum.

A non-thermal component of flatter spectral index in the far-infrared range may also arise in radio-loud AGN, as a high-frequency extension of the radio core spectrum, especially for flat-spectrum "blazar-like" objects such as 3C273 (see Sanders *et al.* 1989 for a compilation of SEDs). For the case of Cygnus A, it is difficult to extrapolate such a component without flux information between 100 and 1000 μm. Antonucci, Barvainis & Alloin (1990) recently presented radio–infrared SEDs of a sample of Lobe-Dominant Quasars (*LDQs*), which show deep minima at rest wavelengths of 1000 μm, presumably due to energy losses in the synchrotron radio spectrum. These results provide some support for a separate, thermal origin of the far-infrared continuum in LDQs, and for Barthel's (1989) "unified scheme" in which LDQs form the "mis-directed jet" population of the core-dominated quasars (which show radio spectrum cut-offs at higher frequencies due to Doppler boosting).

In contrast to the LDQs, Cygnus A shows no such cut-off in its radio–millimetre spectrum (see Salter *et al.* 1989, or Figure 3), which indicates that the core radio spectrum *may* extend into the far-infrared. This is *not* expected in the unified scheme, since the results presented here naturally lead us to re-classify Cygnus A as a LDQ. The reported lack of variability or superluminal motion in Cygnus A (Salter *et al.* 1989, and references therein), as well as the sky-plane orientation of the radio lobes, argues against the presence in Cygnus A of a blazar-like component beamed towards us (cf. 3C273). Instead, it may merely be the case that the radio core of Cygnus A contains a surfeit of (young) high-energy electrons (Wright & Birkinshaw 1984) compared to those LDQs observed to date at 1000 μm. The high-frequency cut-off in Cygnus A would then occur in the (unobserved) sub-millimetre region of its spectrum.

In any case, as noted by many workers, even if the "flat" radio spectrum (spectral index$\simeq -0.25$) extended out to 10 μm, the *IRAS* data show that there remains a significant far-infrared excess, which can only be accounted for by thermal dust emission (Figure 3).

7.2 Thermal (dust) component

From an analysis of their multi-wavelength data for a sample of PG quasars, Sanders *et al.* (1989) favour interstellar dust grains as the primary emitters in the far-infrared domain for non-blazar AGN (see also Barvainis 1990). These quasars display a wide range of optical/UV "bump" strengths in their SEDs. From our estimate of the intrinsic optical luminosity (Section 5.2), or equivalently by normalizing a canonical quasar SED (e.g. Figure 2 of Sanders *et al.* 1989) to L_X or $L_\nu(1\,\mu\mathrm{m})$, it can be shown that the inferred power in the optical/ultraviolet would be more than sufficient to power the entire far-infrared continuum through absorption and subsequent re-emission by dust grains (cf. 3C234, Carleton *et al.* 1984).

It is not possible to gain an accurate picture of the extinction geometry from these arguments, but the optically thick material must intercept a significant fraction of the AGN's optical/UV radiation (assumed emitted isotropically). We do know from the X-ray spectrum that $\simeq$40% of the transmitted 2-10 keV luminosity is absorbed by foreground material (Arnaud *et al.* 1987). On the other hand, although our particular line of sight towards Cygnus A is heavily obscured, the line-emitting high ionization gas (Section 7) and the optical scattering region clearly have a more direct view of the blue–ultraviolet continuum. A covering fraction of $\sim$10–30% for the optically thick material would be in agreement with the torus opening angles suggested by the relative linear sizes of quasars, BLRGs and NLRGs in the unified scheme of Barthel (1989).

Djorgovski *et al.* (1991) fit a single-temperature black-body spectrum to the *IRAS* data for Cygnus A (with emissivity index -1), after subtraction of a parabolic non-thermal continuum. In reality the dust emission from active galaxies must be produced by grains at a range of temperatures, as modelled by Barvainis (1990) and other workers. The lack of a 100 μm detection for Cygnus A, and the possible contributions of other components in the far-infrared, precludes a detailed analysis here. However, we note that the 25–60 μm spectral index of Cygnus A is well within the range of "warm" values found for Seyfert galaxies and quasars by deGrijp *et al.* (1985). The steep 12–25 μm spectral index is consistent with the trend of this quantity with infrared luminosity found for a sample of *IRAS* galaxies by Soifer & Neugebauer (1991), and may be due either to the destruction of the smallest dust grains (which would otherwise emit strongly at these

shorter wavelengths due to to transient heating), or to significant absorption in the 9.7 μm silicate dust feature.

8 The molecular hydrogen line emission

8.1 Luminosity and mass of warm molecular gas

The H_2 v=1–0 S(1) line in Cygnus A is unusually strong, with a luminosity in the line of 1.0×10^{34} W (after including a small correction for the Galactic obscuration given in Table 3). This value is much higher than the average observed for AGN and starburst galaxies, and places Cygnus A amongst the highest luminosity H_2 sources known, comparable with NGC6240, Arp220 and NGC1275.

An important question is whether such strong H_2 line emission is common in high-luminosity AGN. If we assume that the extinction towards the H_2 line emitting regions in Cygnus A is much less than A_V(NC), then the H_2 v=1–0 S(1) line equivalent width would be reduced to approximately 0.3 nm (uncertain by a factor of $\lesssim$2) for an observer with an unobscured view of the nuclear 2.2 μm continuum in Cygnus A (Section 4.3). This equivalent width is comparable to current detection limits, so the paucity of H_2 v=1–0 S(1) detections in high luminosity Seyfert 1s and quasars (Kawara, Nishida & Gregory 1990) may reflect this observational limitation rather than an intrinsic lack of hot molecular gas in these objects.

The H_2 line emission reported here is the first detection of molecular gas in Cygnus A. Mirabel, Sanders & Kazès (1989) searched for CO J=1–0 line emission, and calculated an upper limit of $2\times10^{10}\,M_\odot$ (corrected here to H_0=50) for the mass of cold molecular gas. Although the conversion from CO line luminosity to molecular gas mass in AGN is uncertain (e.g. Maloney & Black 1988), it is still instructive to compare the relative amounts of hot and cold H_2 in Cygnus A with values derived for other AGN under the same assumptions. Following the methods of Kawara, Nishida & Gregory (1990), the mass of hot H_2 obtained from the v=1–0 S(1) line luminosity above is $4\times10^4\,M_\odot$. From the upper limit given by the CO observations we find that the mass ratio of hot H_2 to cold H_2 in Cygnus A is therefore greater than 2×10^{-6}. This limit is higher than the ratios derived for the sample of active galaxies by Kawara, Nishida & Gregory (1990),

but consistent with the ratios of $\sim 10^{-5}$ derived for the central regions of NGC1068 and our own Galaxy (see Rotaciuc *et al.* 1991), if the same conversion factors are adopted.

8.2 Excitation mechanism

The intrinsic H_2 line flux ratio F(v=1–0 S(3))/F(v=1–0 S(1)) is dependent on the particular excitation mechanism of the molecular hydrogen (see Kawara, Nishida & Gregory 1990 for a discussion). However, the uncertainty in our measured ratio (Section 3.2), together with the unknown reddening towards the molecular line emitting regions in Cygnus A, mean that we are currently unable to use this quantity to distinguish between these mechanisms.

Nevertheless, the flux ratio F(v=1–0 S(1))/F(Brγ) does provide a useful diagnostic. Moorwood & Oliva (1990) conclude that for UV fluorescent excitation of H_2 by stars the maximum value of this ratio is about 1.0. The addition of a UV power-law source from an AGN would reduce the ratio further below this value, so we do not consider this a viable mechanism for Cygnus A.

Higher values of this ratio are possible in models in which the molecular gas is heated by X-rays, as discussed by Lepp & McCray (1983) and Krolik & Lepp (1989). The H_2 v=1–0 S(1) line luminosity derived from our observations agrees very roughly with that expected from their model predictions that $\sim 10^{-5}$ to 10^{-3} of the 2–10 keV X-ray luminosity should be radiated in this line. A better diagnostic is provided by the line flux ratios F(v=1–0 S(1))/F(Brγ) and F([OI]630.0 nm)/F(Hα), since the neutral oxygen species is also believed to originate in partially-ionized X-ray heated zones. Division by the hydrogen recombination line fluxes removes the effect of differential extinction, and indicates the energy balance between the ionized and X-ray heated regions (Mouri *et al.* 1989). The values of these ratios for Cygnus A lie close to the relation derived from the X-ray heating model (see Figure 1 of Mouri *et al.*), and represent the most extreme observed values consistent with this model.

A further viable excitation mechanism of the H_2 emission is through shock waves, which may result from star-forming activity or an AGN-driven wind (Mouri *et al.* 1989, and references therein). We are unable to rule out these processes with our current observations. However, the location of Cygnus A on the F(v=1–0 S(1))/F(Brγ) vs.

F([OI]630.0nm)/F(Hα) diagram is in closer agreement with the X-ray heating model than with the separate correlation applicable to the star-forming galaxy nuclei (Mouri *et al.* 1989). The radio jet, with a power $L_{jet} \simeq 5 \times 10^{38}$ W (Blandford & Rees 1974), is a promising power source for the H_2 emission from Cygnus A *if* the jet drives slow shocks into dense molecular material. For shock velocities in the range 30–50 km s^{-1}, the fraction of shock power converted into v=1–0 S(1) line emission has a maximum value of about 0.02 (Draine, Roberge & Dalgarno 1983; Draine & Woods 1990). Thus, if $\sim 10^{-3}$ of the jet luminosity is converted into such shocks, the observed H_2 1–0 S(1) line luminosity in Cygnus A could be produced. As an illustration, the dynamic pressure $L_{jet}/\pi r^2 c$ associated with the jet at the nozzle in the Blandford & Rees (1974) model is 6×10^{-6} Pa. Such a pressure could drive a shock of velocity 30 km s^{-1}if the cloud density were $\simeq 10^6$ H_2 molecules cm^{-3}.

9 [SiVI]1.962 μm and the high-ionization lines

9.1 Sources of [SiVI]1.962 μm emission in galaxies

The Si^{4+} ion has a high ionization potential of 167 eV, and the [SiVI]1.962μm transition has a high critical density of $\sim 10^8$ cm^{-3}, similar to that for the optical transitions of [NeV] and [FeVII] which are commonly observed in the spectra of AGN. The only classes of Galactic source known to display this line are novae (e.g. Benjamin & Dinerstein 1990) and planetary nebulae (Ashley & Hyland 1988). The line has not yet been detected in supernovae or their remnants (see Oliva & Moorwood 1990), although further searches should be made in this difficult part of the K window.

It is a useful exercise to investigate whether the [SiVI] line should be detectable at any level in normal galaxies. We assume that the line arises mainly in Planetary Nebulae (*PNe*), given their longevity relative to the other sources noted above. Optimistically taking the high-excitation PN NGC6302 as typical (Ashley & Hyland 1988), we adopt a [SiVI] line luminosity per PN of 2×10^{27} W. From a study of stellar populations in the Local Group, Maciel (1983) finds the specific density of PNe to be roughly $1\text{–}4 \times 10^{-7}$ $M_\odot{}^{-1}$. Combining this estimate with the relation between stellar mass and K-band (2.2μm) luminosity established for spiral galaxies by Thronson & Greenhouse (1988), we derive a

[SiVI] line equivalent width of ~0.01 nm which is below current detection limits. It is unlikely that the line equivalent width is much higher in other stellar systems, since the late-type stars which usually dominate the K-band luminosity are also the progenitors of PNe.

9.2 [SiVI]1.962 μm emission in Cygnus A

It follows from these considerations, then, that the strong [SiVI] line reported here in Cygnus A cannot arise from a normal stellar population. Similar arguments have been used in the past to establish the non-stellar nature of the high-ionization optical lines. Whilst these optical lines can be strongly attenuated by fairly small amounts of dust extinction, observations of the [SiVI]1.962 μm transition may provide a useful test for the presence of highly ionized gas around heavily dust-enshrouded AGN.

A number of mechanisms have been suggested to explain the formation of the high excitation species in AGN. These include collisional ionization (Nussbaumer & Osterbrock 1970), pure photo-ionization (e.g. Korista & Ferland 1989), and photo-ionization in combination with shock processes (Viegas-Aldrovandi & Contini 1989). Only Korista & Ferland (1989) present predicted strengths for the [SiVI] line. Taking optical line fluxes from Osterbrock & Miller (1975), and correcting for A_V(Gal) and A_V(NL), we find that the Korista & Ferland model is quite successful in accounting for the fluxes of [NeV]342.6 nm, [OIII]500.7 nm, [FeVII]608.7 nm (upper limit), and [SiVI]1.962 μm relative to narrow Hβ. The largest discrepancy is for [OIII], which is underestimated, since Korista & Ferland exclude the "classical" NLR from their model.

In the Korista & Ferland model, the emitting gas is the low-density (n_e~1 cm^{-3}) warm phase of the host galaxy's interstellar medium. Other workers have previously suggested that the high-excitation lines could originate in gas of much higher density, perhaps intermediate in scale between the BLR and NLR (e.g. Penston *et al.* 1984). As pointed out by Roche *et al.* (1991) in connection with their mid-infrared observations of NGC1068 and NGC4151, the 10.52 μm transition of [SiV] in AGN may allow us to discriminate between these possibilities, as this line is predicted to be strong only at densities below its critical density of ~10^4 cm^{-3}. A measurement of this line in Cygnus A has not yet been attempted, but a simple scaling of the Korista & Ferland (1989) model

spectrum by our measured [SiVI] flux predicts a high [SIV]10.52 μm line flux of approximately 1.2×10^{-16} W m^{-2}. If the S^{3+} species is formed in high-density gas, this line should be much weaker due to collisional de-excitation.

Finally, there is the question of the high line width we derive for [SiVI]1.962 μm after de-blending (Section 3.3 and Figure 2). Clive Tadhunter (private communication) reports that the [FeVII] lines in his long-slit optical spectra of Cygnus A exhibit broader profiles (FWHM$\sim$700 km s^{-1}) than the Balmer lines, which lends credence to our result for [SiVI]. The marginally higher line width we find for [SiVI]1.962 μm (FWHM=1200$\pm$300 km s^{-1}) is also consistent with the line-width/critical density correlation established by deRobertis & Osterbrock (1986) for Seyfert 2 galaxies.

10 Conclusions

10.1 Cygnus A as a buried quasar

There is as yet no direct evidence for an obscured BLR in Cygnus A. However, the lack of broad wings to the observed Paschen α line profile can be explained by a line-of-sight extinction A_V(BL)>24 mag. Using a series of reasonable assumptions we are able to estimate the extinction towards the 2.2 μm nuclear continuum source to be A_V(NC)=37$\pm$6 mag, which is consistent with the gas column density derived independently from the low-energy absorption of the compact X-ray component. The strong H_2 v=1–0 S(1) and [OI]630.0 nm line emission from Cygnus A are naturally accounted for by models in which this X-ray source is responsible for heating the neutral gas. The observed non-stellar continuum in the nuclear regions, which is an appreciable fraction of the total at optical and near-infrared wavelengths, may readily be produced by Thomson scattering of $\sim$5% of the nuclear luminosity towards us by electrons with a clear view of the nuclear source.

There is also a more general energetic argument in favor of the hypothesis that Cygnus A is host to a quasar-like nucleus blocked from direct view by a large column of gas and dust. The *total* observed luminosity of Cygnus A (e.g. Tadhunter, Scarrott & Rolph 1990), which in practice means the sum of the infrared (1–1000 μm) and hard X-ray emission, is 6.4×10^{38} W. This luminosity is equal to, or exceeds, that from typical

BLRGs. The far-infrared excess over the interpolated near-infrared to radio continuum is consistent with a redistribution of energy from the optical/ultraviolet into the mid- and far-infrared by circumnuclear dust.

10.2 Future observational tests

A number of key observations could test these conclusions further, and some of them are already underway.

10.2.1 Mid-infrared spectroscopy

Spectroscopy in the 8–13 μm window should reveal a strong 9.7 μm silicate absorption feature, while a measurement of [SIV]10.52 μm would discriminate between some of the current models of the high ionization emission line region. A 10 μm spectrum of Cygnus A was obtained on our behalf by Tom Geballe in May 1991, using the 16-element mid-infrared spectrometer CGS3 with a 3 arcsec aperture. Modelling this spectrum as a power law extinguished by foreground dust of Galactic composition gave a silicate optical depth $\tau_{9.7} \simeq 1.0 \pm 0.3$, and an intrinsic power law spectral index of $\simeq -2$, compatible with the 10–15 μm colours. However, the total flux level in the spectrum is only one third of that expected from the broad-band photometry of Rieke & Low (1972) and the *IRAS* 12-μm flux, possibly due to errors in pointing. If confirmed, the observed value for $\tau_{9.7}$ above would imply a dust column equivalent to $A_V \simeq 20$ mag, in the simple case of foreground absorption by "cold" material.

10.2.2 The far-infrared–sub-millimetre continuum

Stringent limits on the possible *non*-thermal contribution in the far-infrared are required, however, before a more detailed modelling of the dust distribution can be attempted (e.g. Lawrence *et al.* 1991). Sub-millimetre photometry (at 450 μm) will place a constraint on any contribution from a high-frequency extension of the radio spectrum. Such an observation is only just possible using current instrumentation on the James Clerk Maxwell Telescope (*JCMT*) on Mauna Kea, but will become straightforward once the receiver system *SCUBA* (Sub-millimetre Continuum Bolometer Array) is commissioned on this telescope in a few years time.

10.2.3 Detection of the buried quasar in Cygnus A

Optical spectro-polarimetry would confirm the presence of an obscured quasar nucleus through detection of broad polarized components to the Balmer lines, and would shed light on the nature of the scattering medium. The hard X-ray source may exhibit short-term variability (although the amplitude of the variations would be diluted by the extended X-ray emission). Finally, with envisaged ground-based and space-borne instrumentation it may be possible to detect transmitted broad hydrogen recombination line emission from Cygnus A (perhaps by observing the Pfund β line), or to set a better limit on a transmitted broad line component of Paschen α. Such observations would be difficult but feasible in the future.

Acknowledgements

We would like to thank the telescope operators Joel Aycock and Dolores Walther for their expert handling of UKIRT. We are especially grateful to Tom Geballe for his assistance at the telescope, and for performing observations on our behalf through the UKIRT Service Observing programme. We also thank Clive Tadhunter for his comments on earlier versions of this work, and for communicating his results in advance of publication.

References

Antonucci, R. R. J., Barvainis, R. & Alloin, D., 1990. *Astrophys. J.*, **353**, 416.

Antonucci, R. R. J. & Miller, J. S., 1985. *Astrophys. J.*, **297**, 621.

Arnaud, K. A., Fabian, A. C., Eales, S. A., Jones, C. & Forman, W., 1984. *Mon. Not. R. astr. Soc.*, **211**, 981.

Arnaud, K. A., Johnstone, R. M., Fabian, A. C., Crawford, C. S., Nulsen, P. E. J., Shafer, R. A. & Mushotzky, R. F., 1987. *Mon. Not. R. astr. Soc.*, **227**, 241.

Ashley, M. C. B. & Hyland, A. R., 1988. *Astrophys. J.*, **331**, 532.

Barthel, P. D., 1989. *Astrophys. J.*, **336**, 606.

Barvainis, R., 1987. *Astrophys. J.*, **320**, 537.

Barvainis, R., 1990. *Astrophys. J.*, **353**, 419.

Benjamin, R. A. & Dinerstein, H. L., 1990. *Astron. J.*, **100**, 1588.

Binette, L., Calvet, N., Cantó, J. & Raga, A. C., 1990. *Publs astr. Soc. Pacific*, **102**, 723.

Blandford R. J. & Rees, M. J., 1974. *Mon. Not. R. astr. Soc.*, **169**, 395.

Carleton, N. P., Willner, S. P., Rudy, R. J. & Tokunaga, A. T., 1984. *Astrophys. J.*, **284**, 523.

Carleton, N. P., Elvis, M., Fabbiano, G., Willner, S. P., Lawrence, A. & Ward, M. J., 1987. *Astrophys. J.*, **318**, 595.

deGrijp, M. H. K., Miley, G. K., Lub, J. & de Jong, T., 1985. *Nature,* **314**, 240.

deRobertis, M. M. & Osterbrock, D. E., 1986. *Astrophys. J.*, **301**, 727.

Djorgovski, S., Weir, N., Matthews, K. & Graham, J. R., 1991. *Astrophys. J. Lett.*, **362**, L67.

Draine, B. T., Roberge, W. G. & Dalgarno, A., 1983. *Astrophys. J.*, **264**, 485.

Draine, B. T. & Woods, D. T., 1990. *Astrophys. J.*, **363**, 464.

Gaskell, C. M. & Ferland, G. J., 1984. *Publs astr. Soc. Pacific,* **96**, 393.

Hummer, D. G. & Storey, P. J., 1987. *Mon. Not. R. astr. Soc.*, **224**, 801.

Kawara, K., Nishida, M. & Gregory, B., 1990. *Astrophys. J.*, **352**, 433.

Korista, K. T. & Ferland, G. J., 1989. *Astrophys. J.*, **343**, 678.

Knapp, G., Bies, W. & van Gorkum, J., 1990. *Astron. J.*, **99**, 476.

Kriss, G., 1988. *Astrophys. J.*, **324**, 809.

Krolik, J. H. & Lepp, S., 1989. *Astrophys. J.*, **347**, 179.

Lawrence, A., Rowan-Robinson, M., Efstathiou, A., Ward, M. J., Elvis, M., Smith, M. G., Duncan, W. D. & Robson, E. I., 1991. *Mon. Not. R. astr. Soc.*, **248**, 91.

Lepp, S. & McCray, R., 1983. *Astrophys. J.*, **269**, 560.

Lilly, S. J. & Hill, G. J., 1987. *Astrophys. J. Lett.*, **315**, L103.

Maciel, W. J., 1983. in: *Planetary Nebulae*, IAU Symposium No. 131, ed. S. Torres-Peimbert, (Dordrecht: Reidel), p. 73.

Malkan, M. A., 1983. *Astrophys. J. Lett.*, **264**, L1.

Maloney, P. & Black, J. S. 1988. *Astrophys. J.*, **325**, 389.

Mathis, J. S., 1990. *Ann. Rev. Astr. Astrophys.*, **28**, 37.

M^{c}Alary, C. W. A. & Rieke, G. H. 1988. *Astrophys. J.*, **333**, 1.

Mirabel, I. F., Sanders, D. B. & Kazès, I., 1989. *Astrophys. J. Lett.*, **340**, L9.

Moorwood, A. F. M. & Oliva, E., 1990. *Astr. Astrophys.*, **239**, 78.

Morrison, R. & McCammon, D., 1983. *Astrophys. J.*, **270**, 119.

Mouri, H., Taniguchi Y., Kawara, K. & Nishida, M., 1989. *Astrophys. J. Lett.*, **346**, L73.

Neugebauer, G., Green, R. F., Matthews, K., Schmidt, M., Soifer, B. T. & Bennett, J., 1987. *Astrophys. J. Suppl. Ser.*, **63**, 615.

Nussbaumer, H. & Osterbrock, D. E. 1970. *Astrophys. J.*, **161**, 811.

Oliva, E. & Moorwood, A. F. M. 1990. *Astrophys. J. Lett.*, **348**, L5.

Osterbrock, D. E. & Miller, J. S. 1975. *Astrophys. J.*, **197**, 535.

Osterbrock, D. E., 1983. *Publs astr. Soc. Pacific,* **95**, 12.

Penston, M. V., Fosbury, R. A. E., Boksenberg, A., Ward, M. J. & Wilson, A. S., 1984. *Mon. Not. R. astr. Soc.*, **208**, 347.

Pierce, M. J. & Stockton, A., 1986. *Astrophys. J.*, **305**, 204.

Puxley, P. J., 1991. *Mon. Not. R. astr. Soc.*, **249**, 11P.

Rieke, G. H. & Low, F., 1972. *Astrophys. J. Lett.*, **176**, L95.

Roche, P. F., Smith, C. H., Aitken, D. K. & Ward, M. J., 1991. *Mon. Not. R. astr. Soc.*, **248**, 606.

Rotaciuc, V., Krabbe, A., Cameron, M., Drapatz, S., Genzel, R., Sternberg, A. & Storey, J. W. V., 1991. *Astrophys. J. Lett.*, **370**, L23.

Rudy, R. J., 1984. *Astrophys. J.*, **284**, 33.

Salter, C. J. *et al.*, 1989. *Astr. Astrophys.*, **220**, 42.

Sanders, D. B., Phinney, E. S., Neugebauer, G., Soifer, B. T. & Matthews, K., 1989. *Astrophys. J.*, **347**, 29.

Soifer, B. T. & Neugebauer, G., 1991. *Astron. J.*, **101**, 354.

Tadhunter, C. N., Scarrott, S. M. & Rolph, C. D., 1990. *Mon. Not. R. astr. Soc.*, **246**, 163.

Thronson, H. A. & Greenhouse, M. A., 1988. *Astrophys. J.*, **327**, 661.

Viegas-Aldrovandi, S. M. & Contini, M., 1989. *Astrophys. J.*, **339**, 689.

Ward, M. J., Done, C., Fabian, A. C., Tennant, A. F. & Shafer, R. A., 1988. *Astrophys. J.*, **324**, 767.

Wright, M. & Birkinshaw, M., 1984. *Astrophys. J.*, **281**, 135.

Yates, M. G. & Garden, R. P., 1989. *Mon. Not. R. astr. Soc.*, **241**, 167.

Chapter 5

Multiwavelength spectroscopy of Markarian 463(E)

Prologue: The *IRAS* survey in the mid-1980s revealed a new class of active galaxy which had been largely overlooked in previous surveys. These so-called "ultra-luminous" infrared systems have similar bolometric luminosities, and a comparable space density in the local universe, to optically-selected quasars. Unlike classical quasars, however, these objects radiate almost all of their power at far-infrared wavelengths, indicating that dust plays a important role in re-processing the energy emitted by sources hidden from direct view. At least some of these sources are known to harbour non-thermal nuclei, but extinction by dust makes it hard to assess their contribution to the bolometric energy output, or their relationship to more familar samples of active galaxies.

An example of this kind of activity is provided by the eastern nucleus of the galactic merger Markarian 463. In order to learn more about the intrinsic properties of this active nucleus and the effects of extinction on its appearance from X-rays to far-infrared wavelengths, we obtained near-infrared spectra of Markarian 463(E) over the period 1990–1991, and re-examined archival data from the *International Ultraviolet Explorer* satellite.

This work has been prepared for submission to *Monthly Notices of the Royal Astronomical Society* (Blanco, Ward & Wright 1992).

Summary

We present new near-infrared spectroscopy of the eastern nucleus of the luminous merging galaxy Markarian 463, detecting transmitted broad hydrogen recombination line emission from the eastern nucleus for the first time. We find an extinction A_V(NL)=2.2 mag towards the narrow lines in Markarian 463(E), which must arise in foreground dust, and an extinction A_V(BL)=$5.3^{+3.9}_{-2.2}$ mag towards the broad line gas. From the extinction-corrected broad line luminosity, through the line and continuum correlations established for Seyfert 1 galaxies and quasars, we account for the spectral properties

of Markarian 463(E) from far-infrared to X-ray frequencies in terms of an intrinsically luminous, but moderately obscured, Seyfert 1 nucleus. A simple model of the *IRAS* emission ascribes almost all of the high far-infrared luminosity of Markarian 463 to this active nucleus, and recent mid-infrared spectroscopy confirms this conclusion.

While we are unable to exclude a significant contribution from dust scattering to the polarized optical spectrum of Markarian 463(E), we find that electron scattering of ~5% of the nuclear radiation is successful in accounting for the observed soft X-ray and ultraviolet continuum, and the polarization of the continuum at 2.2 μm.

Further observations of the secondary nucleus Markarian 463(W) are necessary to establish the nature of its excitation of the line spectrum, and its contribution at other wavelengths to the total emission from Markarian 463.

1 Introduction

1.1 Background

Of the most luminous sources discovered by the *IRAS* survey, a high fraction have since been shown to be merging or tidally-interacting systems, with optical spectra resembling type 2 Seyferts (Sanders *et al.* 1988a, Leech *et al.* 1989). It has been proposed that a subset of these so-called "ultra-luminous" infrared galaxies, which exhibit high infrared/blue luminosity ratios and "warm" 25–60 μm colours, form an intermediate population in an evolutionary scheme for the origin of quasars (Sanders *et al.* 1988b, Hutchings & Neff 1991), in which a large concentration of gas in the central regions of merging galaxies provides the raw material for a massive starburst, and subsequently fuels a nascent Active Galactic Nucleus (*AGN*). Such ideas are the subject of controversy, however, due to the deeply-buried nature of the heating sources in these objects, and other mechanisms have been proposed (e.g. Harwit *et al.* 1987, Armus, Heckman & Miley 1989, Thronson *et al.* 1990). Therefore it is important to quantify the contributions of the various energy sources proposed to the prodigious energy output of these systems.

Only after accounting for the effects of obscuration and viewing angle can one proceed to establish intrinsic differences between the various classes of AGN. Since the pioneering study of NGC 1068 by Antonucci & Miller (1985) it has been established that at least

some Seyfert 2 galaxies possess Seyfert 1 nuclei which are obscured from direct view at optical wavelengths by a large column of gas and dust. These sources may, however, be visible indirectly either through high-excitation narrow line emission, or through scattering of nuclear radiation towards us (either by dust grains or free electrons), from extended line-emitting regions which have a "clear view" of the continuum source.

While such signatures are useful in identifying obscured nuclear activity, their detectability and strength depend on the properties of the illuminated medium as well as those of the source. However, by making resolved observations of recombination lines in the near-infrared (1–5 μm) it is possible to penetrate the obscuring material in some Seyfert 2 galaxies, and detect direct transmitted line radiation from their optically-obscured Broad Line Regions (*BLRs*) (e.g. Chapter 3), as well as excited line emission from hot molecular gas which may be associated with the obscuring matter. Moreover, the long wavelength baseline afforded by combining optical and infrared spectra of such active galaxies permits accurate extinction estimates to be made for their less obscured narrow line-emitting regions.

1.2 Infrared spectroscopy of Markarian 463

We present here new near-infrared spectra of the the eastern nucleus of the luminous merging system Markarian 463, at a redshift of 0.0505. Optical images of the galaxy show tidal tails indicative of an advanced stage merger between two late-type galaxies (Mazzarella & Boroson 1987). Markarian 463 is known to possess a double nucleus at optical, near-infrared and radio wavelengths, with the eastern component by far the most prominent at the longer wavelengths. Broad- and narrow-band imaging by Hutchings & Neff (1989) has revealed extended [OIII] emission from a region around Markarian 463(E) aligned roughly with the radio continuum structure (Neff & Ulvestad 1988, Condon, Frayer & Broderick 1991). Since the observed ultraviolet continuum of Markarian 463 is relatively weak, it follows that the source of ionizing photons is either intrinsically anisotropic, or obscured from our direct view (cf. Haniff, Wilson & Ward 1991).

Miller & Goodrich (1990) have found that in polarized light the optical spectrum of Markarian 463(E) resembles that of a Seyfert 1 nucleus. The favoured interpretation in terms of the "unified model" described above is that the BLR is hidden from direct view

by a non-spherical distribution of optically thick matter (such as a dusty torus), but remains indirectly visible via scattered radiation from an extended medium (electrons, and/or dust grains) which "mirrors" its more direct view of the AGN towards us.

The new observations presented here provide the first direct view of this optically-hidden AGN, and allow us to estimate the extinction towards its line-emitting regions. We then examine the contribution of these components to the appearance of Markarian 463 at other wavelengths from 10 keV to 1000 μm, either via direct radiation from a quasar nuclear continuum, scattering from this continuum, or absorption and re-radiation of the continuum energy by dust in the circumnuclear regions.

Throughout this chapter we assume H_0=50 km s^{-1}Mpc^{-1}.

2 Observations and reduction

We have obtained new near-infrared spectra of the central regions of Markarian 463(E) in the J and K atmospheric windows, and we have retrieved archival spectra taken with instruments on the *InternationalUltravioletExplorer* satellite (*IUE*). The observations are described below and summarized in Table 1.

Table 1: *Journal of observations.*

UT Date	Telescope/ Instrument	λ–λ (μm)	Resolution [1] (km s^{-1})	Exposure /point (s)
1984 Apr 17	IUE/ SWP	0.120–0.195	980	25500
1984 Apr 18	IUE/ LWR	0.190–0.320	970	24360
1990 Dec 31	UKIRT/ CGS2	1.119–1.227	1010	120 [2]
1991 Apr 11	UKIRT/ CGS4	1.914–2.332	1050	520 [2]

Notes:

1. The quoted resolutions are appropriate to the middle of the wavelength range covered.

2. Exposure times for the infrared spectroscopy at UKIRT include an equal amount of time spent on the source and the sky.

2.1 Infrared spectroscopy

Infrared spectroscopy of Markarian 463(E) was performed at the f/36 Cassegrain focus of the U. K. Infrared Telescope (*UKIRT*). The J-window spectrum shown in Figure 1

was taken with the seven-element spectrometer CGS2, using a 5 arcsec circular aperture which was centred on the peak of 1.2 μm emission in Markarian 463, corresponding to the eastern nucleus Markarian 463(E) (Mazzarella *et al.* 1990). Standard slow-chopping

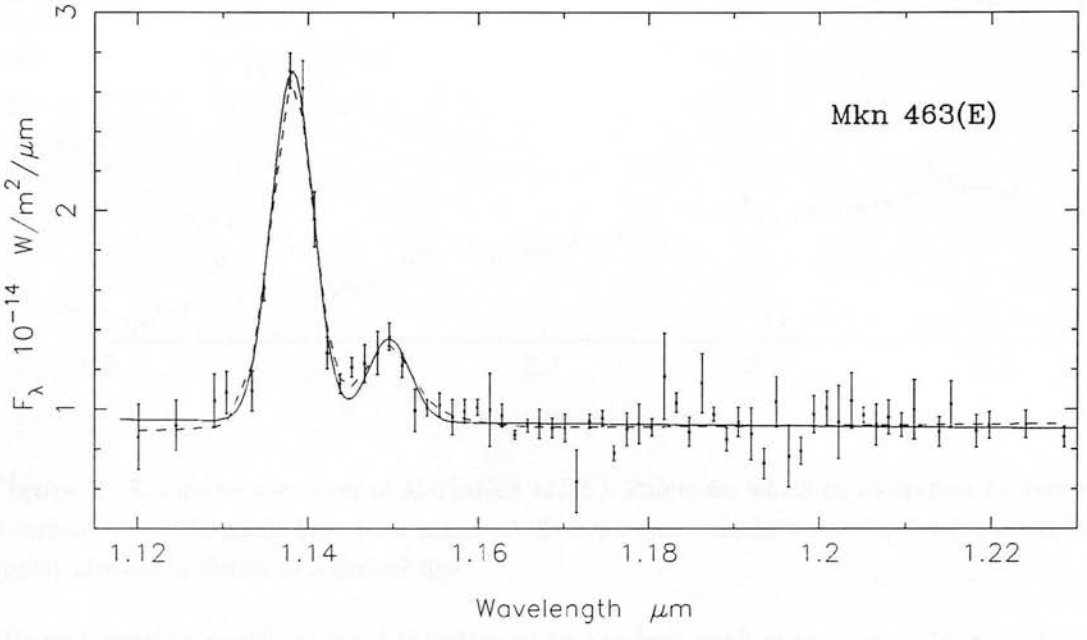

Figure 1: *J-window spectrum of Markarian 463(E), taken with a 5-arcsec circular aperture. The solid line shows the fit of Gaussian profiles to these lines, the dashed line shows the effect of including broad components to these lines.*

procedures were used to subtract the sky background, and the grating was stepped in increments of 1/3 resolution element to achieve adequate sampling of the line profiles. The spectrum was calibrated using the nearby UKIRT standard star BS5235 (spectral type G0IV). Accurate wavelength calibration and determination of the resolution were obtained by observing the HeI 1.0830 μm line in the planetary nebula NGC3242.

The more recent spectrum presented in Figure 2 was obtained as part of the commissioning of the 2D array infrared spectrometer CGS4, which utilizes a 58×62 InSb array as a detector, with the longer dimension oriented perpendicular to the dispersion at a pixel scale of 3 arcsec. The 75 lines/mm grating in first order gave a resolution of 920 km s^{-1} (FWHM over two detectors) through the 3-arcsec wide slit as measured from the spectrum of an arc lamp mounted in the spectrometer's optical path. To provide a greater sampling factor and to minimize gaps in the spectrum due to bad pixels, four

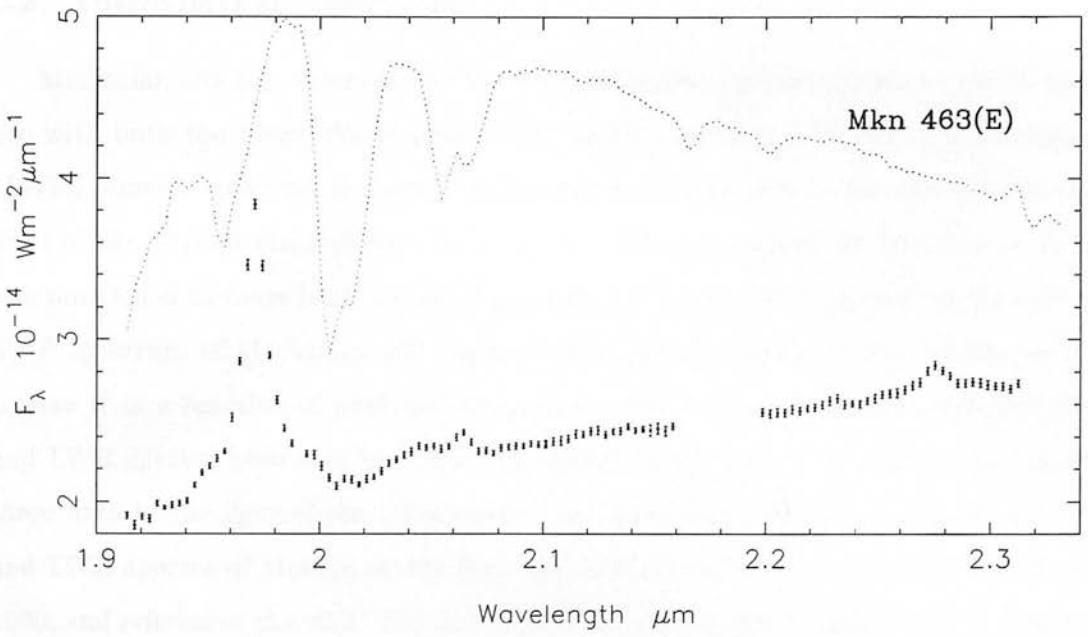

Figure 2: *K-window spectrum of Markarian 463(E). Points for which no correction for telluric absorption could be made have been removed. The raw spectrum of a standard star observed at similar airmass is shown as a dotted line.*

adjacent grating positions were interleaved to produce each spectrum. The seeing was measured to be better than 1 arcsec throughout the observation, which enabled us to centre the spectrum of Markarian 463(E) on a single row of the detector array. Since emission from the host galaxy was detectable over the entire length of the 51-arcsec slit, sky subtraction was achieved by "nodding" the telescope between object and sky after each 20 s exposure; the final spectrum shown is the co-addition of 13 of these (object−sky) pairs.

Correction for telluric absorption was carried out in the manner described in Chapter 2, using the standard star BS5447 (F2V) observed at a similar airmass. The raw spectrum of this early-type star displayed strong Brackett γ absorption; we have therefore removed those points affected from our final spectrum (Figure 2). BS5477 also provided the primary flux calibration, which was checked against other photometric standards observed on the same night, and is believed to be accurate to about 10%.

2.2 Ultraviolet spectroscopy

Markarian 463 was observed by the *InternationalUltravioletExplorer* (*IUE*) satellite with both the Short Wavelength Prime (*SWP*) and Long Wavelength Redundant (*LWR*) cameras spanning the wavelength range from Lyman α to the short-wavelength limit of the Earth's atmosphere (Table 1). For each observation the 10-arcsec wide slit was positioned to cover both nuclei. Kollatschny & Fricke (1984) presented the reduced SWP spectrum of Markarian 463 together with spatial profiles of this continuum and Lyman α as a function of position along the slit 10×15 arcsec slit; the combined SWP and LWR spectra have also been used by Kinney *et al.* (1991). In order to re-examine these data in the light of the other results presented here, we have retrieved the SWP and LWR spectra of Markarian 463 from the *IUE Low Dispersion Archive* (see Murray 1990, and references therein). The combined SWP+LWR spectrum is shown in Figure 3.

The SWP portion of the spectrum is of noticeably inferior quality to that presented

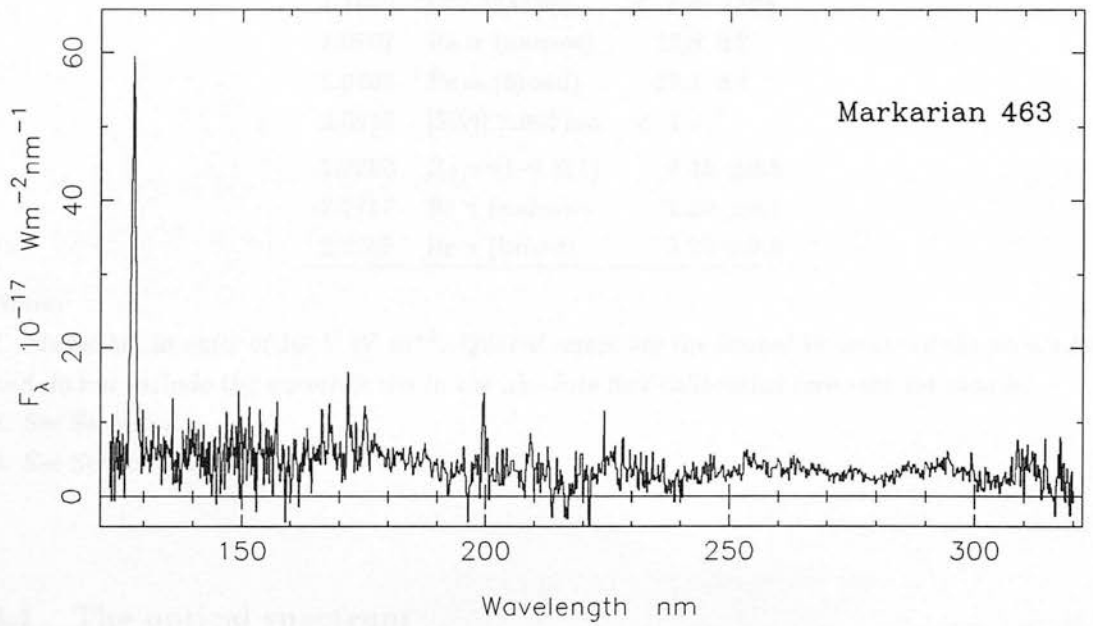

Figure 3: *Combined SWP+LWR spectrum of Markarian 463. In the overlap region, data from the SWP spectrum were used in preference to those of the LWR.*

by Kollatschny & Fricke (1984) produced from the same raw data, since it was reduced with an automatic technique as part of the archiving process. However it is sufficient for our purposes.

3 Results and comparison with existing data

Although at optical wavelengths the emission-line spectrum of Markarian 463(E) resembles that of a classical Seyfert 2, and this similarity appears to extend to the J-band (Figure 1), it is immediately apparent that our K-window spectrum reveals a strong broad component to the Paschen α and Brackett γ lines. Our spectra cover a number of atomic and molecular transitions, for which we have derived fluxes or upper limits listed in Table 2, and which we describe below, after first summarizing the pertinent optical data available in the literature.

Table 2: *Fitted line fluxes for Markarian 463(E).*[1]

λ_{obs}	Line	Flux
0.1278	Ly α	34.1 $\pm$2 [2]
1.1382	HeI 1.0833 μm	10.9 $\pm$0.5
1.1495	Pa γ	2.6 $\pm$0.3
1.1859	OI1.1287 μm	$<$ 1.4 (3σ)
1.9707	Pa α (narrow)	13.8 $\pm$2
1.9707	Pa α (broad)	19.1 $\pm$4
2.0615	[SiVI] 1.962 μm	$<$ 4.2 [3]
2.2292	H_2 v=1–0 S(1)	0.35 $\pm$0.8
2.2757	Br γ (narrow)	1.20 $\pm$0.1
2.2757	Br γ (broad)	3.20 $\pm$0.8

Notes:

1. Fluxes are in units of 10^{-17} W m^{-2}. Quoted errors are the formal 1σ errors of the profile fits, and do not include the uncertainties in the absolute flux calibration (see text for details).

2. See Section 3.3.

3. See Section 3.2.2.

3.1 The optical spectrum

Low resolution spectra covering the optical window, and including both nuclei of Markarian 463 in the same aperture, have been presented by deBruyn & Sargent (1978) and Kinney *et al.* (1991). Spectroscopy at a number of positions has been performed by Hutchings & Neff (1989). Leech *et al.* (1989) also present a spectrum of the eastern nucleus as part of their survey of infrared luminous galaxies.

Shuder & Osterbrock (1981) tabulated line fluxes for Markarian 463(E) and Markarian 463(W), observed at 0.5 nm resolution with a 2.4×4 arcsec aperture. We have confirmed the fluxes of the brighter lines with our own spectrophotometry at lower sensitivity. We therefore use the fluxes tabulated by these authors for comparison with our optical data, and assign a flux calibration uncertainty of 10% to these data.

3.1.1 Markarian 463(E)

The broad, blueward-asymmetric bases to the [OIII], [OII] and Balmer lines are readily apparent in the spectrum of Markarian 463(E) presented by Leech *et al.* (1989), and a more detailed view of these line profiles is presented by Hutchings & Neff (1989). At the lower resolution employed for the ultraviolet and infrared observations we present here, the corresponding lines at these wavelengths appear much more symmetrical. For comparison purposes, we therefore smoothed the Hβ profile presented by Hutchings & Neff (1989) to a comparable resolution to our observations ($\simeq$950 km s^{-1}), and found that the resulting degraded line profile is well described by a Gaussian function of intrinsic FWHM=1200 km s^{-1}.

Miller & Goodrich (1990) also comment on the broad bases to the [OIII] lines in their flux spectrum of Markarian 463(E), and furthermore note that these features appear to be absent in their *polarized* flux spectrum. This could imply a change in polarization across the [OIII] profile which warrants further investigation, in Markarian 463(E) and in other Seyfert 2 galaxies displaying asymmetric profiles.

3.1.2 Markarian 463(W)

Only Shuder & Osterbrock (1981) present line fluxes for this nucleus, though relative spectrophotometry of the Hβ and O[III] lines has been presented by Hutchings & Neff (1989). Their spatial profiles of the blue continuum also show that Markarian 463(W) is more extended than Markarian 463(E), which is suggestive of a star-forming origin of the blue light. Classification of the emission spectrum of this nucleus is difficult due to this underlying strong (stellar) continuum. Shuder & Osterbrock (1981) classified Markarian 463(W) as a Seyfert 2, but the line ratios clearly show that its excitation is much lower than that of Markarian 463(E). To quantify this effect, we examined the

diagnostic line ratios [SII]/Hα, [NII]/Hα and [OI]/Hα, all expressed relative to [OIII]/Hβ (e.g. Veilleux & Osterbrock 1987). Of the other potential diagnostics available in the optical, the [OII]372.7nm line is almost certainly *not* suitable due to contaminating emission from the extended NLR gas photo-ionized by Markarian 463(E) (Hutchings & Neff 1989). The four line flux ratios place Markarian 463(W) in the LINER category, but only just; if the stellar absorption lines underlying this spectrum are stronger than estimated by Shuder & Osterbrock, its nebular emission line spectrum would be that of a high-excitation starburst.

3.2 The infrared spectra of Markarian 463(E)

3.2.1 1.119–1.227 μm

The HeI 1.083μm and Paschen γ lines are clearly resolved in our CGS2 spectrum of Markarian 463(E). The HeI 1.0833μm line has been observed previously by Rudy *et al.* (1989a) at comparable and lower resolutions, but the data presented here are of much higher quality.

At the resolution used for these observations we may neglect the intrinsic asymmetries of these lines and use Gaussian profiles to determine the fluxes. Two Gaussians of equal width and fixed wavelength separation, superimposed on a linear continuum, were therefore fitted to the HeI and Paschen γ lines in our spectrum; the resulting fit is shown as a solid line in Figure 1. The fitted width of these Gaussians corresponds to an intrinsic (resolution-corrected) FWHM of 1125$\pm$50km s^{-1}, in excellent agreement with the value expected from the profile of Hβ (Section 3.1.1).

In the light of the more recent spectrum obtained in the K window, a further fit was made to the J window spectrum in an attempt to detect or set a limit on a broad component to the Paschen γ line. The situation is complicated by the line's proximity to HeI 1.0833μm, which would also be expected to possess broad wings. Therefore we included an additional broad Gaussian component to each of the HeI and Paschen γ lines in the fitting procedure outlined above. The intrinsic narrow component widths were held fixed at 1125km s^{-1} FWHM, while the broad components were constrained to a FHWM of 5000km s^{-1} for reasons given below. To our surprise, we find that the inclusion of such components *did* improve the fits significantly, with a resulting broad

line Paschen γ flux of $(1.9\pm1)\times10^{-17}$ W m^{-2}, and a flux in the narrow component 40% lower than before. Only an upper limit of 4×10^{-17} W m^{-2} was obtained for broad HeI 1.0833 μm. This fit is shown as a dotted line in Figure 1. Obviously it is desirable to confirm this tentative detection at higher signal-to-noise.

One of our main reasons for obtaining the J-window spectrum of Markarian 463(E) was to search for line emission from OI1.1287 μm, which has been reported in IZw1 (Rudy *et al.* 1989a) and 3A0557-38 (Ward 1988a), but has not yet been observed in a Seyfert 2 galaxy. The portion of our spectrum covering this line is of rather poor signal-to-noise, but we may still set an upper limit for the line flux from Markarian 463(E) (Table 2).

3.2.2 1.914–2.332 μm

More remarkable is the spectrum covering Paschen α and Brackett γ, which clearly shows broad wings on the profiles of these lines. Although the effects of residual telluric absorption are visible between 2.0 and 2.1 μm it is nevertheless apparent that the profile of this broad component is intrinsically more *triangular* than Gaussian (after one allows for the effect of the instrumental response of CGS4). The narrow and broad components of Paschen α were therefore separated by fitting a Gaussian plus a triangular profile, both constrained to the same central wavelength and convolved with the instrumental response, on top of a linear continuum. The resulting intrinsic FWHM of $\simeq5000\pm500$ km s^{-1} for the broad component is in rough agreement with the found by Miller & Goodrich (1990) for *scattered* broad Hβ.

A similar fitting procedure was applied to the Brackett γ line, but this time the component widths were held fixed at the values determined from the fit to Paschen α; allowing these widths to vary increased the uncertainties on the component Brackett γ fluxes, but did not change the values significantly.

Of the other lines we might plausibly expect to be detectable, H_2 v=1–0 S(1) is weakly visible in our spectrum at the predicted redshifted wavelength; a similar feature is also present in an earlier spectrum taken at higher resolution with CGS2 (Chapter 2). No strong telluric absorption features are expected at this wavelength; nor are any observed in the raw spectrum of the standard star (Figure 1), so this feature is probably intrinsic to the source. Fitting an unresolved line profile at the appropriate wavelength

(measured relative to the Brackett γ line) yields a detection at the 4σ level, which we list in Table 2.

Our spectrum also covers the expected position of the [SiVI]1.9615μm line, which is blended with H_2 v=1–0 S(3) (e.g. Chapter 3). Unfortunately the portion of our spectrum containing this blend is affected by imperfect cancellation of the atmosphere, visible as a shallow "hump" longward of Paschen α, so no flux can be determined for [SiVI]. (We know that the contribution from H_2 v=1–0 S(3) is negligible from the weak flux of H_2 v=1–0 S(1) above.) In order to estimate an upper limit for this line we fitted a Gaussian profile at the redshifted wavelength with a FWHM (i) constrained to that of narrow Paschen α and (ii) unconstrained, therefore covering most of the bump in the spectrum. The upper limit derived from method (i) is similar to the flux derived from (ii), which assumed that all of the bump structure is due to [SiVI], and so in a sense is also an upper limit. These methods concur in limiting the [SiVI]1.962μm flux to less than 30% of the narrow Paschen α flux (Table 2).

3.3 The ultraviolet spectrum

We determined the total Lyman α flux from Markarian 463 by summing the line above a continuum interpolated from adjacent points in the SWP spectrum (after removal of points affected by reseaux, cosmic rays and geocoronal Lyman α). A similar flux was obtained by Kinney *et al.* (1991); both estimates may include a small contribution from NV emission on the red side of the Lyman α profile (cf. NGC1068—Snijders, Netzer & Boksenberg 1986). This may also account for the higher FWHM (1900 km s^{-1}) we find for the Lyman α line, compared to the profiles of the Balmer lines.

Kollatschny & Fricke (1984) have shown that the Lyman α emission detected in the SWP camera aperture is extended, and probably comes from both nuclei. Using their spatial Point Spread Function (*PSF*), we attempted to separate the contributions from Markarian 463(E) and Markarian 463(W) by fitting a PSF at the positions of each nucleus. The measured and fitted spatial profile are reproduced in Figure 4. This attempted deconvolution suggests that about 2/3 of the Lyman α emission comes from Markarian 463(E), but the uncertainty of this fraction is harder to evaluate; we therefore adopt a fraction of 0.62±0.05, with all values in this range equally probable. The value

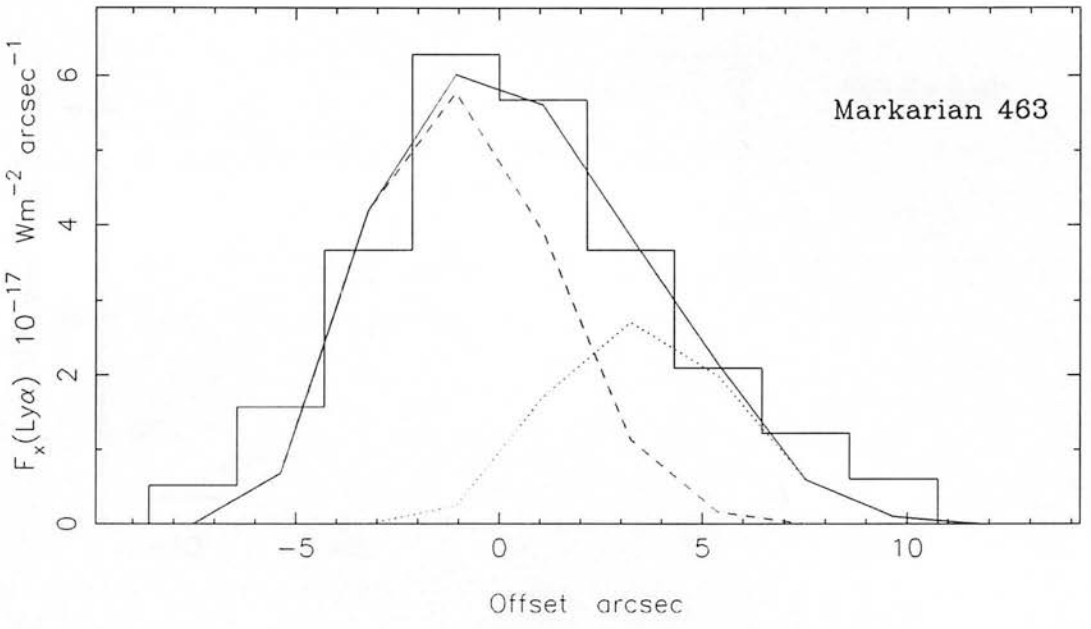

Figure 4: *Spatial profile of Lyman α emission in Markarian 463 at position angle 279 degrees. Kollatschny & Fricke (1984). Spatial offsets are given relative to the position of Markarian 463(E), and the individual bins are 2.15 arcsec wide. The solid line shows a fit to this profile consisting of a sum of unresolved emission components at the positions of Markarian 463(E) (dashed line) and Markarian 463(W) (dotted).*

and error given in Table 2 for the Lyman α flux have been calculated using this fraction.

A similar procedure was applied to the SWP continuum profile, which we have calibrated and reproduced for completeness in Figure 5, but in this case an extended stellar background is required in addition to the nuclei. This is expected if a large fraction of this continuum comes from an extended star-forming region. We estimate that fractions of 0.25 and 0.35 of the total SWP continuum arise from Markarian 463(E) and Markarian 463(W) respectively; we assign an uncertainty of 0.2 to these quantities. The relative strengths of the SWP continuum from each nucleus are consistent with the spatial profile in blue light presented by Hutchings & Neff (1989), which was taken with a much narrower slit than the *IUE* aperture, and hence includes a smaller fraction of stellar emission from the host galaxy.

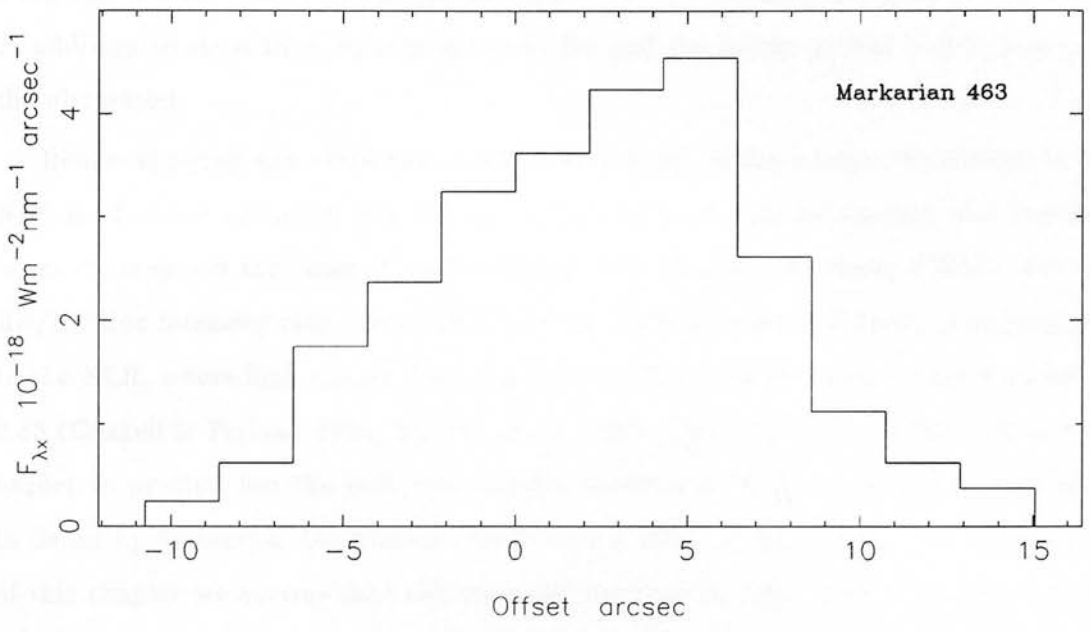

Figure 5: *Spatial profile of the SWP continuum from Markarian 463 at position angle 279 degrees, taken from Kollatschny & Fricke (1984) and calibrated using the data shown in Figure 3. Offsets are given relative to the position of Markarian 463(E), and individual data bins are 2.15 arcsec wide.*

4 Line emission and extinction in Markarian 463(E)

The new infrared spectroscopy presented here allows us to study properly the quantity and location of dust along our line of sight to the line-emitting regions of Markarian 463(E), when combined with existing data at optical wavelengths. In the following derivations we use the interstellar extinction law as tabulated by Mathis (1990), and take "case B" hydrogen recombination line ratios from Hummer & Storey (1987) for $T = 10^4$ K and $n_e = 10^4\,\mathrm{cm}^{-3}$.

4.1 The narrow line region

4.1.1 Reliable extinction estimates

Our observations of the Paschen lines and Brackett γ extend the wavelength baseline over which hydrogen recombination line radiation has been measured in Markarian 463(E) by two octaves. In particular, the line ratios Paα/Hβ and Paγ/Hδ are excellent extinction indicators; each pair of transitions shares the same upper energy

level, and so their relative intensities are unaffected by collisional excitation in the NLR. In addition to these lines we may also add Hγ and Hα in the optical and Lyman α in the ultraviolet.

Before applying any extinction model a knowledge of the intrinsic line ratios in the NLR is of course essential. For the higher Balmer lines and the Paschen and Brackett series we may use the "case B" values taken from Hummer & Storey (1987). For the Hα/Hβ line intensity ratio we assume that an intrinsic value of 3.2±0.2 is appropriate to the NLR, where high energy electrons enhance this ratio above the "case B value" of 2.85 (Gaskell & Ferland 1984, Binette *et al.* 1990). The intrinsic Lyα/Hβ ratio is even harder to predict, but the radiative transfer problem in NLR clouds has been studied in detail by Ferland & Osterbrock (1986) over a range of conditions. For the purpose of this chapter we assume that this ratio lies between 23 (the "case B" value) and 100 (the highest values considered by these authors). Using only those line ratios expected to be close to their "case B" values we derive the foreground extinction estimates listed in Table 3.

Table 3: *Hydrogen line ratios and NLR extinction (A_V(NL)) in Markarian 463(E)*

Line pair	flux ratio (error)	A_V(NL) (mag)
Brγ/Hβ	0.21 (16%)	2.24±0.2
Paα/Hβ	2.87 (20%)	2.25±0.2
Paγ/Hδ	3.88 (18%)	2.45±0.2
Hγ/Hβ	0.32 (10%)	2.68±0.7
Hδ/Hβ	0.14 (10%)	2.83±0.5

Note:
Balmer line data are taken from Shuder & Osterbrock (1981), other data from Table 2. Quoted errors are calculated from those in Table 2 added in quadrature to the uncertainties of the absolute flux calibrations.

The line fluxes quoted by Shuder & Osterbrock (1981) have been subjected to a small correction for stellar absorption, which we do not consider significant for the other lines. It can be seen from the Table that the hydrogen line ratios considered are in excellent agreement with "case B" plus a foreground extinction A_V(NL)≃2.2 mag towards the NLR. Since the estimates in Table 2 are not all independent, we simply adopt a value

A_V(NL)=2.25±0.2 mag determined from the Paα/Hβ ratio.

In Figure 6 we show the effect of foreground extinction on the observed line strengths relative to Hβ. The fact that the derived foreground extinction does not increase with

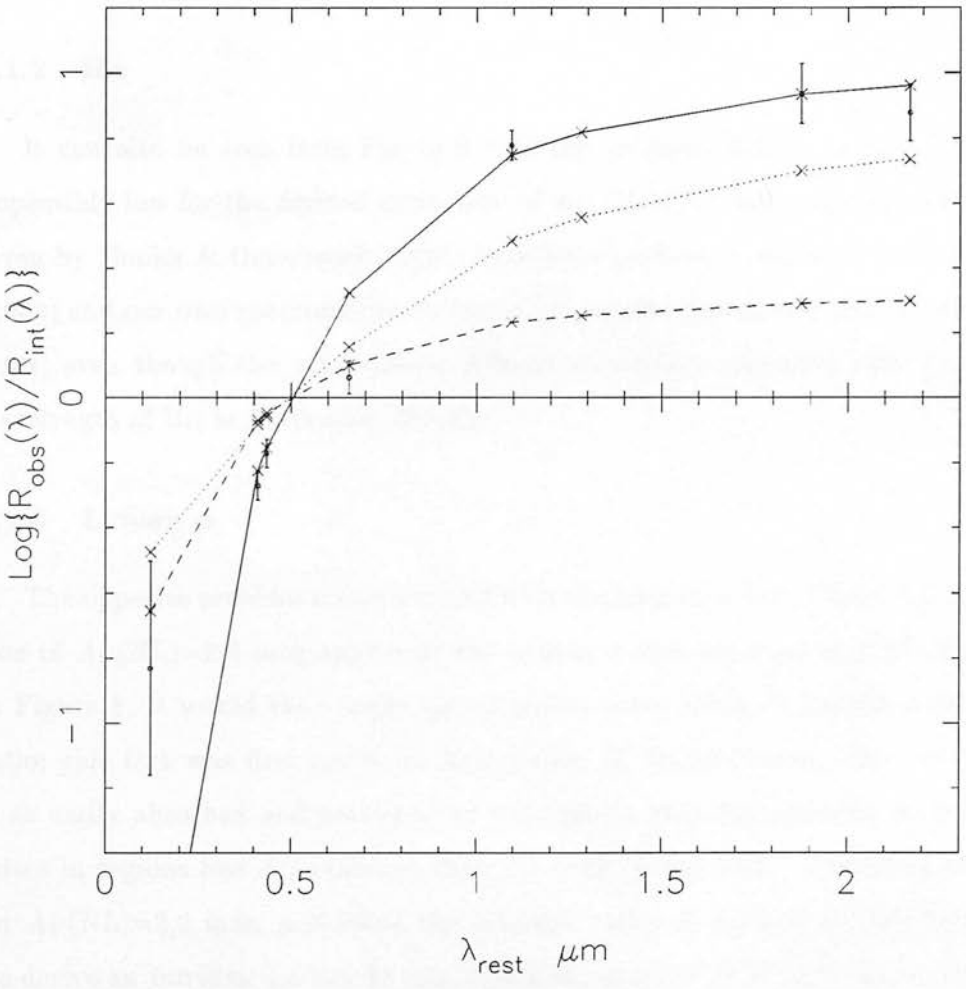

Figure 6: *Narrow hydrogen line flux ratios (R_{obs}) relative to Hβ, divided by their expected intrinsic ratios (R_{int}—see Section 3.2). The solid line connects the values expected for a foreground extinction* A_V *(NL)=2.25 mag (solid line) which is derived from the Paschen* α*/H*β *ratio* $R(1.875\,\mu m)$*. The dashed line represents a extinction of* A_V*=0.8 mag, which was derived by Malkan (1983) from consideration of the forbidden lines. Also shown (connected with a dotted line) are the values expected for* internal *extinction equivalent to* A_V*=7 mag.*

the wavelengths of the lines used rules out significant extinction by dust mixed in with the line-emitting gas; such a model is shown as a dotted line in the Figure, and clearly is

unable to account for the high infrared/optical line ratios, even for the large dust column implied by the 9.7-μm silicate optical depth (Section 5.4).

It should be borne in mind, though, that the much lower values of A_V(NL)$\simeq$0.7 mag derived by consideration of the [OII] and [SII] line ratios by Malkan (1983), together with the strong observed Lyman α emission discussed below, may indicate that some regions suffer much less extinction.

4.1.2 Hα

It can also be seen from Figure 6 that the intrinsic Balmer decrement of $\simeq$1.7 is impossibly low for the derived extinction of A_V(NL)=2.2 mag. The Hα and Hβ fluxes given by Shuder & Osterbrock (1981) have been confirmed respectively by Leech *et al.* (1989) and our own spectroscopy, so we do not ascribe this discrepancy to measurement error, even though the atmospheric A-band absorption coincides with the redshifted wavelength of Hα in Markarian 463(E).

4.1.3 Lyman α

The opposite problem is encountered with the Lyman α flux (Figure 6). If an extinction of A_V(NL)=2.2 mag applies to the Lyman α flux reported in Table 2 and shown in Figure 6, it would then imply an unfeasibly *large* intrinsic Lyman α/Hβ intensity ratio; this fact was first noted by Kollatschny & Fricke (1984). However, Lyman α is so easily absorbed and scattered by dust grains that the emission we see probably arises in regions less extinguished than the bulk of the NLR. Correcting the Hβ flux for A_V(NL)=2.2 mag, and using the intrinsic ratios of Ferland & Osterbrock (1986), we derive an *intrinsic* narrow Lyman α flux of $\sim 2.5\times10^{-14}$ W m^{-2}, uncertain by a factor of $\sim$3. Since the observed flux is only 1% of this, it may either arise from a less extinguished regions whose emission is unimportant at longer wavelengths, or possibly through scattering of NLR radiation by dust and/or electrons (Section 6), in which case the line should be polarized.

4.2 OI 1.1287 μm and OI 844.6 nm

The 1.1287 μm transition of OI, and its associated transition at 844.6 nm are believed to arise from Lyman β fluorescence in high optical depth regions of the NLR (e.g. Morris & Ward 1989, and references therein). Confirmation of this mechanism in IZw1 was obtained by Rudy, Rossano & Puetter (1989b), who observed that the 844.6 nm/1.1287 μm *photon* flux ratio in this AGN is close to unity, as expected from Bowen line fluorescence.

If this mechanism is also operating in Markarian 463(E), then we are able set an upper limit of 9×10^{-17} W m^{-2} on the flux of the (as yet unobserved) OI 844.6 nm line (without correction for extinction). Even with this limit it would still be possible for OI844.6 nm emission to be present at a level of $\simeq$0.03 times Hα, which is well within the range of values observed in X-ray-selected AGN (e.g. Morris & Ward 1989—see also Chapter 2). Confirmation of the dominance of the Bowen fluorescence mechanism through measurements of OI1.1287 μm in a sample of these relatively unreddened AGN would encourage us to trust the OI 1.1287 μm/844.6 nm line flux ratio as a potential reddening indicator in the future.

4.3 H_2 v=1–0 S(1) and molecular line emission

We have just managed to detect the H_2 v=1-0 S(1) line in our CGS4 spectrum of Markarian 463(E), and in an earlier spectrum taken at lower signal-to-noise with CGS2 (see Chapter 2). Unfortunately the associated v=2–1 S(1) transition at 2.2477 μm (rest wavelength) is outside the range of our spectrum—the presence of this line is a good diagnostic of UV fluorescent excitation in low density molecular gas (see Chapter 4). Using similar arguments to those presented in Chapter 4 for Cygnus A, we find that the reddening-insensitive line flux ratios F[H_2 v=1–0 S(1)]/F(Brγ) and F([OI]630.0 nm)/F(Hα) are consistent with models in which a hard X-ray source excites the nuclear gas (Mouri *et al.* 1989, and references therein).

If the assumptions of Kawara, Nishida & Gregory (1990) are valid in converting the H_2 v=1–0 S(1) line luminosity into a mass estimate, the line emission in Markarian 463(E) corresponds to $\sim2\times10^4$ M$_\odot$ of hot molecular gas. Cooler molecular material has also been detected in Markarian 463 by Sanders *et al.* (1989a), who infer a total H_2 mass of 2×10^{10} M$_\odot$ (corrected to H_0=50) from their measurement of the CO J=1–0

transition. This is much greater than the total mass of HI ($4.2\times10^9\,M_\odot$) determined from a measurement of the 21 cm line by Hutchings, Price & Gower (1987). The high implied molecular/atomic hydrogen mass ratio for Markarian 463 is comparable to the highest ratios claimed for early-type spiral galaxies (Young & Knezek 1989). It is therefore possible that the molecular mass may be overestimated by this method. Uncomfortably high apparent H_2/HI mass ratios in other active galaxies (e.g. Meixner *et al.* 1990) also suggest that the CO luminosity/molecular mass conversion factor does not apply to these systems, at least in their central regions where molecular clouds may be heated to higher temperatures through the presence of the AGN (e.g. Krolik & Lepp 1989).

However, we note that the implied hot/cold H_2 mass ratio of $\simeq10^{-6}$ is comparable to those found for Seyfert 1s and quasars when the same conversion factors are applied (Kawara, Nishida & Gregory 1990). Higher values of $\sim10^{-5}$ similar to those found in the central regions of NGC1068 and our own Galaxy are also admissible given the vastly different beam sizes used in the Markarian 463(E) observations. The comparable width (FWHM$\simeq$300 km s^{-1}) of the CO and HI lines argues for a similar extent of the emission, though observations of other infrared-luminous systems generally indicate that the molecular line emission is often more centrally concentrated. (For an up-to-date review of such observations, and the assumptions behind their interpretation, see Henkel, Baan & Mauersberger 1991.)

4.4 [SiVI]1.962 μm and the high ionization lines

This section is necessarily short since we did not detect the line in Markarian 463(E). In those galaxies known to emit this line to date (Oliva & Moorwood 1990, Moorwood & Oliva 1991; see also Chapter 3) [SiVI]1.962 μm is observed to be at least twice as strong as narrow Brackett γ. Our upper limit (Table 2) is not a stringent one in this respect, but we can show it is at least consistent with the strengths of its optical analogues and the predictions of the photo-ionization model of Korista & Ferland (1989).

Since the [FeVII]608.7 nm line also has a high critical density and the Fe^{6+} species should form in a region close to Si^{5+}, we expect the relative strengths of these lines to be similar over a range of conditions, as long as photo-ionization by the hard ultraviolet continuum of an AGN is the dominant mechanism (cf. Viegas-Aldrovandi & Contini

1989). Scaling the Korista & Ferland (1989) model spectrum to the [FeVII]608.7nm line flux in Markarian 463(E) (Shuder & Osterbrock 1981), and correcting for A_V(NL)=2.2 mag we predict a [SiVI]1.962μm line flux $\sim 1\times10^{-17}$ W m^{-2}, which is comfortably within our upper limit.

The assumption underpinning the Korista & Ferland (1989) ionization model, that the emitting gas is the extended low-density interstellar medium ($n_e \simeq 1$ cm^{-3}), has been called into question for the case of NGC1068 by the non-detection of strong [SiV]10.52μm (Roche *et al.* 1991). However, the relative line strengths of [FeVII] and [SiVI] which we have predicted from this model should be fairly insensitive to density, due to the high critical densities of these forbidden transitions.

4.5 The broad line region in Markarian 463(E)

We have clearly detected broad Paschen α emission transmitted from an optically-obscured BLR. From the flux of scattered broad Hβ reported by Miller & Goodrich (1990), and the lack of reddening in their spectrum, we may conclude that the contribution of scattered broad line radiation at this wavelength is negligible, irrespective of the polarigenic mechanism.

In order to estimate the extinction A_V(BL) towards the BLR, at least two broad line observations well separated in wavelength are necessary. However some general arguments do place limits on this quantity. If A_V(BL) were less than about 4 mag, broad wings of FWHM$\simeq$3000–5000km s^{-1} would be easily visible on the Hβ line in the transmitted optical spectrum of Markarian 463(E). On the other hand, very high extinctions of $\gtrsim$100 mag would either render the BLR undetectable even at 2μm (e.g. NGC1068—Depoy 1987), or alternatively would imply an unrealistically large intrinsic broad line luminosity inferred from the observed flux.

A more accurate extinction estimate is furnished through our J-band spectrum covering Paschen γ (Section 3.2.1), which does allow a broad component to this line at the 2σ level. Taking the intrinsic broad Paschen line intensity ratio to be close to its "case B" value, we find that the observed line flux ratio then implies a broad line extinction $A_V(\mathrm{BL})=5.3^{+3.9}_{-2.2}$ mag (67% confidence interval). The flux we find for broad Brackett γ is also consistent with the "case B" excitation ratio and this value of A_V(BL).

5 Implications for the continuum at other wavelengths

Since relatively unreddened Seyfert 1 AGN exhibit well-defined correlations between their optical emission line, X-ray and far-infrared luminosities (e.g. Ward *et al.* 1988), our measurement of the intrinsic BLR luminosity of Markarian 463(E) enables us to predict the appearance of this AGN at these wavelengths, under the assumption of course that Markarian 463(E) also obeys them. In addition, a knowledge of the quantity of obscuring matter along the line of sight to the continuum source(s) allows us to account for the effects of of this material on the transmitted spectrum.

Many of the important correlations established for Seyfert 1s and quasars are formulated in terms of their broad Hα luminosities $L(\mathrm{H}\alpha)$ (given here in Watts). To convert our broad Paschen α measurement to Hα, we assume an intrinsic broad Paα/Hα line intensity ratio of 0.13±0.12; this is typical of the flux ratios measured in quasars by Yates & Garden (1989), and in agreement with the models of Avrett & Loeser (1988). From this ratio and the broad infrared line fluxes measured above we then infer $\log L(\mathrm{H}\alpha)$=36.5±0.25.

In Figure 7 we present the Spectral Energy Distribution (*SED*) of Markarian 463(E) as best as it can be determined with current observations, together with some of the results derived in the following sections. It should be remembered that the *IUE* observations, and possibly also the *IRAS* fluxes, contain substantial emission from Markarian 463(W) and the circumnuclear regions.

5.1 Hard X-rays (2–10 keV)

A good indicator of the bolometric power of an active nucleus is its hard (2–10 keV) X-ray luminosity L_X (Ward *et al.* 1987). For relatively unobscured Seyfert 1 AGN this is known to be correlated with the Hα luminosity, with fairly small intrinsic scatter. From this correlation (as presented in Ward *et al.* 1988) we find that the intrinsic broad Hα luminosity of Markarian 463(E) derived above implies that $\log L_X$=37.5±0.4.

This luminosity corresponds to a transmitted 2–10 keV flux of about 2.5×10^{-14} W m^{-2} from Markarian 463(E) (uncertain by a factor of 2.5) which is just above the sensitivity limit of the *HEAO*1-*A*2 survey (Piccinotti *et al.* 1982). Until such time as Markarian 463(E) is detected in the future, we assume that the intrinsic X-ray spectrum of

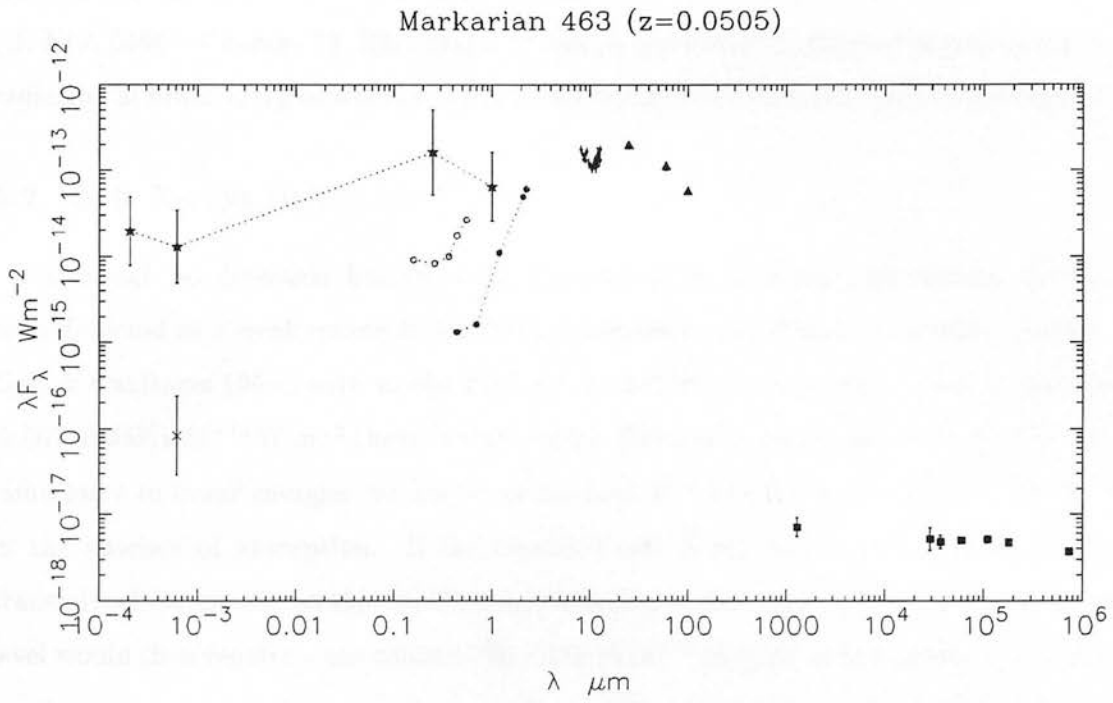

Figure 7: *Spectral Energy Distribution of Markarian 463(E) and its environs. Dotted line segments merely connect related spectral components, and are not intended to interpolate between them. Symbols are as follows: filled squares—radio and submillimetre fluxes at 1.3 mm (18 arcsec beam: Chini, Kreysa & Biermann 1989), 2.9 cm and 3.7 cm (2.7 and 40 arcsec beams respectively: Kojoian* et al. *1976), nuclear fluxes at 6, 11, 18 and 73 cm (Ulvestad, Wilson & Sramek 1981; Unger* et al. *1986); filled triangles—IRAS coadded fluxes of Markarian 463 from Mazzarella, Bothun & Boroson (1991); •—nuclear fluxes from Hutchings & Neff (1989) together with small-aperture near-infrared fluxes from this work; ○—broad-band fluxes including both nuclei (10×15 arcsec aperture: IUE and 14.5 arcsec aperture: Peterson, Fricke & Biermann 1981); ⋆—intrinsic continuum flux at 6(1+z) keV predicted from the $L(H\alpha)/L_X$ correlation, together with predicted intrinsic fluxes at 2(1+z) keV 250(1+z) nm and 1.0(1+z) μm (Section 5); ×—Einstein IPC flux (Kruper, Urry & Canizares 1990), converted to a flux density at 2(1+z) keV assuming a spectral index of −0.7.*

Markarian 463(E) is well described by a power law with a 'typical' energy index of -0.7 ± 0.2 (Turner & Pounds 1989). This spectrum may, of course, be modified by interstellar absorption along the line of sight (Morrison & M^{c}Cammon 1983); the value derived for A_V(BL) corresponds to a minimum expected column density of only $\sim 10^{22}\,\mathrm{cm}^{-2}$, which would not reduce the total 2–10 keV flux significantly.

However, these estimates for the intrinsic hard X-ray flux and column density are, of course, strictly upper and lower limits respectively, since an additional column of

(presumably dust-free) gas may exist between the BLR and X-ray continuum source (cf. NGC5506—Chapter 3). This material will be particularly effective at absorbing X-radiation at lower energies where the photo-electric absorption cross-sections are highest.

5.2 Soft X-rays (0.2–4.5 keV)

Although no detection has yet been reported in hard X-rays, Markarian 463 has been detected as a weak source at soft X-ray energies by the *Einstein* satellite (Kruper, Urry & Canizares 1990), with an observed 0.2–4.0 keV flux in the 68% confidence interval $[0.007, 0.058]\times10^{-14}$ W m^{-2} (best fit value 0.02). Extrapolating the predicted hard X-ray luminosity to lower energies we derive an intrinsic 0.2–4 keV flux of 3.2×10^{-14} W m^{-2} in the absence of absorption. If the observed soft X-ray flux is entirely due to the transmitted component of this continuum, reduction of the intrinsic flux to the observed level would then require a gas column $N_H=33\pm15$ cm^{-2} in front of the power-law source.

A similar column density was found for the Seyfert 2 galaxy Markarian 3, whose 2–10 keV spectrum was measured by *GINGA* (Awaki *et al.* 1990). Such a high column density would also diminish the hard (2–10 keV) X-ray flux received from Markarian 463(E) to about 30% of its unabsorbed level, which would then place Markarian 463 below the detection threshold of previous hard X-ray surveys.

Whilst such high column densities are not commonly seen, there are further reasons to suppose that the gas column towards Markarian 463(E) may be even higher, if the observed soft X-ray flux has another origin. We must first consider the contribution to the soft X-ray flux from circumnuclear star-forming regions in Markarian 463 and the blue secondary nucleus Markarian 463(W), since these also fall within the effective beam size of the *Einstein* observations. Assuming for the moment that Markarian 463(W) can be classified as a starburst we may use the correlation established between the B-band and soft X-ray luminosities of spiral galaxies established by Fabbiano, Gioia & Trinchieri (1988). Taking the integrated B-band luminosity of Markarian 463 from Hutchings & Neff (1989) this correlation predicts a 0.5–4.5 keV flux of $\simeq10^{-18}$ W m^{-2}. A slightly higher value of $\simeq5\times10^{-18}$ W m^{-2} is predicted from the Brackett γ X-ray luminosity correlation established for starburst galaxies by Ward (1988b), where instead we use the Hα flux of Markarian 463(W) given by Shuder & Osterbrock (1981), but this is still

much less than the observed value.

Therefore we can be certain that if line emission in Markarian 463(W) is derived from star formation, the contribution from this source at X-ray energies would be negligible. If Markarian 463(W) is host to non-thermal activity, however, a higher contribution would be expected. The correlations established for Seyfert 2s and LINERS between soft X-ray flux and Hβ line width, and between soft X-ray flux and [OIII]/Hβ line ratio, both suggest that the soft X-ray emission from Markarian 463(W) would be no more than $\sim 5 \times 10^{-15}$ W m^{-2} (Kriss, Canizares & Ricker 1980). The Hβ/soft X-ray flux correlation also presented by these authors would admit a higher contribution, provided of course that *all* of this flux was produced by non-thermal activity. We ignore this possibility until future observations of Markarian 463(W) are performed at optical and shorter wavelengths to determine the nature of the line-exciting source.

A more promising alternative origin for the flux detected by *Einstein*, which was also considered by Awaki *et al.* (1990) for the case of Markarian 3, is electron scattering of an unabsorbed nuclear continuum. If this mechanism accounts for a large fraction of the soft X-ray flux, then the gas column blocking transmitted soft X-rays from Markarian 463(E) would have to be even larger than the value derived above, and may attenuate the hard X-rays even further (cf. NGC1068). We defer a discussion of scattering in Markarian 463(E) to Section 6. However, the firm conclusion we may draw from these considerations is that unless we have somehow overestimated L_X above by a large factor, a substantial column of gas must exist between the BLR and hard X-ray source in Markarian 463(E), at least along our particular line of sight, in order for its intrinsic properties to resemble those of un-extinguished Seyfert 1 AGN.

5.3 Near-infrared (1–4 μm)

Kriss (1988) has shown that the low-energy X-ray luminosities of quasars as measured by the *Einstein* satellite correlate with their 1 μm luminosities. We may use this correlation to estimate the contribution of the active nucleus to near-infrared wavelengths. Applying the correlation presented by Kriss for radio-quiet quasars this implies a 1 μm luminosity $L_{1\,\mu\mathrm{m}} = 2.5 \times 10^{23}$ W Hz^{-1}, with an uncertainty of about 0.4 in the logarithm. The corresponding 1.05 μm flux density of $\simeq$20 mJy is much higher than the

value of 3.5 mJy found from extrapolation of the continuum in our J-band spectrum (Figure 1). If, however, we correct this observed continuum for an extinction equivalent to $A_V(\mathrm{BL})=5.3^{+3.9}_{-2.2}$ mag, the corrected and predicted continuum levels are brought into excellent agreement.

The uncertainties involved in this comparison ($\simeq$0.5 in the logarithm for each quantity), and the presence of some host galaxy emission in our near-infrared spectrum, weaken this result somewhat. Nevertheless, it does suggest that at a crude level, the X-ray/near-infrared luminosity correlation might be used as an extinction indicator in AGN in much the same way as we have used L_X and $L(\mathrm{H}\alpha)$, even though the existence of the former relation is harder to explain. Although the $L_X/L(\mathrm{H}\alpha)$ correlation naturally connects the ionizing luminosity with the broad line radiation, the physical links responsible for the X-ray/near-infrared correlation are much less clear given, for instance, the absence of correlated variability observed between them in radio-quiet AGN (e.g. Done *et al.* 1990).

5.4 Far-infrared (12–1300 μm)

Markarian 463(E) is one of a small number of 'ultra-luminous' infrared galaxies detected by *IRAS*, with a bolometric luminosity of 10^{12} $\mathrm{L}_\odot$ and a 'warm' 25–60 μm colour temperature (Sanders *et al.* 1988b). For this class of objects it is of great interest to establish whether their high far-infrared luminosities can be ascribed to non-thermal nuclear activity, or to stellar processes heating the interstellar medium (Wright *et al.* 1988, Thronson *et al.* 1990), or, as Sanders *et al.* (1988b) suggest, a combination of these processes as one form of activity evolves into another.

The relatively flat 25–60 μm spectral slope of Markarian 463, which is a good secondary indicator of Seyfert activity (e.g. de Grijp *et al.* 1985) would suggest that an AGN is the likely dominant far-infrared emitter in this system. Rowan-Robinson & Crawford (1989) modelled the far-infrared emission of a large sample of *IRAS* galaxies, including Markarian 463, with three components: 'Seyfert', 'starburst' and 'disk'. For the case of Markarian 463 they found that the luminosity of the 'Seyfert' component, L_S, accounted for 80% of the total far-infrared luminosity of the system, with only a 5% formal error on their fitted parameters.

In the same paper Rowan-Robinson & Crawford also show that for those galaxies in their sample which have been detected in hard X-rays, L_S correlates significantly with L_X, as expected if their modelling is realistic. A similar, but purely empirical, correlation was established by Ward *et al.* (1988) between L_X and the 25–60 μm luminosities of X-ray-selected AGN. Using our predicted hard X-ray luminosity of the eastern nucleus, and their value of L_S fitted to the large-aperture *IRAS* fluxes, we find that Markarian 463 lies well within the scatter of these correlations.

As for the major contributor to the remaining 2×10^{11} $L_\odot$ of the infrared luminosity, it is difficult to distinguish between dust heating by a kiloparsec-scale starburst (Wright *et al.* 1988) or by the evolved stellar population (Thronson *et al.* 1990) on the basis of *IRAS* data alone. This is due to the diversity of spectral shapes of the underlying far-infrared 'disk' (or 'cirrus') emission in galaxies, and the similar range of dust temperatures generated by active star formation. Optical and near-infrared images could be used to map the non-uniform extinction and the young stellar population in the nuclear regions of Markarian 463. Much of the emission not associated with Markarian 463(E) may arise from weaker non-thermal or star-forming activity in the secondary (western) emission-line nucleus of this system.

These predictions were confirmed by the 8–13 μm spectrum of Markarian 463(E) presented by Roche *et al.* (1991), who found that almost all of the emission detected by *IRAS* at 12 μm fell within their 4.5 arcsec beam. Moreover, the spectrum itself clearly shows a 9.7 μm silicate absorption feature with an optical depth $\tau_{9.7}$ of 0.47 (see Figure 7). This optical depth corresponds to $A_V\simeq$7–8 mag for dust of Galactic composition, which is in in good agreement with the value of A_V(BL) derived independently from the broad hydrogen lines (Section 4.5). The simplest interpretation of this result is that the mid-infrared continuum in Markarian 463(E) is produced by a compact source viewed through a foreground column of $A_V\simeq7$ mag of "cold" dust, though more realistic dust emission models are probably also consistent with the data. The 9.7 μm silicate absorption is responsible for the steep 12–25 μm colour of Markarian 463, but it also implies that the emission at 25 μm and longer wavelengths is optically thin. This would explain the similarity of Markarian 463(E)'s *IRAS* colours to those observed in samples of relatively AGN. Further observations of the silicate feature at 18 μm and of the submillimetre continuum are required, however, before one can attempt a detailed modelling of the dust

distribution (e.g. Lawrence *et al.* 1991). The red JHK colours of Markarian 463(E) also indicate that hot dust emission may even dominate at shorter wavelengths (Mazzarella *et al.* 1990, see also Figure 7).

Although Markarian 463(E) is not a "radio-loud" AGN (Figure 7), it should be noted that the 1.3 mm flux density reported by Chini *et al.* (1989) is close to that expected from the high-frequency extension of the non-thermal radio spectrum, This component is probably not important at shorter wavelengths (cf. Cygnus A: Chapter 4), and indeed the high far-infrared/radio luminosity ratio of Markarian 463 compared with normal and star-forming galaxies is also a definite signature of non-stellar activity (Condon, Frayer & Broderick 1991).

6 Scattering in Markarian 463

6.1 The optical spectrum

Miller & Goodrich (1990) were the first to unambiguously identify an optically-obscured BLR in Markarian 463(E) through the use of spectropolarimetry to isolate the nuclear radiation which is scattered towards us. Their polarized flux spectrum shows clear evidence for broad Hα and Hβ emission, with possible contribution from FeII multiplets, with equivalent widths similar to those of un-extinguished AGN of comparable luminosity. In polarized light, then, the spectrum of Markarian 463(E) resembles a Seyfert 1.

Our estimate of the *intrinsic* broad Hα luminosity of Markarian 463(E) in Section 5 enables us to calculate the efficiency with which broad line radiation is scattered towards us from Markarian 463(E)—a quantity which Miller & Goodrich (1990) had to assume in the absence of other information. From the scattered Hβ flux used in their paper we derive a scattered Hα luminosity L^{scat}(Hα) of 1.4×10^{35} W (we assume a broad line Balmer decrement of 3.5). Comparing this with the value we find for L(Hα) above we find that a fraction $f=10^{-1.34\pm0.25}$ of the broad line radiation is scattered. Under the reasonable assumption that the optical continuum is also scattered with the same efficiency (see Miller & Goodrich 1990), the broad Hβ equivalent width in the polarized flux spectrum implies that Markarian 463(E) would resemble a high luminosity quasar,

when viewed by an observer with a direct view of the nuclear source.

6.2 Soft X-rays

In the classical Seyfert 2 galaxy NGC1068, our direct view of the hard X-ray source is believed to be completely blocked by a column of $N_H \sim 10^{24}\,\mathrm{cm}^{-2}$, and yet nuclear X-radiation is still able to reach us via scattering by electrons outside the plane of the blocking material (e.g. Koyama *et al.* 1989). The weak soft X-ray emission of Seyfert 2 galaxies as a class may have a similar origin, though as yet there is insufficient spectral information to test this possibility (Kruper *et al.* 1990).

It is conceivable, then, that the observed soft X-ray emission from Markarian 463(E) may contain a component from an unabsorbed, but intrinsically weak, electron scattered nuclear continuum. If all of $L^{scat}(\mathrm{H}\alpha)$ derived above from Miller & Goodrich's spectropolarimetry is due to wavelength-independent electron scattering, the hard X-ray/broad Hα luminosity correlation utilized in Section 5.1 then leads us to expect a scattered 2–10 keV flux of $10^{-15}\,\mathrm{W\ m}^{-2}$, uncertain by a factor of 2. For a typical AGN spectral energy index of -0.7, we find that this scattered flux would then correspond to $1.2\times10^{-15}\,\mathrm{W\ m}^{-2}$ in the 0.2–4 keV band, which is marginally *higher* than the observed soft X-ray flux. This result is only weakly dependent on extinction, since it turns out that any dust extinction affecting the scattered Hα flux would similarly affect the scattered soft X-ray flux similarly (averaged over the 0.2–4 keV band with our assumed spectral index) due to photo-electric absorption by the associated gas (Morrison & M$^{\mathrm{c}}$Cammon 1983).

However, dust may play a role in scattering the broad line radiation, as evidenced by the blueward-rising polarization spectrum presented by Miller & Goodrich, which would reduce our estimate above for the scattered X-ray component; if dust scattering dominates in the optical, the soft X-ray emission is more likely due to a component of a highly absorbed power-law continuum as considered in Section 5.1 which would rise towards higher energies as the absorption decreases, though the presence of an entirely separate soft component cannot be completely ruled out.

Without spectral information it is impossible to distinguish between these origins, for Markarian 463(E) and for Seyfert 2 galaxies as a whole, or the alternative of an

intrinsically soft component entirely separate from the hard X-ray continuum.

6.3 The ultraviolet continuum

Kinney *et al.* (1991) used the *IUE* spectrum of Markarian 463, together with large-aperture spectrophotometry, to argue in favour of an electron scattering origin for the ultraviolet continuum in Markarian 463(E) and other Seyfert 2s. However, we have already shown in Section 3.3 that the ultraviolet continuum received in the SWP is mainly produced from Markarian 463(W), so in this case these authors' arguments are not valid. Although they point out that the SWP continuum has a similar spectral slope to that of Seyfert 1 AGN (Figure 3), this slope is not unique to active galaxies, but is also found in LINER and starburst nuclei, (e.g. NGC2782—Kinney *et al.* 1984).

Kriss (1988) also presented a correlation between the soft X-ray and ultraviolet luminosities of his quasar sample. The large intrinsic scatter is due to the diversity of spectral shapes of quasars at ultraviolet wavelengths. Nevertheless, if Markarian 463(E) has a typical quasar SED, this correlation implies an ultraviolet continuum luminosity (in W Hz^{-1}) given by $\log L_{250\,\mathrm{nm}}=23.2\pm0.5$.

Although we find that only $\simeq$25% of the observed SWP continuum comes from Markarian 463(E), a correction for an extinction equivalent to $A_V\simeq0.7$ mag (Malkan 1983; Section 4.1) would imply a luminosity of 7×10^{21} W Hz^{-1} at 250 nm at the source, uncertain by a factor of 2. This luminosity corresponds to a fraction $10^{-1.4\pm0.5}$ of the intrinsic flux density predicted above, which is in excellent agreement with the scattered fraction of broad line radiation. Although the close agreement is contrived given the large uncertainties involved and the sensitivity to extinction, these arguments at least demonstrate that wavelength-independent electron scattering *could* account for the observed ultraviolet continuum, which is indirect evidence in favour of this mechanism in Markarian 463(E).

6.4 Near-infrared

The steep near-infrared slope of the SED of Markarian 463(E) indicates that hot dust is likely to dominate the emission at 2.2 μm and beyond. Nevertheless, R. R. J. Antonucci (private communication) was able to detect a K-band polarization of 2.69±0.54%, at a

position angle of 87±7 degrees in a 4-arcsec aperture.

This position angle is very close to that reported by Miller & Goodrich (1990) for the optical continuum, and is also perpendicular to the radio continuum and [OIII] structure, (e.g. Hutchings & Neff 1989). These results argue strongly in favour of a common origin for the polarization, and rules out scattering by dust due to the inefficiency of this mechanism at infrared wavelengths. Although other mechanisms are possible (e.g. transmission through aligned dust grains, cf. Hough *et al.* 1991), wavelength-independent electron scattering is the most likely candidate for the polarization. We also note that the ratio of polarized optical and 2.2 μm fluxes is within the range expected for a typical quasar continuum SED (e.g. Sanders *et al.* 1989b), which also argues in favour of this mechanism.

7 Conclusions

In summary, then, we find that once the effects of obscuration are taken into account, the spectral properties of Markarian 463 are not too different from those of luminous Seyfert 1 nuclei. From the extinction-corrected broad line luminosity we find that the circumnuclear interstellar matter in Markarian 463 scatters a high fraction (~5%) of its optical broad line emission towards us. If the scattering medium consists of electrons, this mechanism naturally accounts for the near-infrared polarization, and may contribute to the ultraviolet and low-energy X-ray fluxes. Finally we note that our conclusions are supported by a simple model of the far-infrared emission from Seyfert galaxies, and by independent mid-infrared spectroscopy. Taken together, these results provide convincing evidence that that the dominant source of luminosity in the Markarian 463 system is the (compact) active nucleus Markarian 463(E).

Our conclusions suggest a number of observational tests. The most obvious and fundamental test would be a search for hard X-ray emission from Markarian 463(E), which should be possible with planned space missions ($ASTRO-D, JET-X$ and $AXAF$). Even for the columns $N_H \sim 30 \times 10^{22}\,\mathrm{cm}^{-2}$ considered in Section 5.2, we predict that Markarian 463(E) should be detectable above 5 keV. At lower energies, pointed observations by the Position-Sensitive Proportional Counter ($PSPC$) aboard $ROSAT$ may distinguish between a scattered and a transmitted origin of the low-energy soft

X-ray flux, while its High Resolution Imager could discriminate between emission from Markarian 463(E) and Markarian 463(W). The possible presence of $\sim$0.7 mag (A_V) extinction in the nuclear regions may, however, reduce the X-ray fluxes significantly at these low energies.

In the optical, high quality spectrophotometry would allow us to distinguish between the various narrow line extinction models discussed in Section 4.1 unambiguously, and to check the anomalous Balmer decrement we find, when compared to other hydrogen line ratios. Measurements longward of 800 nm would also be particularly useful for evaluating the contribution to the continuum from hot stars (via the Ca Triplet), and in searching for emission from OI844.6 nm. Similarly, an improved spectrum in the J atmospheric window in the near-infrared should allow us to search for OI1.1287 μm, and more importantly attempt to confirm the broad line component of Paschen γ. High-quality optical spectrophotometry of Markarian 463(W) should identify the exciting source of its line emission. We note that only two galaxies (AN0248+43 and Markarian 266; Kollatschny *et al.* 1991, and references therein) are known to contain a double Seyfert nucleus, so this phenomenon is extremely rare.

Finally we consider the relation of Markarian 463(E) to other luminous objects detected in the *IRAS* survey which show "warm" 25–60 μm colours (Sanders *et al.* 1988b). Although the 25–60 μm colour criterion only selects a small fraction of those galaxies known to possess active nuclei, this method suffers little contamination (Condon, Frayer & Broderick 1991), and is insensitive to *moderate* dust optical depths. We can therefore confidently predict that broad infrared line emission should be readily observable in this sample, since the high optical depths suppressing the K-window Paschen and Brackett lines would also significantly alter the 12- and 25 μm colours (cf. Arp 220—Depoy, Becklin & Geballe 1987). In particular, we find that amongst those objects considered by Sanders *et al.* (1988b), IRAS0518-2524 is remarkably similar in its properties to Markarian 463(E) in its morphology, energy distribution, near-infrared colours and optical spectrum. Jones & Klebe (1989) found a high near-infrared polarization towards the brighter nucleus of IRAS0518-2524, which they interpreted as emission from a blazar-like core. By analogy with Markarian 463(E), however, we prefer to interpret their results in terms of scattering from a luminous (but highly-obscured) Seyfert 1 nucleus, and we consider IRAS0518-2524 an excellent candidate for the detection of broad line emission

in its infrared (transmitted) and in the optical (polarized) emission-line spectrum.

We note that the extinction we derive towards Markarian 463(E) cannot apply to every line of sight to this AGN, as evidenced by the extended [OIII] emission, and the high-ionization lines in the optical spectrum (cf. Haniff, Ward & Wilson 1991), which argue strongly in favour of angle-dependent obscuration of the central source. The different timescales of star-forming and nuclear activity, and the dominance of the latter in these systems (as opposed to a composite appearance) provide indirect supporting evidence that these objects are not "intermediate" in an evolutionary sense, but in a geometrical one.

Acknowledgements

It is our pleasure once again to give thanks to the telescope operators Joel Aycock and Thor Wold, and to Phil Puxley for his assistance with the observations. Pat Roche and Ski Antonucci kindly communicated their results in advance of publication. Richard Dixon and Penelope Smith are thanked for improving earlier drafts by their critical reading. Support for PRB was generously provided by the DSS and PATT.

References

Antonucci, R. R. J. & Miller, J. S., 1985. *Astrophys. J.*, **297**, 621.

Armus, L. Heckman, T. M. & Miley, G. K., 1989. *Astrophys. J.*, **347**, 727.

Avrett, E. H. & Loeser, R., 1988. *Astrophys. J.*, **331**, 211.

Awaki, H., Koyama, K., Kunieda, H. & Tawara, Y., 1990. *Nature*, **346**, 544.

Binette, L., Calvet, N., Cantó, J. & Raga, A. C., 1990. *Publs astr. Soc. Pacific*, **102**, 723.

Chini, R., Kreysa, E. & Biermann, P. L., 1989. *Astr. Astrophys.*, **219**, 87.

Condon, J. J., Frayer, D. T. & Broderick, 1991. *Astron. J.*, **101**, 362.

deBruyn, A. G. & Sargent, W. L. W., 1978. *Astron. J.*, **83**, 1257.

deGrijp, M. H. K., Miley, G. K., Lub, J. & de Jong, T., 1985. *Nature*, **314**, 240.

Depoy, D. L., 1987. in: *Infrared Astronomy with Arrays*, p. 426, eds Wynn-Williams, C. G. & Becklin, E. E. (Honolulu: University of Hawaii press).

Depoy, D. L., Becklin, E. E. & Geballe, T. R., 1987. *Astrophys. J. Lett.*, **316**, L63.

Done, C., Ward. M. J., Fabian, A. C., Kunieda. H., Tsuruta, S., Lawrence, A., Smith. M. G. & Wamsteker, W., 1990. *Mon. Not. R. astr. Soc.*, **243**, 713.

Fabbiano, G., Gioia, I. M. & Trinchieri, G., 1988. *Astrophys. J.*, **324**, 749.

Ferland, G. J. & Osterbrock, D. E., 1986. *Astrophys. J.*, **300**, 658.

Gaskell, C. M. & Ferland, G. J., 1984. *Publs astr. Soc. Pacific*, **96**, 393.

Haniff, C. A., Ward, M. J. & Wilson, A. S., 1991. *Astrophys. J.*, **368**, 167.

Harwit, M., Houck, J. R., Soifer, B. T. & Palumbo, G. G. C., 1987. *Astrophys. J.*, **315**, 28.

Henkel, C., Baan, W. A. & Mauersberger, R., 1991. *Astr. Astrophys. Rev.*, **3**, 47.

Hough, J. H., Brindle, C., Wills, B. J., Wills, D. & Bailey, J., 1991. *Astrophys. J.*, **372**, 478.

Hummer, D. G., & Storey, P. J., 1987. *Mon. Not. R. astr. Soc.*, **224**, 801.

Hutchings, J. B. & Neff, S. G., 1989. *Astron. J.*, **97**, 1306.

Hutchings, J. B. & Neff, S. G., 1991. *Astron. J.*, **101**, 434.

Hutchings, J. B., Price, R. & Gower, A. C., 1987. *Astron. J.*, **93**, 6.

Jones, T. J. & Klebe, D., 1989. *Astrophys. J.*, **341**, 707.

Kawara, K., Nishida, M. & Gregory, B., 1990. *Astrophys. J.*, **352**, 433.

Kinney, A. L., Bregman, J. N., Huggins, P. J., Glassgold, A. E. & Cohen, R. D., 1984. *Publs astr. Soc. Pacific*, **96**, 398.

Kinney, A., Antonucci, R. R. J., Ward, M. J., Wilson, A. S. & Whittle, M., 1991. *Astrophys. J.*, **377**, 100.

Kojoian, G., Sramek, R. A., Dickinson, D. F., Tovmassian, H. & Purton, C. R., 1976. *Astrophys. J.*, **203**, 323.

Kollatschny, W. & Fricke, K. J., 1984. *Proc. 4th European IUE Conference*, ESA SP-218. p. 91.

Korista, K. T. & Ferland, G. J., 1989. *Astrophys. J.*, **343**, 678.

Koyama K, Inoue, H., Tanaka, Y., Awaki, H., Takano, S., Ohashi, T. & Matsuoka, M, 1989. *Publs astr. Soc. Japan*, **41**, 731.

Kriss, G. A., 1988. *Astrophys. J.*, **324**, 809.

Kriss, G. A., Canizares, C. R. & Ricker, G. R., 1980. *Astrophys. J.*, **242**, 492.

Krolik, J. H. & Lepp, S., 1989. *Astrophys. J.*, **347**, 179.

Kruper, J. S., Urry, C. M. & Canizares, C. R., 1990. *Astrophys. J. Suppl. Ser.*, **74**, 347.

Lawrence, A., Rowan-Robinson, M., Efstathiou, A., Ward, M. J., Elvis, M., Smith, M. G., Duncan, W. D. & Robson, E. I., 1991. *Mon. Not. R. astr. Soc.*, **248**, 91.

Leech, K. J., Penston, M. V., Terlevich, R., Lawrence, A., Rowan-Robinson, M. & Crawford, J., 1989. *Mon. Not. R. astr. Soc.*, **240**, 349.

Malkan, M. A., 1983. *Astrophys. J. Lett.*, **264**, L1.

Mathis, J. S., 1990. *Ann. Rev. Astr. Astrophys.*, **28**, 37.

Mazzarella, J. M. & Boroson, T. A., 1987. *Bull. Am. astron. Soc.*, **19**, 699.

Mazzarella, J. M., Bothun, G. D. & Boroson, T., 1991. *Astron. J.*, **101**, 2034.

Mazzarella, J. M., Gaume, R. A., Soifer, B. T., Graham, J. R., Neugebauer, G. & Matthews, K., 1990. *Bull. Am. astron. Soc.*, **22**, 88.

Meixner, M., Puchalski, R., Blitz, L., Wright, M. & Heckman, T., 1990. *Astrophys. J.*, **354**, 158.

Miller, J. S. & Goodrich, R. W., 1990. *Astrophys. J.*, **355**, 456.

Moorwood, A. F. M. & Oliva, E., 1991. *ESO Messenger*, **63**, 57.

Morris, S. L. & Ward, M. J., 1989. *Astrophys. J.*, **340**, 713.

Morrison, R. & McCammon, D., 1983. *Astrophys. J.*, **270**, 119.

Mouri, H., Taniguchi, Y., Kawara, K. & Nishida, M., 1989. *Astrophys. J. Lett.*, **346**, L73.

Murray, J., 1990. *Starlink User Note 20.3* (Starlink Project: Rutherford Appleton Laboratory).

Neff, S. G. & Ulvestad, J. S., 1988. *Astron. J.*, **96**, 841.

Oliva, E. & Moorwood, A. F. M., 1990. *Astrophys. J. Lett.*, **348**, L5.

Peterson, B. M., Fricke, K. & Biermann, P., 1981. *Publs astr. Soc. Pacific*, **93**, 281.

Piccinotti, G., Mushotzsky, R. E., Boldt, E. A., Holt, S. S., Marshall, E. E., Serlemitsos, P. J. & Shafer, R. A., 1982. *Astrophys. J.*, **253**, 485.

Roche, P. F., Smith, C. H., Aitken, D. K. & Ward, M. J., 1991. *Mon. Not. R. astr. Soc.*, **248**, 606.

Rowan-Robinson, M. & Crawford, J., 1989. *Mon. Not. R. astr. Soc.*, **238**, 523.

Rudy, R. J., Cohen, R. D., Rossano, G. S., Puetter, R. C. & Chapman, S. C., 1989a. *Astrophys. J.*, **341**, 120.

Rudy, R. J., Rossano, G. S. & Puetter, R. C., 1989b. *Astrophys. J.*, **342**, 235.

Sanders, D. B., Soifer, B. T., Elias, J. H., Madore, B. F., Matthews, K., Neugebauer,G. & Scoville, N. Z., 1988a. *Astrophys. J.*, **325**, 74.

Sanders, D. B., Soifer, B. T., Elias, J. H., Neugebauer, G. & Matthews, K., 1988b. *Astrophys. J. Lett.*, **328**, L55.

Sanders, D. B., Scoville, N. Z., Zensus, A., Soifer, B. T., Wilson, T. L., Zylka, R., and Steppe, H, 1989a. *Astr. Astrophys.*, **213**, L5.

Sanders, D. B., Phinney, E. S., Neugebauer, G., Soifer, B. T. & Matthews, K., 1989b. *Astrophys. J.*, **347**, 29.

Shuder, J. M. & Osterbrock, D. E., 1981. *Astrophys. J.*, **250**, 55.

Snijders, M. A. J., Netzer, H. & Boksenberg, A., 1986. *Mon. Not. R. astr. Soc.*, **222**, 549.

Thronson, H. A., Majewski, S., Descartes, L. & Hereld, M., 1990. *Astrophys. J.*, **364**,456.

Turner, T. J. & Pounds, K. A., 1989. *Mon. Not. R. astr. Soc.*, **240**, 833.

Ulvestad, J. S., Wilson, A. S. & Sramek, R. A., 1981. *Astrophys. J.*, **247**, 419.

Unger, S. W., Pedlar, A., Booler, R. V. & Harrison, B. A., 1986. *Mon. Not. R. astr. Soc.*, **219**, 387.

Veilleux, S. & Osterbrock, D. E., 1987. *Astrophys. J. Suppl. Ser.*, **63**, 295.

Viegas-Aldrovandi, S.M. & Contini, M., 1989. *Astrophys. J.*, **339**, 689.

Ward, M. J., 1988a. *Adv. Space. Res.*, **8**, 39.

Ward, M. J., 1988b. *Mon. Not. R. astr. Soc.*, **231**, 1P.

Ward, M. J., Done, C., Fabian, A. C., Tennant, A. F. & Shafer, R. A., 1988. *Astrophys. J.*, **324**, 767.

Ward, M. J., Elvis, M., Fabbiano, G., Carleton, N. P., Willner, S. P. & Lawrence, A., 1987. *Astrophys. J.*, **315**, 74.

Wright, G. S., Joseph, R. D., Robertson, N. A., James, P. A. & Meikle, W. P. S., 1988. *Mon. Not. R. astr. Soc.*, **233**, 1.

Yates, M.G. & Garden, R. P., 1989. *Mon. Not. R. astr. Soc.*, **241**, 167.

Young, J. S. & Knezek, P. M., 1989. *Astrophys. J. Lett.*, **347**, L55.

Chapter 6

Concluding remarks

Prologue: We have only just begun to realistically test unified models of active galaxies, but the results presented so far are encouraging. "More data" is a clichéd plea at the end of every dissertation, and this is no exception, though "more-of-the-same" is certainly not the author's wish. Below we consider the consequences of some of the results presented in the previous chapters, and the directions for future research they suggest.

1 Searches for obscured nuclear radiation

It is not clear whether infrared spectroscopy is the best tool for testing the predictions of unified schemes of AGN. Although the extinction at infrared wavelengths is an order of magnitude less than in the visible (Figure 1 of Chapter 1), there are obviously objects which contain material so optically thick that not even near-infrared radiation can escape absorption by dust, and even hard X-rays are also affectively quenched by the associated gas.

It might be thought that one should then simply observe lines at longer wavelengths (e.g. the Pfund recombination lines of hydrogen) to circumvent this limitation, but the law of diminishing returns is unfortunately a strong function of wavelength. The higher recombination lines of common elements are generally intrinsically weaker than their optical counterparts, and beyond a few microns wavelength the steeply rising near-infrared continua of active galaxies reduces the equivalent widths of these lines to well below the level of detectability, even from planned space-based observatories. Cygnus A (Chapter 4) probably represents the detectable limit of obscured nuclear activity in the infrared, since although we did not detect broad Paschen α emission in this galaxy, sufficient radiation in the broad-band continuum enabled the nuclear point source to be identified. (Detection of broad Pfund β emission in Cygnus A, at rest wavelength $4.65\,\mu$m, might *just* be possible from Mauna Kea, if conditions were perfect). In this sense, then, near-infrared (1–$5\,\mu$m) spectroscopy represents the "last chance" to detect

obscured nuclear activity at longer wavelengths, but the steep slope of the infrared extinction law (Figure 1 of Chapter 1) ensures that this spectral region should still uncover nuclear activity over a far wider range of extinction ($A_V \lesssim 35$ mag) than is possible with optical observations (dependent of course on sensitivity constraints).

2 Excitation and extinction in narrow line regions

These considerations aside, we should not under-estimate the other useful results gained through infrared observations of the AGN under study here.

The long wavelength baseline afforded by combining optical and near-infrared line fluxes enables accurate extinctions to be estimates even when the infrared lines themselves are measured with inferior accuracy—the flux ratios and corresponding extinction estimates presented for Markarian 463(E) in Table 3 of Chapter 4 are an excellent example of this. The insensitivity of the [SiVI] line to moderate amounts similarly makes it a useful probe of the dusty narrow line regions of AGN (see "Radio galaxies" below). In addition, only near-infrared observations probe the hot molecular gas component through emission from excited H_2. The K-band spectrum of Cygnus A (Figure 1 of Chapter 4) is just a taste of what future observations of narrow-line AGN may bring forth, once investigations with faster 2D array detectors are underway. Since such spectra demonstrate that it is possible in principle to detect three diverse phases of the interstellar medium in a single observation, further studies of large samples may allow us to extend the traditional diagnostic line ratio diagrams for classifying nuclear activity (e.g. Veilleux & Osterbrock 1987) to embrace these near-infrared features.

A few brief notes summarizing the key achievements of this thesis are in order, and we use these as a springboard for projecting similar studies into the future.

3 Seyfert 2 galaxies

We have clearly strong emission from a broad line region in two so-called *Narrow Line X-ray Galaxies*, where, at best, the evidence for such emission at shorter wavelengths was controversial, and certainly nothing like that expected from Seyfert 1s of comparable X-ray luminosity. Much of the extinction towards their nuclei appears to take place between

the classical narrow line and broad line regions, and in NGC5506 a further column of (dust-free) gas is known to exist towards the hard X-ray source. The extended high ionization gas in all three galaxies under study attests to the existence of much less obscured line of sight to these AGN, along observers would classify them as Seyfert 1s. One limitation of our conclusions throughout this thesis has been the tacit assumption that this ionizing continuum is emitted *isotropically* at the source, and the observed anisotropy is then presumed to result from "shadowing" of this source along certain directions (including our own line of sight).

After the work presented in Chapter 3 was completed, a number of Seyfert 2 AGN were subsequently detected by the *GINGA* satellite (e.g. Markarian 348—Warwick *et al.* 1989; Markarian 3—Awaki *et al.* 1990). These AGN exhibit large amounts of low-energy absorption ($N_H \sim 10^{23}\,\mathrm{cm}^{-2}$), and there are indications that such objects may even be sufficiently numerous to contribute to the hard X-ray background (Setti & Woltjer 1989).

Ironically, it is this background which currently limits the sensitivity of large area proportional counters aboard X-ray satellites. In this thesis we have made much of the fruitful interplay between X-ray and near-infrared observations. This is to be expected, since not only are the luminosities in each band correlated, but it also turns out that for a typical column of interstellar medium, the optical depths of a 2-μm and a 2-keV photons are comparable. Although deeply-buried AGN have been detected in X-rays for which near-infrared nuclear emission is hard to discern (e.g. NGC4388–Chapter2) improvements in infrared technology may reverse the situation in the future.

4 Radio galaxies

Although we did not detect broad line emission in Cygnus A, we show that the detection of a point source at hard X-rays and at 2.2 μm is consistent with this galaxy harbouring a quasar nucleus obscured by A_V=37$\pm$7 mag—one of the highest extinctions "measured" towards an active nucleus to date. The exceptionally strong emission from H_2 (which we did not expect to see) *may* arise in a compact region associated with the obscuring dust, though observations at higher resolution are needed to test this conclusion.

The detection of a strong [SiVI]1.962 μm line in Cygnus A presents an interesting

prospect for further work. One of the major objections to Barthel's (1989) scheme for unifying powerful radio galaxies and quasars has been provided by Jackson & Browne (1990), who find that radio galaxies are systematically *less luminous* in [OIII]500.7nm emission than a comparison sample of quasars. To reconcile this with the "unified scheme" it is necessary to invoke angle-dependent obscuration not just of the BLR, but also of the NLR (by $A_V \simeq 2$–3 mag). The [SiVI]1.962μm line would be virtually unaffected by an extinction, and since the line cannot be produced by star formation (unlike [OIII]) it would provide an excellent extinction-insensitive measure of an AGN's hard ultraviolet luminosity, and hence enable a more definite test to be made.

5 "Ultra-luminous" infrared galaxies

Since their discovery by the *IRAS* survey, the origin of the luminosity in infrared-luminous systems has been the subject of over 5 years of observational effort, with little progress in their understanding. This now seems hardly surprising, given the enormous column depths towards the heating sources in these objects inferred from recent radio observations (Condon, Huang & Yin 1991; Sopp & Alexander 1991), which also favour a compact starburst origin for the radio continuum structure. Such objects will be optically thick even to near-infrared radiation and hard X-rays, however, so this conclusion will be hard to test, though mid-infrared spectroscopy of the silicate absorption feature should yield reliable dust optical depths towards these regions.

However, near-infrared spectroscopy of Markarian 463(E)—a member of the "warm" sub-sample of ultraluminous infrared galaxies—has revealed a moderately obscured (compact) Seyfert 1 nucleus which is able to account for almost *all* of the high far-infrared luminosity detected by *IRAS*. The [OIII] emission line structure, and the efficient scattering of nuclear radiation towards us (probably by electrons, and possibly by by dust as well) indicate that clear lines of sight do exist towards this AGN. Although the extinction we find may be evidence of a concentration of dusty molecular material in the nuclear regions, we do not interpret Markarian 463 as a "transition stage" in the Sanders *et al.* (1988) scheme for the origin of quasars. For a sample of of infrared-bright galaxies, Roche *et al.* (1991) reached similar conclusions through mid-infrared their spectroscopy of infrared-bright galaxies, finding very few objects which displayed composite

Seyfert+starburst signatures.

6 Broad line active galaxies

Although no new observations of Seyfert 1s or quasars have been presented in this thesis, the research would of course have been impossible without the wealth of observational data available for these broad line AGN. Near-infrared spectroscopy can still add to this knowledge in some useful ways relevant to this work, and these are outlined below.

6.1 Line/continuum correlations in the near-infrared

Extensive use has been made in this thesis of correlations established between the broad line, X-ray and infrared luminosities of quasars and Seyfert 1 galaxies. Typically the fundamental parameter considered is the hard X-ray luminosity, which is taken as a measure of the energy output of the central source. At visible wavelengths, a correlation is also observed between the continuum luminosity and broad Hα equivalent width, which is a consequence of photo-ionization. It would be interesting in the future to investigate whether a correlation of similar strength and slope is observed between 1 μm luminosity and the 1.282 μm line equivalent width in low-redshift Seyfert 1 AGN. Given that these quantities are supposed to be dependent on hard X-ray luminosity, a correlation is certainly expected, but if it is weaker or significantly different from its optical analogue then the presence of another continuum component (e.g. a dense stellar cluster?—Lawrence *et al.* 1991, and references therein) could then be inferred.

6.2 Angle-dependent obscuration in Seyfert 1s and quasars

While it has been convincingly demonstrated that at least some narrow line AGN would appear as broad line, quasar-like objects if viwed from other angles, it still remains to be conclusively proven that the inverse is true. One plausible piece of evidence is the detection of Fe Kα line emission in the X-ray spectra of Seyfert 1s, often accompanied by lower-energy absorption. The frequency and equivalent widths of these features indicates a non-spherical distribution of matter in these AGN, but detailed variability studies are

needed to constrain the extent of this material (e.g. Kunieda *et al.* 1990).

Another approach is to search for emission from *molecular* material, and this has been pursued by Kawara, Nishida & Gregory (1990). Despite some encouraging detections by these authors, we show in Chapter 4 that the expected equivalent widths of the H_2 lines, when observed against an unobscured quasar continuum, are at the very limits of detectability from the ground. Infrared spectrometers with improved quantum efficiency and higher resolution may still yield useful results in this area, though again the location of the emission may not necessarily be confined to a compact obscuring torus (cf. NGC1068—Rotaciuc *et al.* 1991).

7 And finally...

Clearly it would be desirable to perform future studies on complete samples selected without bias of extinction or beaming. Such samples may be furnished by the recently-completed *IRAS* Faint Source Survey database for Seyfert and infrared-luminous galaxies, and the complete "10-Jansky" sample of Laing, Riley & Longair (1983) for powerful radio galaxies. Whatever results are furnished by statistical studies of unified schemes in the future, near-infrared spectroscopy promises to provide an important tool for testing them.

References

Awaki, H., Koyama, K., Kunieda, H. & Tawara, Y., 1990 *Nature*, **346**, 544.

Barthel, P. D., 1989. *Astrophys. J.*, **336**, 606.

Condon, J. J., Huang, Z.-P. & Yin, Q. F., 1991. *Astrophys. J.*, **378**, 65.

Jackson, N. & Browne, I. W. A., 1990. *Nature*, **343**, 43.

Kawara, K., Nishida, M. & Gregory, B., 1990. *Astrophys. J.*, **352**, 433.

Kunieda, H., Turner, T. J., Awaki, H., Koyama, K., Mushotzsky, R. .& Tsusaka, Y., 1990. *Nature*, **345**, 786.

Laing, R. A., Riley, J. M. & Longair, M. S., 1983. *Mon. Not. R. astr. Soc.*, , **204**, 157.

Lawrence, A., Rowan-Robinson, M., Efstathiou, A., Ward, M. J., Elvis, M., Smith, M. G., Duncan, W. D. & Robson, E. I., 1991. *Mon. Not. R. astr. Soc.*, **248**, 91.

Roche, P. F. Smith, C. H., Aitken, D. K. & Ward, M. J., 1991. *Mon. Not. R. astr. Soc.*, **248**, 606.

Rotaciuc, V., Krabbe, A., Cameron, M., Drapatz, S., Genzel, R., Sternberg, A., & Storey, J. W. V., 1991. *Astrophys. J. Lett.*, **370**, L23.

Sanders, D. B. Soifer, B. T., Elias, J. H., Madore, B. F., Matthews, K., Neugebauer,G. & Scoville, N. Z., 1988. *Astrophys. J.*, **325**, 74.

Setti, G. & Woltjer, L., 1989. *Astrophys. J.*, **224**, L21.

Sopp, H. M. & Alexander, P., 1991. *Mon. Not. R. astr. Soc.*, **251**, 112.

Veilleux, S. & Osterbrock, D. E., 1987. *Astrophys. J. Suppl. Ser.*, **63**, 295.

Warwick, R. S., Koyama, K., Inoue, H., Takano, S., Awaki, H. & Hoshi, R., 1989. *Publs astr. Soc. Japan*, **41**, 739.

Mon. Not. R. astr. Soc. (1990) **242,** *Short Communication,* 4P–8P

Broad infrared line emission from the nuclei of Seyfert 2 galaxies

Philip R. Blanco
Department of Astronomy, University of Edinburgh, Blackford Hill, Edinburgh EH9 3HJ

Martin J. Ward
Institute of Astronomy, Madingley Road, Cambridge CB3 0HA

Gillian S. Wright
Joint Astronomy Centre, 665 Komohana Street, Hilo, HI 96720, USA

Accepted 1989 October 5. Received 1989 October 4

SUMMARY

We report spectroscopic observations at $\lambda/\delta\lambda \simeq 300$ of the Paschen β hydrogen recombination line in the narrow line X-ray galaxies NGC 5506 and A0945 − 30 (= MCG-5-23-16), and in the Seyfert 2 galaxy NGC 4388. The line profiles of NGC 5506 and A0945 − 30 are both found to possess broad components of FWHM > 1500 km s^{-1}; this removes the previous controversy concerning the presence of broad line components in their Hα line profiles. We use optical, X-ray and mid-infrared data to estimate the extinction towards the line and continuum sources in these objects in order to test the hypothesis that they are in fact moderately obscured Seyfert 1 nuclei.

The non-detection of a broad Paschen β line profile in NGC 4388 is consistent with a scattered (as opposed to a transmitted) origin for the observed off-nuclear broad Hα emission, in agreement with models of the optical emission-line geometry in this galaxy.

Mon. Not. R. astr. Soc. (1990) **242,** *Short Communication,* 4P–8P

Broad infrared line emission from the nuclei of Seyfert 2 galaxies

Philip R. Blanco
Department of Astronomy, University of Edinburgh, Blackford Hill, Edinburgh EH9 3HJ

Martin J. Ward
Institute of Astronomy, Madingley Road, Cambridge CB3 0HA

Gillian S. Wright
Joint Astronomy Centre, 665 Komohana Street, Hilo, HI 96720, USA

Accepted 1989 October 5. Received 1989 October 4

SUMMARY

We report spectroscopic observations at $\lambda/\delta\lambda \simeq 300$ of the Paschen β hydrogen recombination line in the narrow line X-ray galaxies NGC 5506 and A0945−30 (=MCG-5-23-16), and in the Seyfert 2 galaxy NGC 4388. The line profiles of NGC 5506 and A0945−30 are both found to possess broad components of FWHM > 1500 km s^{-1}; this removes the previous controversy concerning the presence of broad line components in their Hα line profiles. We use optical, X-ray and mid-infrared data to estimate the extinction towards the line and continuum sources in these objects in order to test the hypothesis that they are in fact moderately obscured Seyfert 1 nuclei.

The non-detection of a broad Paschen β line profile in NGC 4388 is consistent with a scattered (as opposed to a transmitted) origin for the observed off-nuclear broad Hα emission, in agreement with models of the optical emission-line geometry in this galaxy.

1 INTRODUCTION

There is increasing evidence that the diversity of spectral shapes of Seyfert Active Galactic Nuclei (AGN) from infrared to X-ray frequencies is due at least in part to the effects of obscuring material along the line-of-sight (Lawrence & Elvis 1982; Ward *et al.* 1987). In particular, observations at X-ray energies have revealed that a subset of those AGN which have narrow lines of hydrogen and helium in their optical spectra (and are hence classified as Seyfert 2s, Weedman 1977) emit hard X-rays at luminosities characteristic of Seyfert 1 nuclei. This is despite the fact that at lower X-ray energies, Seyfert 2s are roughly one hundred times less luminous than Seyfert 1s (Kriss, Canizares & Ricker 1980). A step towards understanding these so-called *Narrow Line X-ray Galaxies* resulted from a study of the archetypcal Seyfert 2 galaxy NGC 1068 by Antonucci & Miller (1985). Using spectropolarimetry they discovered a polarized (scattered) broad line component to the optical permitted lines, which implies that the true Seyfert 1 nucleus is hidden by a very large column of obscuring material. The amount of dust and gas is so great (e.g. $A_V > 100$ mag, Depoy 1987), that even the hard X-rays are extinguished.

It has been suggested that the nuclei of many Seyfert 2 galaxies harbour a Broad Line Region (BLR), which together with the powerful Seyfert 1 ionizing continuum source is hidden from direct view by intervening gas and dust; the much larger Narrow Line Region (NLR) would then extend beyond this 'blocking' material (e.g. Krolik & Begelman 1986). The geometry of this obscuring matter is, however, not well known. If it is in the form of a simple torus, then the column of material intercepted by our line-of-sight will depend on its inclination. An alternative possibility is that the active nucleus is completely enshrouded by dust (i.e. a covering factor of unity). However, this seems unlikely in those AGN where there is strong narrow line emission from He II, [Fe VII] and [Ne V], which requires a hard, unreddened ultraviolet continuum for excitation. Since the spectra of Seyfert 2 nuclei often display lines of such high-excitation species (Koski 1978), the detection of heavily reddened BLRs in them provides a test for models involving collimation of the ionizing continuum. This may be produced either by intrinsic physical processes, or simply by angle-dependent absorption ('shadowing') of the continuum source.

The extinction along our line-of-sight to the BLR in a Seyfert nucleus will of course be a variable parameter from object to object. This is supported by the existence of an intermediate class of Seyfert galaxy–Seyfert 1.9 (Osterbrock

1981). The optical spectra of these AGN display weak broad wings on the Hα line, whereas this component is almost undetectable at shorter wavelengths due to the differential extinction of dust grains. The extinction towards the BLRs in these galaxies must be $A_V \lesssim 5$ mag for the broad Hα line components to be visible at all. This leads us to expect that there may be many AGN in which the BLR is obscured in the visible by more than this (hence resulting in their classification as Seyfert 2s), but which emit broad line radiation directly observable in the near-infrared (1–4 μm) where the dust extinction is less.

We report here observations of the 1.282-μm Paschen β line in three Seyfert 2 galaxies. The extinction due to dust at this wavelength is related to that in the optical by $A_{1.28\,\mu m} \simeq 0.3\,A_V$, i.e. the line is attenuated only by a factor of 4 for a visual extinction of 5 mag. The achievable limit in practice for detecting broad lines depends of course on the signal-to-noise ratio of the spectrum and the equivalent widths of the broad and narrow line components.

2 OBSERVATIONS AND REDUCTION

The spectra presented in Fig. 1 were taken at the United Kingdom Infrared Telescope (UKIRT) in 1989 February with the cooled grating spectrometer CGS 2, using a 637 lines mm^{-1} grating in first order and a circular aperture 5.0 arcsec in diameter. The resolution of the instrument is fixed by the finite size of the detector elements. The aperture was centred on the optical nuclei of NGC 5506 and A0945 − 30, and a position 3 arcsec north, 4 arcsec east of the optical nucleus of NGC 4388 for reasons described later (Section 3.1). The grating was stepped successively so that adjacent points in the spectrum were spaced by one quarter of a detector width. Standard chopping and beamswitching procedures were followed to subtract the background emission, and atmospheric absorption features were removed by dividing each galaxy spectrum with that of a late-type star close in the sky. Although conditions were not photometric, on both nights the cancellation of telluric absorption features was excellent (remaining features are at less than 3 per cent of the continuum level). An approximate flux calibration of 15–20 per cent accuracy was obtained by observing standard stars at similar airmasses. For NGC 5506 the flux calibration is accurate to within 10 per cent, because we were able to calibrate the peak line flux from an earlier, lower signal-to-noise spectrum taken in photometric conditions. Wavelength calibration and determination of the instrumental profile were performed by observing the Paschen β line in bright planetary nebulae using the same configuration of the instrument. The observations are summarized in Table 1.

The Paschen β line was detected close to its predicted redshifted wavelength in all three programme objects, and its profile was significantly broader than the instrumental

Table 1. Journal of observations.

Object Name	Recession z	UT Date	Integration /point	Spectral Standard
NGC 4388 3^{m}N, 4^{m}E	0·0084	1989 Feb 25	140s	BS 4777
NGC 5506	0·0059	1989 Feb 26	220s	BS 5384
A0945-30=MCG-5-23-16	0·0086	1989 Feb 26	310s	BS 3833

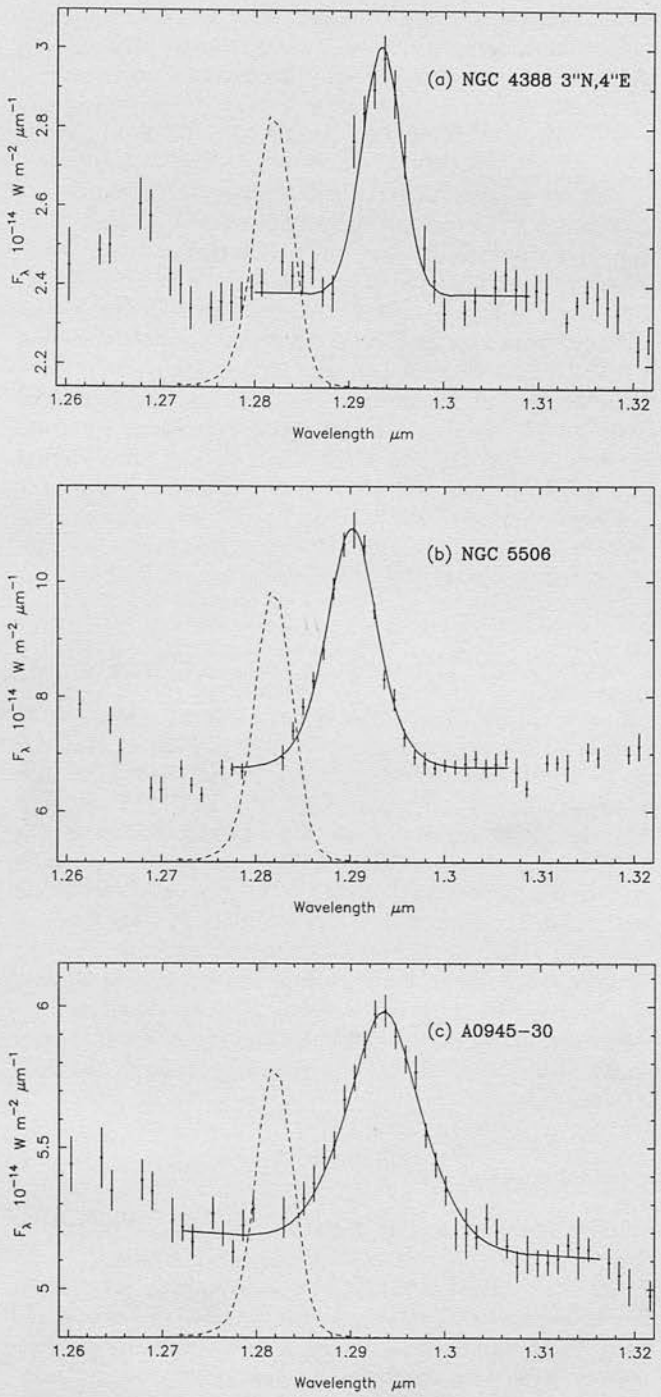

Figure 1. Near-infrared spectra of three Seyfert 2 Galaxies. Each spectrum has been smoothed with a Gaussian of FWHM equal to half of that of the instrumental profile. Also shown for each spectrum is the model fit to the Paschen β line profile (solid line), and the smoothed instrumental resolution as derived from observations of planetary nebulae (broken line), which has a FWHM of 1100 km s^{-1}. (a) NGC 4388, 3 arcsec north, 4 arcsec east of the optical nucleus, (b) NGC 5506 and (c) A0945 − 30 = MCG-5-23-16.

response in the cases of NGC 5506 and A0945 − 30. The divided spectra were smoothed with a Gaussian function of FWHM = 0.00215 μm (equal to one half of a detector width), and then re-binned on to a uniform wavelength scale. This procedure removes the worst of the pixel-to-pixel vari-

ations which arise from changes in the atmospheric transmission and seeing while the grating is being scanned. An identical treatment was applied to the planetary nebulae line observations; the resulting instrumental response function is well described by a Gaussian profile with FWHM = 1100 km s^{-1}.

In order to separate the broad and narrow components of the Paschen β lines a least-squares fit was made to each spectrum. The continuum level was determined by linear interpolation between points on each side of the Paschen β line, excluding the region near 1.26 μm which contains a contribution from He I and [Fe II] emission. To the Paschen β profile itself we then fitted a Gaussian function of FWHM set equal to that of the narrow Hα line, and an additional Gaussian of variable FWHM, both convolved with the instrumental profile and constrained to the same central wavelength. In the case of NGC 4388 the inclusion of a Gaussian profile broader than the narrow line width did not improve the fit significantly. The results of the fitting procedure for each object are presented in Table 2.

3 COMPARISON WITH EXISTING DATA

All three objects observed have been studied extensively at optical wavelengths and show different degrees of evidence for broad line components on the Hα line. We discuss each galaxy in order of increasing hard X-ray (2–10 keV) luminosity. By combining the measured Paschen β fluxes with optical spectroscopy it is possible to derive the extinction towards the line-emitting regions in these objects. We use the interstellar dust extinction law as interpolated from Rieke & Lebofsky (1985), and we make the assumption that the intrinsic Hα/Paschen β line ratio is close to its case B value of 17.6. For NGC 5506 and A0945 − 30 these extinction estimates can be compared with the obscuration towards their nuclear continuum sources as derived from X-ray and mid-infrared data.

3.1 NGC 4388

Despite being the nearest of the three Seyferts discussed in this paper (taking the distance of the Virgo cluster to be 18 Mpc), NGC 4388 has not yet been reported as a detection in hard X-rays. However, it has been detected at lower X-ray energies by the *Einstein* satellite (Green *et al.* 1989). This edge-on galaxy was the subject of an extensive Hα line imaging study by Shields & Filippenko (1988, hereafter SF88) who found broad wings on this line at a number of positions close to the optical nucleus. The infrared spectrum shown in Fig. 1(a) was taken at the peak of the broad Hα emission reported by SF88, which they gave as 3 arcsec north, 4 arcsec east of the optical nucleus. It can be seen from the spectrum that there are no detectable broad wings on the Paschen β line. Although a smaller aperture was used for the optical observations, and our 5-arcsec beam averages the line emission over a region of non-uniform broad Hα emission, we can at least be certain from our upper limit for the corresponding broad component of Paschen β (Table 2) that the average extinction suffered by the broad line emission at this position in NGC 4388 is $A_V < 6.5$ mag.

Pogge (1988) compares the optical emission line geometry of this galaxy to that of NGC 1068, in which the radiation from the BLR is believed to be scattered into our line-of-sight, either by electrons or perhaps by dust grains. In both NGC 1068 and NGC 4388 the high excitation gas (as defined by the ratio of [O III] to Hα emission) has a cone-like morphology. In terms of the 'obscured Seyfert 1' hypothesis described in Section 1, the large column of gas prevents us from observing hard X-rays directly from the active nucleus, while the associated dust blocks the direct (transmitted) broad line emission even in the near-infrared. The *scattered* off-nuclear broad line emission, on the other hand, is not expected to be highly reddened, since the scattering region 'mirrors' its less obscured view of the BLR. Our non-detection of broad Paschen β is consistent with this origin of the broad Hα emission in NGC 4388, as it rules out transmitted broad line radiation from a highly reddened source. However, as noted by SF88, spectro-polarimetry of the optical permitted lines at a number of off-nuclear positions is essential to confirm this picture.

3.2 NGC 5506

This edge-on galaxy is noted for its rapid X-ray variability and high 2–10 keV luminosity (Turner & Pounds, in preparation, hereafter TP90). Although these properties are characteristic of Seyfert 1 activity, the optical spectrum of this galaxy is that of a Seyfert 2 with permitted lines of FWHM = 370 km s^{-1} (Shuder 1980). The Paschen β spectrum shown in Fig. 1(b) displays an additional broad line component of FWHM = 1550 km s^{-1}, providing unambiguous evidence of an obscured BLR in this galaxy.

Traditionally, studies of reddened Seyfert nuclei have concentrated on searches for broad wings on the Hα line (e.g. Véron *et al.* 1980). The blending of this line with emission from [N II] and uncertainty over the intrinsic profile of the narrow component have meant that different workers have arrived at discrepant results for the case of NGC 5506 (e.g. Whittle 1985; Boisson & Durret 1986). Fortunately, though, there is a secondary indicator of Seyfert 1 activity in the optical, provided that the extinction towards the BLR is not too great. Line emission from O I at 8446 Å is believed to arise from Lyman β fluorescence in high optical depth, high-density clouds (Grandi 1980). This line was detected in NGC 5506 and NGC 7314 by Morris & Ward (1985), who suggested that its presence is closely related to the Seyfert 1 phenomenon. Taking the sample of unobscured Seyfert 1s with fluxes reported for this line (Grandi 1980; Morris & Ward 1988) we find that the median value of the line flux ratio (O I 8446 Å/Hα) is approximately 0.038, which implies an intrinsic (O I 8446 Å/broad Paβ) line ratio of $\simeq 1.5$. Comparing this characteristic value for Seyfert 1s with the ratio observed for NGC 5506 (Morris & Ward 1985, 1988) implies $A_V \simeq 6$ mag for the BLR gas. Similarly, if we take the broad Hα flux reported by Durret & Bergeron (1988, hereafter DB88) we obtain $A_V = 5.0 \pm 0.5$ mag from the broad (Hα/Paβ) ratio.

From the low-energy cut-off in the X-ray spectrum of NGC 5506 TP90 derive a gas column density of $N_H = 2.8 \pm 0.5 \times 10^{22}$ cm^{-2} towards the hard X-ray source. Note that the BLR visual extinction determined above implies that a column of approximately 1.7×10^{22} cm^{-2} of

his gas is situated between the BLR and the hard X-ray source, assuming that a standard dust-to-gas ratio of $A_V = 4.5 \times 10^{-22} N_H$ applies exterior to the BLR.

An estimate of the dust extinction towards the infrared continuum emission is provided by the 8–13 μm spectrum of Roche *et al.* (1984). From the optical depth of the 9.7-μm silicate feature they derive an equivalent visual extinction of 20 ± 2 mag to the 10-μm source (taking $A_V = 15\ \tau_{9.7}$). If this is correct, our estimate of the BLR extinction above would imply that a large amount of silicate dust exists between the non-thermal source and the BLR, a situation we consider unlikely since these grains could not survive so close to the source of ultraviolet photons (e.g. Barvainis 1987). Noting this difference we adopt an extinction to the BLR gas of $A_V = 5.7 \pm 1$ mag, which is consistent with the optical observations within the uncertainties.

3.3 A0945 − 30 = MCG-5-23-16

Slightly more luminous at hard X-ray energies than NGC 5506 (TP90), A0945 − 30 has also been optically classified as a Seyfert 2, with permitted recombination lines of FWHM 270 km s^{-1} (Wilson, Baldwin & Ulvestad 1985). Véron *et al.* (1980) tentatively fitted a broad component to the Hα line profile, while more recently DB88 reported a broad line flux an order of magnitude higher from their line profile fitting. In our Paschen β spectrum shown in Fig. 1(c), the broad line emission (FWHM = 2150 km s^{-1}) dominates the total line profile with negligible contribution from the narrow component. Combining the broad Hα flux from DB88 with our observed broad Paschen β flux (Table 2) gives a BLR extinction of $A_V = 4.0 \pm 0.7$ mag. Following the same arguments as for NGC 5506 above, we find that this extinction value is just consistent with the observed upper limit on the O I 8446 Å line flux (Morris & Ward 1989), which yields $A_V > 6$ mag.

The gas column density towards the hard X-ray source of $N_H = 1.06 \pm 0.4 \times 10^{22}$ cm^{-2} reported by TP90 would imply a similar visual extinction of 4.8 ± 2.5 mag for a standard galactic dust abundance. For the purpose of this paper we therefore adopt a broad line extinction of $A_V = 5.0 \pm 1.5$ mag. Finally, we note that Aitken & Roche (1985) determined an extinction of $A_V = 6 \pm 1.5$ mag to the 10-μm source from the depth of the 9.7-μm silicate feature, which in this case is in agreement with the other extinction estimates.

Table 2. Fitted Paschen β line widths and fluxes.

	Narrow Line		Broad Line		Continuum
Object	FWHM	Flux	FWHM	Flux	F_λ (1·29 μm)
NGC 4388	230 [a]	3·3±0·2	2000 [a]	<1·5 (3σ)	2·4 (15%)
NGC 5506	370 [b]	11±3	1550±300	18±3	6·8 (10%)
A0945-30	270 [c]	<2·5 (3σ)	2150±250	7·5±0·7	5·2 (20%)

Notes: (1) Line fluxes are in units of 10^{-17} W m^{-2}; line widths (corrected for the instrumental profile) are in km s^{-1}. The errors given for these are the formal 1σ uncertainties obtained from the fitting procedure. (2) The continuum flux densities at 1.29 μm are in units of 10^{-14} W m^{-2} μm^{-1}. The quoted percentage errors reflect the uncertainty in the *absolute* flux calibration.

References: (a) Shields & Filippenko (1988); (b) Shuder (1980); (c) Wilson, Baldwin & Ulvestad (1985).

4 NGC 5506 AND A0945 − 30: OBSCURED SEYFERT 1 NUCLEI

Although we have detected broad Paschen β line emission from both NGC 5506 and A0945 − 30, it still remains to be shown that they are in fact moderately obscured, but otherwise typical, Seyfert 1 nuclei. (It is conceivable, for instance, that this class of AGN could have an intrinsically underluminous BLR, which escapes detection in the optical without the need for significant obscuration.)

For relatively unobscured Seyfert 1 AGN there exists a well-established correlation between broad Hα and 2–10 keV luminosity (e.g. Ward *et al.* 1988). By correcting the broad Paschen β fluxes presented in Table 2 for the BLR extinction values adopted above (Section 3) we can estimate the intrinsic (i.e. de-reddened) broad Hα luminosity for NGC 5506 and A0945 − 30. The results of this procedure are presented in Table 3. The positions of NGC 5506 and A0945 − 30 on a plot of L(2–10 keV) versus L(Hα) (e.g. as presented in fig. 5 of Ward *et al.* 1988; note that they use CGS units) lie close to the correlation line for X-ray selected Seyfert 1s, once this correction for extinction has been made. Hence our observations provide direct support for the Seyfert 1 nature of the BLRs in these galaxies.

Table 3. Adopted BLR extinctions and derived extinction-corrected luminosities.

	A_V	$\log_{10} L$ (Watt)	
Object	(mag) [a]	broad Hα [a]	2–10 keV [b]
NGC 5506	5·7±1·0	35·3±0·1	36·1
A0945-30	5·0±1·5	35·1±0·4	36·3

Note: We take $H_0 = 50$ km s^{-1} Mpc^{-1} and assume isotropic emission.

References: (a) See Section 4 of the text; (b) Turner & Pounds (in preparation).

It should be noted that for each of the methods used above to determine the extinction towards the BLRs of NGC 5506 and A0945 − 30, no information can be obtained as to the location of the obscuring matter along the line-of-sight. However, some indirect arguments can be made. NGC 5506 appears on photographs as a dusty edge-on disc galaxy. One can reasonably assume that most of the BLR extinction takes place in the interstellar medium of the disc over several kiloparsec. On the other hand, the host galaxy of A0945 − 30 appears to be of type S0. Based on the narrow line optical ratios (DB88) and the upper limit we find for the flux of the narrow component of Paschen β (Table 2), the NLR gas is obscured by only $A_V \simeq 2.5$ mag, so in this case a large fraction of the nuclear extinction takes place within, or more likely just outside, the BLR of this active nucleus.

5 DISCUSSION

In attempts to unify the classification of AGN it is often proposed that at least some Seyfert 2 galaxies possess obscured Seyfert 1 nuclei (e.g. Lawrence 1987). NGC 5506 and

A0945 − 30 represent an extension of the Seyfert 1.9 class; their broad Hα emission is barely detectable, and has thus been the subject of previous controversy.

Observations of the Paschen β line are sensitive to extinctions in the range $5 \lesssim A_V \lesssim 10$ mag. This is because if the BLR extinction is less, we would detect clear broad components on the Hα line, but for values much more than this the broad Paschen β components would also be extinguished. The latter is probably the case for NGC 4388 and NGC 1068, which display only scattered off-nuclear broad line emission. However, a detailed search for transmitted broad line emission from these nuclei, perhaps slightly offset from the peaks of their continuum emission, is necessary to confirm this.

All three galaxies discussed in this paper contain large quantities of extended high-excitation narrow line gas (Wilson, Baldwin & Ulvestad 1985 - NGC 5506 and A0945 − 30; Pogge 1988 - NGC 4388). It follows that this gas must be exposed to a less obscured view of the active nucleus, in comparison to our own particular line-of-sight, otherwise there would be far too few hard ultraviolet photons to produce the observed line strengths. This provides an indirect argument for anisotropic continuum emission in these objects (e.g. Wilson, Ward & Haniff 1988), in which the obscuring material along our line-of-sight also serves to collimate the ionizing continuum.

6 CONCLUSIONS

We have detected broad (FWHM > 1500 km s^{-1}) components in the Paschen β line of NGC 5506 and A0945 − 30, removing the previous controversy over the existence of an obscured BLR in these objects. In NGC 4388 the upper limit we find for the broad Paschen β flux at the peak of broad Hα emission is consistent with the scattered broad emission line geometry proposed for this and other Seyfert 2 galaxies.

We also find that the strength of the O I 8446 Å line in NGC 5506, and the upper limit reported for A0945 − 30, are consistent with other estimates of the BLR reddening in these objects. On the basis of our results for this line we predict that NGC 7314 should display broad Paschen β emission of similar strength to A0945 − 30.

With the recent increase in the performance of ground-based infrared spectroscopy it is now becoming possible to detect (or set stringent upper limits on) dust-obscured broad line emission in Seyfert 2 galaxies. Resolved spectroscopy of the 2.17-μm Brackett γ line ($A_{2.17\,\mu m} \simeq 0.1\ A_V$) and the 4.05-$\mu$m Brackett α line ($A_{4.05\,\mu m} \simeq 0.05\ A_V$) will be able to explore the highly extinguished regions of AGN to greater dust optical depths than is possible with the Paschen β line utilized here. Unfortunately the increased thermal background radiation at these wavelengths, combined with the steeply rising 1–10 μm continua of Seyfert galaxies and the correspondingly small equivalent widths of the Brackett lines, make these observations much more difficult in practice. However, further observations of infrared recombination lines in a sample of Seyfert 2 galaxies *not* known to be strong emitters of hard X-rays are needed to establish their relationship, if any, to luminous Seyfert 1 nuclei.

ACKNOWLEDGMENTS

It is a pleasure to thank Tom Geballe, Phil Puxley and Dolores Walther for their assistance at the telescope. We would also like to acknowledge the UKIRT Service observing programme for obtaining the initial spectrum of NGC 5506 which prompted this work. Pat Roche contributed valuable advice and encouragement during the analysis of the data. These observations were made possible by the technical skill of Rosemary Chapman and the members of the CGS 2 upgrade team in Edinburgh and in Hilo, to whom we are indebted for the improvements made to the instrument shortly before our observing run. PRB is in receipt of a SERC studentship.

REFERENCES

Aitken, D. K. & Roche, P. F., 1985. *Mon. Not. R. astr. Soc.*, **213**, 777.
Antonucci, R. R. J. & Miller, J. S., 1985. *Astrophys. J.*, **297**, 621.
Barvainis, R., 1987. *Astrophys. J.*, **320**, 537.
Boisson, C. & Durret, F., 1986. *Astr. Astrophys.*, **168**. 32.
Depoy, D. L., 1987. In: *Infrared Astronomy with Arrays*, p. 426, eds Wynn-Williams, C. G. & Becklin, E. E., University of Hawaii Press, Honolulu.
Durret, F. & Bergeron, J., 1988. *Astr. Astrophys. Suppl.*, **75**, 273 (DB88).
Grandi, S. A., 1980. *Astrophys. J.*, **238**, 10.
Green, P. J., Ward, M. J., Anderson, S. F., Margon, B., de Grijp, M. H. K. & Miley, G. K., 1989. *Astrophys. J.*, **339**, 93.
Koski, A. T., 1978. *Astrophys. J.*, **223**, 56.
Kriss, G. A., Canizares, C. R. & Ricker, G. R., 1980. *Astrophys. J.*, **242**, 492.
Krolik, J. H. & Begelman, M. C., 1986. *Astrophys. J.*, **308**, L55.
Lawrence, A., 1987. *Publs astr. Soc. Pacif.*, **99**, 309.
Lawrence, A. & Elvis, M., 1982. *Astrophys. J.*, **256**, 410.
Morris, S. L. & Ward, M. J., 1985. *Mon. Not. R. astr. Soc.*, **215**, 57P.
Morris, S. L. & Ward, M. J., 1988. *Mon. Not. R. astr. Soc.*, **230**, 639.
Morris, S. L. & Ward, M. J., 1989. *Astrophys. J.*, **340**, 713.
Pogge, R. W., 1988. *Astrophys. J.*, **332**, 702.
Osterbrock, D. E., 1981. *Astrophys. J.*, **249**, 462.
Rieke, G. H. & Lebofsky, M. J., 1985. *Astrophys. J.*, **288**, 618.
Roche, P. F., Aitken, D. K., Phillips, M. M. & Whitmore, B., 1984. *Mon. Not. R. astr. Soc.*, **207**, 35.
Shields, J. C. & Filippenko, A. V., 1988. *Astrophys. J.*, **332**, L55 (SF88).
Shuder, J. M., 1980. *Astrophys. J.*, **240**, 32.
Véron, P., Lindblad, P. O., Zuiderwyk, E. J., Véron, M. P. & Adam, G., 1980. *Astr. Astrophys.*, **87**, 245.
Ward, M. J., Done, C., Fabian, A. C., Tennant, A. F. & Shafer, R. A., 1988. *Astrophys. J.*, **324**, 767.
Ward, M. J., Elvis, M., Fabbiano, G., Carleton, N. P., Willner, S. P. & Lawrence, A., 1987. *Astrophys. J.*, **315**, 74.
Weedman, D. W., 1977. *Ann. Rev. Astr. Astrophys.*, **15**, 69.
Whittle, M., 1985. *Mon. Not. R. astr. Soc.*, **216**, 817.
Wilson, A. S., Baldwin, J. A. & Ulvestad, J. S., 1985. *Astrophys. J.*, **291**, 627.
Wilson, A. S., Ward, M. J. & Haniff, C. A., 1988. *Astrophys. J.*, **334**, 121.